ISBN 978-82-326-4764-4 (printed version)
ISBN 978-82-326-4765-1 (electronic version)
ISSN 1503-8181

NTNU
Norwegian University of
Science and Technology

Stian Skaalvik Sandøy

Doctoral theses at NTNU, 2020:208

NTNU

Doctoral Thesis

NTNU
Norwegian University of
Science and Technology
Faculty of Engineering
Department of MarineTechnology

Doctoral theses at NTNU, 2020:208

Stian Skaalvik Sandøy

Acoustic-Based Probabilistic Localization and Mapping for Unmanned Underwater Vehicles in Aquaculture Operations

NTNU
Norwegian University of
Science and Technology

Stian Skaalvik Sandøy

Acoustic-Based Probabilistic Localization and Mapping for Unmanned Underwater Vehicles in Aquaculture Operations

Thesis for the degree of Philosophiae Doctor

Trondheim, June 2020

Norwegian University of Science and Technology
Faculty of Engineering
Department of MarineTechnology

NTNU
Norwegian University of
Science and Technology

NTNU
Norwegian University of Science and Technology

Thesis for the degree of Philosophiae Doctor

Faculty of Engineering
Department of MarineTechnology

© Stian Skaalvik Sandøy

ISBN 978-82-326-4764-4 (printed version)
ISBN 978-82-326-4765-1 (electronic version)
ISSN 1503-8181

Doctoral theses at NTNU, 2020:208

Printed by Skipnes Kommunikasjon as

Preface

This thesis is submitted in partial fulfillment of the requirements for the degree of Philosophiae Doctor (Ph.D.) at the Norwegian University of Science and Technology (NTNU). The thesis contains work carried out from August 2016 to May 2020. It was funded by the Norwegian University of Science and Technology (NTNU) under the Norwegian Research Council project Reducing Risk in Aquaculture (254913). Professor Ingrid Schjølberg was the principal supervisor, and Professor Ingrid Bower Utne was the co-supervisor.

The target audience for this thesis is personnel working on the study and development of underwater navigation systems for unmanned underwater vehicles (UUVs), both in industry and academia. The findings of the research herein may help to improve the future development of autonomous underwater vehicles performing operations such as inspection, maintenance, and repair tasks in aquaculture.

At present, all operations in aquaculture that are performed by UUVs need continuous control and supervision on site. Increasing our knowledge about how to use today's available technology to make these operations less reliant on humans is crucial to achieving a safe, efficient, and sustainable aquaculture industry. This thesis addresses challenges and solutions for UUVs with greater personnel independence and is, therefore, a step toward autonomous operations in aquaculture.

Abstract

The aquaculture industry needs automation to meet the world's increasing demand for fish protein. However, it is considered to be one of the most dangerous occupations in Norway due to the required amount of manual labor with heavy equipment in demanding weather conditions. One of the operations in need of improvement is the inspection of submerged equipment, which, nowadays, is performed by divers and remotely underwater vehicles (ROVs). The former is a high-risk operation for personnel, and the latter demands heavy lifting during launch and recovery, which is also considered a high-risk task.

Autonomous vehicles could perform these tasks to reduce risk; however, many challenges need to be solved before this becomes a reality, one of which is navigation in an aquaculture environment. This thesis addresses this challenge, presents tank and field experiments to validate some suggested methods, and compares the suggestions against existing methods. The thesis examines four novel algorithms in terms of two topics. The topics are localization and mapping using exteroceptive sensors, which measures the environment from a vehicle's egocentric perspective, and localization using environmental sensors, which measures position from an external point of reference. The external point of reference means that the sensors have a known location in the environment. From an egocentric perspective, there is a group of methods called simultaneous localization and mapping (SLAM). SLAM is a mature field; however, there are still challenges related to the use of sonar as an exteroceptive sensor. The high number of outliers and the nonlinear noise distributions pose a challenge to current methods.

The first method presented is primarily a sonar likelihood model that addresses outlier measurement issues. The likelihood model is integrated into a scan-matching method and in a Rao-Blackwellized particle filter SLAM method, and then compared with other SLAM methods. The results show that the suggested method has a better runtime and localization accuracy than the other methods.

The second issue addressed is the mapping of an aquaculture environment, or more specifically, the mapping of a dynamic fish cage using exteroceptive sensors such as sonar. Conventional methods involve memory consumption that scales cubically with volume. The suggested approach, named polar map, scales quadratically with the size of the environment. It not only makes the method far more memory-efficient in large environments, but gives a lower runtime complexity than conventional mapping representations when used in SLAM solutions. The verification of the map representation used tank experiments, where an unmanned underwater vehicle (UUV) performed SLAM using the suggested representation. This thesis also compares the use of two other map representations, namely the 3D occupancy grid map and the octomap, with the polar map.

The third issue addressed is the use of an environmental sensor to create a map representation of an anchor line. Hydrophones obtain the positions of acoustic tags placed on the line, which generate the map. This work presents field experiments, and the results show that the performance of the equipment had satisfactory accuracy for generating an initial map of an environment.

The fourth challenge addressed is the use of a hydroacoustic positioning system in the wave zone. Having a positioning system close to the surface simplifies the mounting and maintenance of equipment; however, wave-induced motion generates an oscillatory error in the position estimates of a UUV. The suggested solution is to use an extended Kalman filter that uses a wave filter to remove the wave motion in the final localization estimates of the UUV.

Thus, to summarize, the thesis presents four suggested methods for increasing automation in underwater inspections using a UUV in an aquaculture environment.

In dedication to my parents.
Ann Helen Skaalvik Sandøy
Pål Jørgen Sandøy

Acknowledgments

This thesis would not have been a possibility without guidance, help, and support from numerous people.

Firstly, I would sincerely thank my supervisor Professor Ingrid Schjølberg for her guidance and for helping me to stay positive. She has encouraged me to pursue my ideas, and the flexibility and support she has given are an essential factor in me being able to finish this thesis. I would also like to thank my co-supervisor, Professor Ingrid Utne, for her guidance, interesting discussions, and help in proof-reading articles. Thanks to Professor Jo Arve Alfredsen for sharing his insight and his assistance in the collection of hydroacoustic experimental data. Also, thanks to the project Exposed for providing me with valuable insight into the aquaculture industry.

I would like to thank Professor Toshihiro Maki at the University of Tokyo for inviting me and giving excellent guidance throughout my research stay. I would also like to thank the researchers Dr. Takumi Matsuda and Dr. Mehul Sangekar for our successful collaboration on multiple research articles. Thanks for sharing all your insight and your help in obtaining experimental data.

Thanks to my office mate in Trondheim, Bent Oddvar A. Haugaløkken, for fun discussions on both life and research, and numerous successful collaborations. Thanks to Jeevith Hedge for the cooperation on the polar map article and great talks on the topic. Furthermore, thanks to my training mates, Magnus Nygaard Holm, Einar Ueland, and Stian Sørum. The workout sessions have been of great importance after long office hours.

Last but not least, I would like to thank my family for their support. In particular, my mother, Ann Helen, my father Pål, my sister Ann Sophie, and my grandparents Åsmund and Eldbjørg.

Stian Skaalvik Sandøy
Trondheim, Norway

Contents

Contents **ix**

List of Figures **xi**

List of Tables **xiii**

Nomenclature **xv**

I Main Report **1**

1 Introduction **3**
- 1.1 Aquaculture in Norway . . . 3
- 1.2 Unmanned Underwater Vehicles in Aquaculture . . . 4
- 1.3 Framework of Unmanned Underwater Vehicles . . . 5
  - 1.3.1 Software Modules . . . 6
  - 1.3.2 Probabilistic Underwater Localization and Mapping . . . 8
  - 1.3.3 Navigation Sensors . . . 10
- 1.4 Research Objectives . . . 16
- 1.5 Overview of Articles and Contributions . . . 18
- 1.6 Thesis Outline . . . 21

2 Relevant Methods in Localization and Mapping **23**
- 2.1 Underwater Localization with Environmental Acoustics . . . 23
  - 2.1.1 Circular and Hyperbolic Localization . . . 23
  - 2.1.2 Delusion of Precision . . . 25
  - 2.1.3 Probabilistic Nonlinear Estimators . . . 25
- 2.2 Localization and Mapping with Exteroceptive Acoustics . . . 28
  - 2.2.1 Motion Model Using Doppler Velocity Log and Gyro . . . 28
  - 2.2.2 Sensor Model Using an Imaging Sonar . . . 29
  - 2.2.3 Occupancy Grid Mapping . . . 30
  - 2.2.4 Scan Matching . . . 32
  - 2.2.5 Outlier Robustness . . . 34
  - 2.2.6 SLAM Using RBPF with Occupancy Grid Maps . . . 35

3 Research Methods **39**

3.1 Underwater Localization and Mapping with Exteroceptive Acoustics 39
3.2 Underwater Localization with Environmental Acoustics 40

4 Summary of Research Results 43
4.1 Underwater Simultaneous Localization and Mapping 43
4.2 Polar Map: A New Map Representation for Localization and Mapping in Fish Cage Structures 46
4.3 Underwater Mapping Using Multiple Acoustic Tags 50
4.4 Positioning Error Correction for Ocean Wave Induces Long Baseline Navigation System 52

5 Conclusions and Further Work 55
5.1 Conclusions 55
5.2 Further Work 56

References 59

II Collection of Articles 69

Article J1 71

Article J2 95

Article J3 107

Article C1 125

Article C2 135

Article C3 145

Article C4 157

III Published Theses at Department of Marine Technology - NTNU 167

Theses 169

List of Figures

1.1 A Norwegian fish farm. Courtesy [10] 3
1.2 ROV in aquaculture inspection operation. Courtesy of [82]. 4
1.3 Fish cage deformations with varying current. Courtesy [51] 6
1.4 Overview of an autonomy framework for a UUV 6
1.5 ECEF, NED and Body frame 9
1.6 Acoustic sensors from a side view, where the blue colored areas indicate the trace of the acoustic pulse for each sensor. 13
1.7 Echo intensity measurement 15
1.8 UUV localization and mapping in a fish cage. 17
1.9 Linking each article to the scope of the thesis 18

2.1 Geometrical solution of circular and hyperbolic localization. 24
2.2 Geometrical examples of delusion of precision. 25
2.3 Target and proposal distribution in a PF 28
2.4 Reference systems and notation of the vehicle from the top view. . . . 28
2.5 Range extraction from echo intensity measurements 30
2.6 Grid mapping 31
2.7 Octree representation. Courtesy of [40]. 31
2.8 The 2.5D bathymetry map 32
2.9 Scan matching 33
2.10 Examples of loss functions 34
2.11 RBPF importance weighting with occupancy grid maps 36
2.12 RBPF resampling 37
2.13 Map estimation 37

3.1 The hovering AUV Tri-Dog 1 developed at the University of Tokyo, and the setup of the tank experiment. 40
3.2 On the left: The ROV used for recording the Abandoned Marina Dataset. On the right: an overview of the abandoned marina, courtesy of [80] and Google Maps. 40
3.3 Experimental setup in the marine cybernetics lab 41
3.4 Acoustic tag experiment 41

4.1 Sensor suite 44
4.2 SLAM in tank using MSIS 45

4.3 Results using the open Abandoned Marina dataset as a test case for the suggested method 46
4.4 Illustration of a typical fish cage 47
4.5 Section-wise discretization of a solid cylinder by angle, θ, and depth, z. The range r is the variable that describes the edge of the cylinder for each section. 47
4.6 Top view of the discretized structure (left) and the uncertainty model of a single section (right) in the 2.5D polar map representation 48
4.7 2.5D Polar map representation of a fish cage 48
4.8 PF-based SLAM in tank using polar map 49
4.9 Time-series for RMSE of tag ID 32 with the EKF and PF for Case Studies 1 (top subplot) and 2 (bottom subplot). The blue line is the RMSE for the PF, the red line for the EKF. 51
4.10 Visualization of the interpolated anchor line from Article J1 52
4.11 Estimated states with EKF in x direction 53

List of Tables

1.1 Navigation sensors 11
1.2 Sonar two-way working ranges. Courtesy of [16]. 15
1.3 Overview of articles 20

4.1 RMSE for uncompensated versus compensated 53

Nomenclature

List of abbreviations

2.5D	Two point five dimensional
2D	Two dimensional
3D	Three dimensional
ADCP	Acoustic Doppler current profiler
AUV	Autonomous underwater vehicle
CTD	Conductive-temperature-depth
DOF	Degree of freedom
DVL	Doppler velocity log
EKF	Extended Kalman filter
FOG	Fiber optic gyro
GNSS	Global navigation satellite system
ICP	Itterative closest point
IMR	Inspection, maintenance and repair
LBL	Long baseline
Lidar	Light detection and ranging
MEMS	Micro-electro-mechanical system
NED	North-East-Down
PF	Particle filter
pIC	probabilistic iterative correspondence
RBPF	Rao-Blackwellized particle filter
RMSD	Root mean square deviation
RMSE	Root mean square error
ROV	Remotely operated vehicle

SBL	Short baseline
SLAM	Simultanious localization and mapping
Sonar	Sound navigation and ranging
TDOA	Time difference of arrival
TOF	Time of flight
USBL	Ultra short baseline
UUV	Unmanned underwater vehicle

List of symbols

$\boldsymbol{\xi}$	x-y-ψ transformation vector
$\boldsymbol{u}$	Surge, sway and yaw velocities $[\frac{m}{s}, \frac{m}{s}, \frac{rad}{s}]$
$\boldsymbol{x}$	2D pose $[m, m, rad]$
$\Delta\theta_k$	Difference in bearing $[rad]$
Δr_k	Difference in range$[m]$
Δt	Small time step
$\dot{x}$	Time derivetive of some variable x
$\frac{\delta f(\cdot)}{\delta x}$	Partial derivetive of function $f(\cdot)$ for some variable x
$\mathbb{R}$	A scalar real number
$\mathbb{R}^{n\times m}$	A matrix of real numbers with dimention n times m
$\mathbb{R}^n$	A vector of real numbers with dimention n
$\mathbf{m}$	Map
$\mathbf{p}$	Position of acoustic transponder/receiver $[m]$
$\mathbf{z}$	Range and bearing measuremet [m,rad]
ψ	Heading in NED frame $[rad]$
$\rho.$	Loss function
σ_θ	White noise standard deviation for bearing $[rad]$
σ_r	White noise standard deviation for range$[m]$
θ	Bearing of range measurements $[rad]$
c_o	Speed of sound $[\frac{m}{s}]$
D	Water depth $[m]$
dt_{TDOA}	Time difference of arrival $[s]$
$f(\cdot)$	Nonlinear function

$h(\cdot)$	Nonlinear function
i	Particle number
k	Time step
N	Number of particles
N_{eff}	Effective number of particles
$O(\cdot)$	Big O notation. Run time complexity given inputs.
p	Proability distribution
r	Angular velocity in yaw $[\frac{rad}{s}]$
r	Range measurement $[m]$
$R_{xy\psi}$	Rotation matrix in for $\mathbf{x}$
R_{xy}	Rotation matrix in the x-y vector
S	Salinity [‰]
T	Temperature $[\,^{\circ}C]$
t_{TOF}	Time of flight $[s]$
W	Set of weights
w	Particle weight
X	Set of particles
x	Random variable x
x	x position in NED frame $[m]$
y	Random variable y
y	y position in NED frame $[m]$
z	z position in NED frame $[m]$

Part I

Main Report

Chapter 1

Introduction

1.1 Aquaculture in Norway

AQUACULTURE is one of the fastest-growing food-production industries in the world [72]. In Norway, it has experienced large growth during the last forty years, and in 2017 it produced approximately 1.3 million tons of fish every year, with a value of about 65 billion NOK. Along with the fishery industry (20 Billion NOK), aquaculture is the second-largest export industry in Norway [72]. As of December 2018, production (mainly of salmon and trout) has been underway in 1015 aquaculture fish farms [20], where one fish farm may consist of multiple fish cages, as seen in Figure 1.1.

The standard size of a fish cage is about 30 m in diameter and 40 m deep. To increase production volumes requires installations of a more substantial scale and

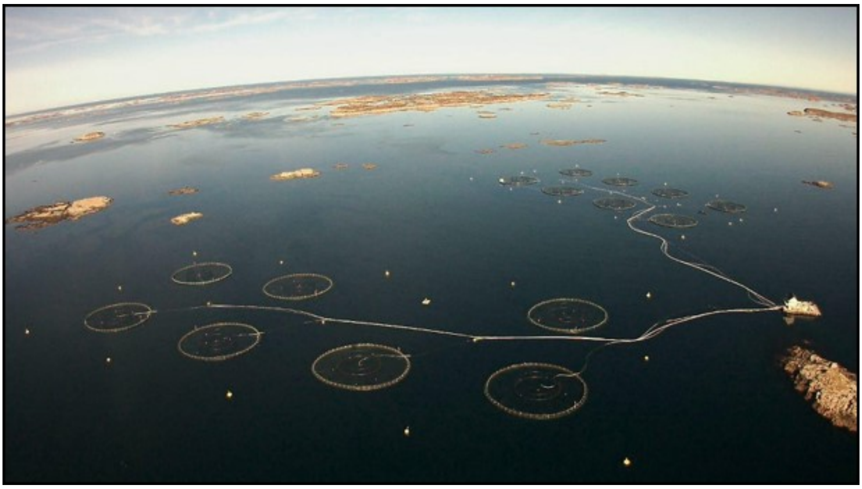

Figure 1.1: A Norwegian fish farm. Courtesy [10]

.

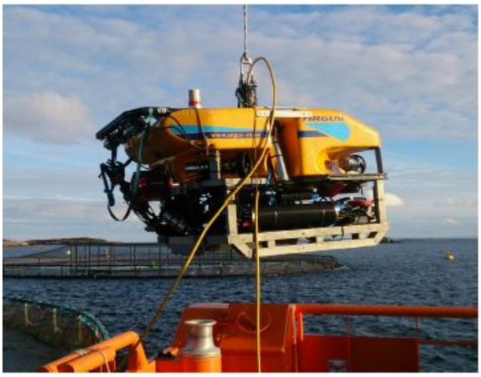

Figure 1.2: ROV in aquaculture inspection operation. Courtesy of [82].

adoption of more exposed sites, due to the lack of available sheltered locations [10]. Increased production calls for better autonomous underwater operations solutions in inspection, maintenance, and repair (IMR) tasks [83]. Inspection and maintenance activities are vital for cost-efficient and safe aquaculture operations, but sea-based fish farming is a dangerous occupation. The combination of the harsh environmental conditions, high manual workload for the operators, utilization of heavy equipment, as well as high work efficiency pressure contribute to the occupational risks [39].

Furthermore, there are risks to the environment, such as the escape of fish, which is influenced by interactions between the equipment, the hard physical working environment, and the operator's workload, work pressure, training, skills, experience, co-operation, communication, and safety management. Fish escape incidents harm the environment because they are a threat to biodiversity and wild fish [90].

Moreover, they cause economic losses and attract considerable negative attention from the public, with corresponding losses to the fish farm reputation. Fish cages are prone to damage, such as holes in the fishnets made by predators and boat collisions, and abrasion and general handling [44]. On average, 372,000 salmon and trout have escaped annually since 2001 [21]. Equipment wear is why sea-based aquaculture fish farms require periodic maintenance [71] performed by human divers or remotely-operated vehicles (ROVs) [93]. Figure 1.2 shows an ROV that is ready to be deployed for fish cage inspection.

1.2 Unmanned Underwater Vehicles in Aquaculture

Diving is hazardous and costly, and the improved utilization of unmanned underwater vehicles (UUVs) for visual inspection in aquaculture can reduce the risk of personal injury and fatality. A UUV is defined as follows:

Definition: Unmanned underwater vehicle

An underwater vehicle that does not have a human on board and is controlled either remotely or by an autonomous system.

Nowadays, ROVs perform some inspection operations; however, this can be dangerous and costly due to the need for a supply vessel with a crane and multiple human operators. ROVs have an umbilical due to the lack of high communication bandwidth in underwater environments. Tethers are a hazard in the management of the vehicle in confined areas and during high tidal currents, which encourages the use of cable-free UUVs with a higher degree of autonomy. In addition to environmental factors, some other arguments include the decreased need for the online transfer of data, as the UUV can gather information autonomously and then transfer it after inspection to the operators, and the possibility of having resident UUVs inspecting aquaculture structures in the future [13, 60].

Resident UUVs may increase the sustainability of underwater activities, as well as reduce costs and personal risk and enhance efficiency, as a reduced need for equipment transportation could lead to a reduction in greenhouse gas emissions. To enable this type of system, all significant parameters that could affect the operation must be taken into account, so that the UUV can make the best decisions possible; however, due to the challenges of operating in an underwater environment, the parameters are not easily determined. Environmental problems in the inspection of fish cages using UUVs include ocean currents and waves, which deform the fish cage [52, 77], as seen in Figure 1.3 and induce slowly varying forces on the vehicle. Challenges for underwater navigation sensors in aquaculture are high water turbidity and high attenuation of electromagnetic waves, which limit the use of camera, radar, and lidar systems due to limited range, although in ideal conditions, some electromagnetic-based systems can be used [17, 78]. The high attenuation of electromagnetic waves is why acoustic sensors are a better alternative, despite having a lower resolution. Furthermore, challenges related to computer processing in online operations include memory and computational power constraints. Even though the processors radically increase in speed every second year [66], there is still a need for efficient algorithms, not only to reduce the cost but also to make autonomous operations possible.

1.3 Framework of Unmanned Underwater Vehicles

Figure 1.4 shows a UUV framework divided into three main components. The operators monitor or manually control the vehicle depending on the level of autonomy [95, 94], the hardware components sense and interact with the environment, and the software interprets sensor information and sends commands to the actuators. “V2O” is an abbreviation for vehicle-to-operator communication through either an umbilical or an acoustical modem. High data transfer operations require an umbilical during online camera monitoring, as the acoustic modems have a limited data

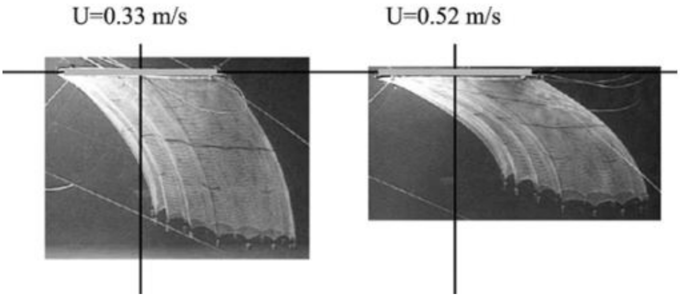
U=0.33 m/s
U=0.52 m/s

Figure 1.3: Fish cage deformations with varying current. Courtesy [51]

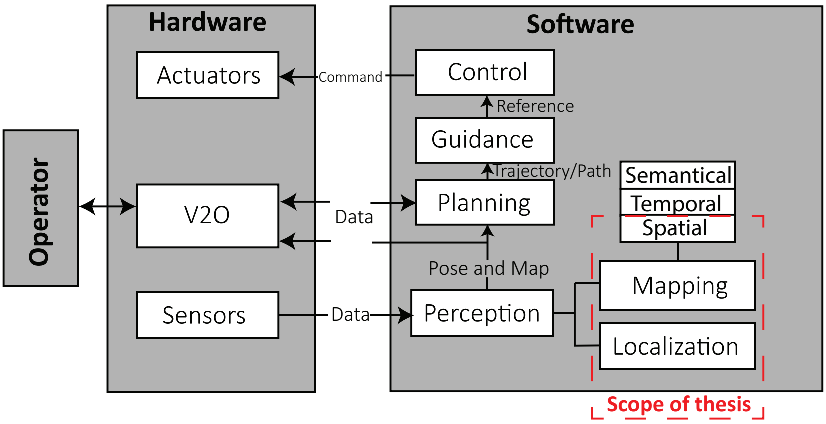
Hardware
Software
Operator
Actuators
Command
Control
Reference
Guidance
Trajectory/Path
Semantical
Temporal
Spatial
V2O
Data
Planning
Pose and Map
Mapping
Sensors
Data
Perception
Localization
Scope of thesis

Figure 1.4: Overview of an autonomy framework for a UUV

transfer and a time delay, which reduces the controlling ability of the operator. UUVs with a higher level of autonomy can reduce the required data transfer and thereby avoid the use of a tether.

Figure 1.4 shows the scope of this thesis with a red dashed line. The thesis addresses the spatial mapping of an aquaculture environment and UUV localization. Localization and mapping are fundamental problems to be solved for the development of planning, guidance, and decision-making algorithms that can perform the proper actions for an autonomous inspection of fish cages.

1.3.1 Software Modules

Figure 1.4 shows the software modules in an autonomous online system. “Online” means that computational processing is performed during operation, and therefore there are constraints on memory and processing requirements, which need to be taken into account when the algorithms are designed. There are three submodules in the software structure:

- perception,
- planning, and
- guidance and control.

From an inspection operation point of view, *robot perception* is the ability to sense and understand the environment through sensors; this also includes the filtering or smoothing of sensor signals.

Definition: Robot Perception

is a robot's spatial-temporal and semantical representation of an environment, and its own location within the environment, as obtained through sensors.

This thesis divides perception into two topics, as seen in the figure. *Mapping* refers to the process of representing a map relative to a reference, such that the robot obtains a spatial, temporal, and semantical understanding; however, herein, it will be limited to the spatial representation. *Localization* is the process of estimating the robot's position and orientation relative to the spatial environment; this also includes inertial navigation. Section 1.3.2 will present this topic in more detail, as it is one of the main issues of this thesis. All preceding modules depend on the perception module in some manner.

Planning refers to the vehicle's ability to reach higher-order goals; this can, for example, be to inspect a fish cage and cover a whole area.

Definition: Planning

is the process of bringing a UUV from a start to a goal location, using optimization or heuristics based on the robot's perception.

Here, planning includes both offline and online planning. Offline planning is prior-mission computations using known environmental characteristics, which does not constrain the algorithms to low computational complexity or limited memory. Online planning deals with planning during operations such as for collision avoidance or unexpected events that call for the replanning of the mission. Planning may include three main modules [76]: Firstly, mission planning governs the overall goal of the task, for example, stipulating a global path to follow. One method uses cost evaluation algorithms such as Dijkstra's algorithm [19] or A* [35] to generate a global path using the available information. Secondly, behavioral planning is the decision-making module that monitors all processes, for example, through a finite state machine, which manages time-to-collision or failures. Motion planning or path planning, which is a well-studied domain, [15, 28, 53, 54, 91] generates paths that withhold certain constraints such that the path is flyable for the vehicle. Flyable means that the vehicle can follow the path. Motion constraints can be, for example, based on the kinetic properties of the vehicle. Planning consists again of various methods, which depend on the available perception representation. [84] is a reference containing motion planning algorithms for further interest.

The guidance and control modules interpret the received input into actuator commands such that the robot follows the path or trajectory. Guidance controls the generation of references [28], and the actuators receive commands from the output of the controller computation. Both depend on control theory [14, 48].

Definition: Guidance

is the process of interpreting a path or trajectory into reference commands such that the vehicle can follow the desired trajectory

Definition: Control

is the process of interpreting reference commands into actuator commands such that the robot reaches a goal position in the desired manner.

1.3.2 Probabilistic Underwater Localization and Mapping

Robotic localization and mapping is a broad field of research that is of interest in most applications where there is robotic motion, from terrestrial satellite navigation in space to a simple robotic manipulator moving in a constrained environment. The underwater robotics field is highly interdisciplinary, and includes sensor systems [32], statistics and probability theory [91], control system theory [14, 48], numerical optimization [70], algorithm design [18], marine craft [28], and more.

This thesis focuses on fully actuated underwater vehicles, meaning they have roll and pitch stability. The neglect of roll and pitch allows the system to be modeled with four degrees of freedoms (DOFs) by x-, y-, and z-directions, and by a yaw angle. Figure 1.5 shows the reference frames used to describe the environment and the motion of the vehicle. The vehicle motion is herein relative to a fixed north-east-down (NED) frame near the site of the inspection. In the NED frame, the x-axis points towards true north, the z-axis points down, and y-axis points eastward. The origin of the earth center fixed frame (ECEF) is in the center of mass of the earth, the z-axis points towards true north, the x-axis points toward zero degrees longitude and latitude, and the y-axis completes the right-hand rule. The reason for choosing a fixed NED frame close to the region of inspection is that the size of one fishnet is on the order of meters, and therefore an assumption of a flat earth is reasonable. For further background on the transformation between the reference frames the reader is referred to [27, 28, 32].

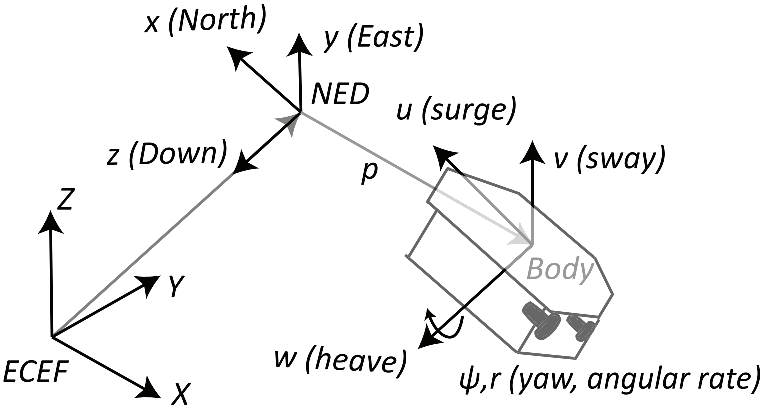

Figure 1.5: ECEF, NED and Body frame

This thesis addresses localization and mapping with a main emphasis on probabilistic methods [91]. Probability comes from the Latin word *probabilitatem*, which means ”something likely to be true.” Therefore, the probabilistic method describes multiple likely solutions to a problem. In probability theory, probability distributions represent the solutions, often approximated by the well-known Gaussian normal distribution. Depending on the sensor setup and knowledge of the environment before the operation, there are three different approaches to localization and mapping:

- Mapping with known position,
- localization with a known map, and
- simultaneous localization and mapping (SLAM).

Mapping with a known position means that the location of the vehicle is known, and therefore exteroceptive sensors can be used to map the environment. In aquaculture, the position can be found through aided navigation, meaning with the use of environmental sensors such as short base line (SBL) or ultra short baseline (USBL) positioning systems [82], along with proprioceptive sensors.

Localization with a known map is particularly tricky in aquaculture inspection without the continuous monitoring of the fish cage, which involves mounting landmarks or tags along with the use of environmental sensors, meaning the environment is modified. Another possibility may be to model the dynamics of the fish cage from the waves, currents, and solidity of the net, and predict the position [52]; however, uncertainties will occur which may be too large for the successful localization of the UUV. A third possibility is to use known terrain information [64, 69] below the fish cage; however, this approach requires a texture-rich seafloor in order to determine a position.

The third type of perception is SLAM, for which there are numerous approaches [26, 55, 59, 61, 80, 85, 91]. Nevertheless, to the author's knowledge, none has addressed this problem in the context of fish cage inspection. As the name SLAM suggests, the problem consists of both finding a map and localizing the vehicle within that map. It originated in the 1990s [56] and has since been heavily researched in all robotic domains [12]. SLAM is one of the fundamental problems to be solved in order to attain a truly autonomous system. There are three main techniques for SLAM implementation: based on the extended Kalman filter (EKF) [61], the graph [59], and the particle filter (PF) [85]. The main focus in this thesis is the PF, and the main reason for choosing PF-based SLAM is its applicability to occupancy grid maps, which can map unstructured environments such as a fish cages, and the computational tractability for online application demonstrated by [30]. Computational tractability is still a challenge with graph-based SLAM [31]; however, applications are emerging in vehicles with high processing speed [42, 59].

The localization and mapping approaches require the fusion of proprioceptive and exteroceptive sensors. Localization using exteroceptive sensors requires that the environment have sufficient texture or detectable landmarks. Also, temporal perception is relevant in the occurrence of a violation of the static assumption. The static assumption states that the actual position of an observed object in space does not change relative position with a given time frame. This assumption is of importance for SLAM because if violated, the vehicle's observations of the same object cannot provide the location unless the temporal perception of the object is accounted for. Therefore, when using the fish cage as a texture for localization, it is an essential assumption either that the fish cage deformations are negligible over the inspection period, or the map accounts for the temporal changes.

1.3.3 Navigation Sensors

A sensor detects a physical phenomenon and represents it as signals that can be interpreted by a computer. Examples of physical phenomenon in underwater environments are acoustic waves, pressure, optics, magnetics, and mechanical forces. Figure 1.4 shows that navigation sensors are used in the perception of an environment and are fundamental for a UUV to be able to perform planning, guidance, and control. The next section presents current navigation sensor technology, and in particular, acoustic sensors.

Navigation Sensors Overview

There are many ways to classify the underwater navigation sensors [74] of a UUV. The sensors are categorized into four groups:

Table 1.1: Navigation sensors

Sensor Name	Type	Technology	Active/ passive
Doppler velocity log	Proprioceptive	Acoustic	Active
Inertial measuring unit	Proprioceptive	Optical/Mechanical	Passive
Thrust feedback	Proprioceptive	Optical/Mechanical	Passive
Compass/Gyro Compass	Exteroceptive	Electromagnetic/Optical	Passive
Pressure sensor	Exteroceptive	Mechanical	Passive
Sonar	Exteroceptive	Acoustic	Active
Lidar	Exteroceptive	Optical	Active
Camera	Exteroceptive	Optical	Passive
LBL/SBL/USBL	Environmental	Acoustic	Active
GNSS	Environmental	Electromagnetic	Active
CTD	Auxiliary	Electromagnetic/Mechanical	Passive
Turbidity meter	Auxiliary	Optical	Passive

- proprioceptive,
- environmental,
- exteroceptive, and
- auxiliary.

In addition to these four groups, each sensor can be classified as active or passive. An active sensor generates, for example, an acoustic or electromagnetic wave and measures the echo or backscatter, e.g., sound navigation and ranging (sonar). A passive sensor does not emit any pulse, but measures the environment's natural phenomena, e.g., camera, which measures the natural scattering of light. Table 1.1 list the relevant sensors and their classification. There is also a technology column that notes the nature of the sensor.

A proprioceptive sensor measures the internal motion of the vehicle, meaning its acceleration or velocity, and is used for inertial navigation.

Definition: Proprioceptive sensor

senses the robot's internal motion and orientation. Position estimates have unbounded error.

Proprioceptive sensors obtain a position by integration; however, uncertainties accumulate due to the integration of noise, and the uncertainty of the position increases over time. Another term for this is unbounded error. Examples of proprioceptive sensors are the Doppler velocity log (DVL) (e.g. [86]), an inertial measuring unit (IMU), and thrust feedback. A DVL measures velocity through the Doppler shift between multiple acoustic pulses emitted at a fixed frequency and the pulses' echo. The echo comes from the backscatter from either the seafloor or from the water column [37]. Note that a fishnet also creates a backscatter if the pulse emitted has a sufficiently high frequency [82].

An IMU is an integrated sensor consisting of multiple accelerometers and gyroscopes. The accelerometer measures the forces along an axis, and a gyro measures the angular velocities around an axis. There are multiple accelerometer and gyro technologies with different noise levels and financial costs. One type, used in the experiments for this thesis, is the fiber optic gyro (FOG). FOG uses the property that light behaves as a wave by splitting a light beam into two and sending each through opposing circular coils around an axis. Because light behaves as a wave, a frequency difference will occur between the spliced beams when there is rotation [32]. This frequency difference is proportional to the angular rotation of the device. Another proprioceptive sensor is the thrust force. A system can, for example, measure the number of rotations of the shaft of the thruster and from it computes the forces generated based on hydrodynamical properties. Then, a navigation algorithm uses the forces to compute the position using double integration [28].

Environmental sensors measure a global spatial position relative to the NED frame.

Definition: Environmental sensor

measure position with bounded error relative to a fixed and external reference.

These sensors bound the error of the position estimate; however, they require external mounting and calibration. A global navigation satellite system (GNSS) [32] is such a system. It is used to obtain a position for a surfaced UUV, or a reference position at the sea surface, as for acoustic transponders. A GNSS uses the TOF (TOF) from at least four satellites in order to triangulate a position. There are also different grades of accuracy. The one used in this work is Europe's regional satellite-based augmentation system, which yields sub-meter-level accuracy.

The third group of sensors is the exteroceptive sensors. They take measurements of external references that are relative to the body frame of the vehicle.

Definition: Exteroceptive sensor

sense the external environment from the body frame.

The most widely used exteroceptive sensor in robotics is the camera. In aquaculture, visual inspection is used to obtain information on the state of equipment and the health of the fish. Cameras are an essential source of navigational information for land vehicles; in contrast, the underwater environment has turbid water that creates light backscatter, which limits the applicability of cameras in navigation. Other geophysical properties include bathymetry, pressure, earth's magnetism, and hydroacoustics. Pressure sensors are a vital sensor that bound the horizontal position error by depth. Even though the surface varies due to tidal currents, the horizontal accuracy is at a cm resolution. It is important to note that pressure varies with the salinity and temperature profile of the water column. Magnetic compasses and magnetometers measure the magnetic North Pole, but they are prone to biases due to magnetic distortions. An alternative is gyro-compassing, which uses the rotation of the earth to determine the direction of true north; however, this approach requires a high-grade IMU. A review of gyro-compassing and other methods for determining heading can be found in [29].

There are some auxiliary sensors for the support of the navigational sensors.

Definition: Auxiliary sensors

measure parameters to support the navigation sensors.

An example of an auxiliary sensor is the conductivity–temperature–depth (CTD) sensor that measures the salinity, temperature, and depth of saltwater. This sensor is particularly useful for the computation of the speed of sound, which depends on multiple factors [41] and is elaborated in the next section.

Acoustic Underwater Sensors

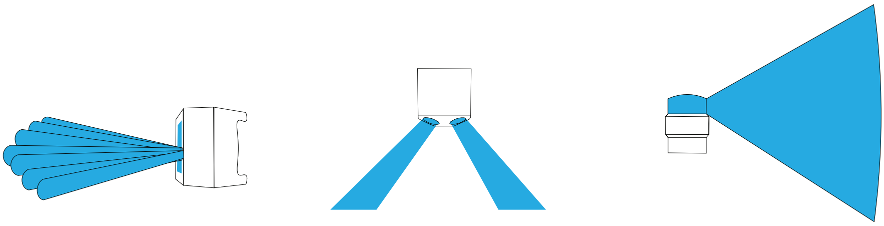

(a) Multibeam echo sounder (b) Doppler velocity log (c) Imaging sonar

Figure 1.6: Acoustic sensors from a side view, where the blue colored areas indicate the trace of the acoustic pulse for each sensor.

The ingenuity of the animal kingdom has inspired acoustic localization technology. For example, dolphins use biological sonar to localize in underwater environments. They can perform complex tasks as shown in [68], where they do a navigation task blindfolded using only ultra-high acoustical frequencies in a challenging acoustical environment. In robotic underwater localization, acoustic-based solutions have proven to be a robust choice [74] in comparison with electromagnetic-based sensors, e.g., cameras, which suffer in high turbidity due to their dependency on light conditions. Acoustics are mechanically-generated pressure waves that have quite low attenuation in seawater compared with electromagnetic signals [32]. Acoustic systems rely on piezoelectric transducers that generate and measures acoustic waves by using a particular crystal material that changes its electrical properties according to acoustic-mechanical stress [41]. The piezoelectric elements are reciprocal and can both emit and receive acoustic pulses. Distances are measured based on the speed of sound and TOF, which assumes that the acoustic pulse travels the shortest path. Common errors in acoustic navigation are due to the bending effects from differences in the speed of sound, timing errors due to clock error, and external acoustical noise. A significant error factor can be the multipath of a pulse; this means that a pulse is bounced off an object, seafloor, or sea surface, thereby violating the assumption of the pulse traveling the shortest path. This error is, in particular, challenging during a high-sea state, because echoes from the surface may be largely due to the bouncing angle of the waves. The properties of the medium in which the sound wave propagates determine the speed of the pulse, c_0. An empirical formula presented in [41] formulates the relation as follows:

$$c_0 = 1448.6 + 4.6418T - 0.0523T^2 + 1.25(S - 35) + 0.017D, \tag{1.1}$$

where c_0, T, S, and D correspond to the speed of sound in the seawater $[m/s]$, the temperature $[^\circ C]$, salinity [‰], and depth $[m]$, respectively.

Other essential acoustic properties are the maximum range and resolution of the pulse. The former is inversely proportional to the frequency of the pulse, and the latter is proportional to the frequency. These relations mean that there is a tradeoff between maximum range and resolution. Table 1.2 shows the frequency, wavelength, and distance relation for acoustic waves in saltwater. Note that the hearing frequency range of salmon which is the most farmed fish in Norway, were reported in [36] to be 380 Hz. Therefore, the acoustic navigation system should have frequencies far above 380 Hz, to avoid stressing the fish.

Sonar is an active exteroceptive sensor that emits a short acoustic pulse and measures the two-way TOF and the returning echo intensities. The output of one echo is multiple discrete distances with an intensity. Figure 1.7 shows the concept of a sonar pulse at the bottom and the echo intensity signal versus range. The echo intensity peak marks the distance to an object, and the weaker intensities are the result of backscatter from the water column. In reality, the echo intensity is corrupted with ambient noise and is not as smooth as illustrated in the figure.

Table 1.2: Sonar two-way working ranges. Courtesy of [16].

Frequency	Wave length	Distance
100 Hz	15 m	1000 km or more
1 kHz	1.5 m	100 km or more
10 kHz	15 cm	10 km
25 kHz	6 cm	3 km
50 kHz	3 cm	1 km
100 khz	1.5 cm	600 m
500 khz	3 mm	150 m
1 MHz	1.5 mm	50 m

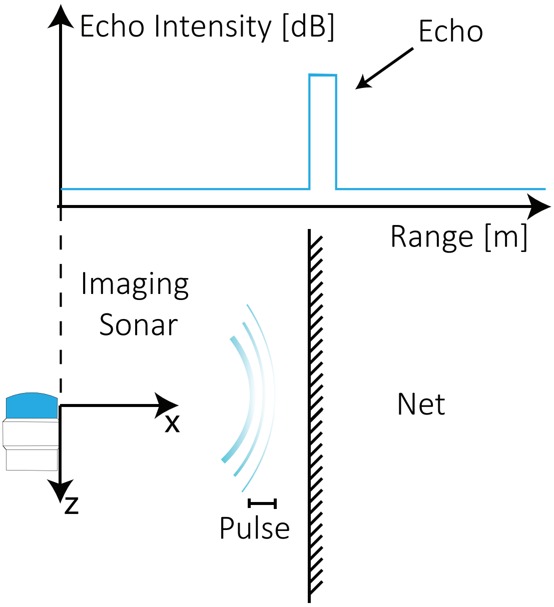

Figure 1.7: Echo intensity measurement

The signal resolution and range depend on the pulse's frequency, as seen in Table 1.2. The former means that in order to measure the distance to a fishnet, the pulse needs a sufficiently high frequency. The width of a fishnet thread is approximately 3 mm, which means that a frequency higher than 500 kHz may be sufficient [82]. The pulse length of the signal is also important for measuring the frequency difference in the Doppler effect, and an increase in pulse length increases the accuracy of the frequency estimate, but decrease the accuracy in ranging.

An acoustic transducer array consists of multiple piezoelectric elements on a small surface and can create directed acoustic beams with a specified vertical and cross-track angle. The angle of the beams determines if a sonar is an imaging or profiling sonar. The former has a high vertical angle, which can be, for example, approximately 60°. The latter has a lower angle beam, for example, 3°. The angle of the vertical and cross-track, with new lens-based technology, can be reduced to 0.5° [6]. There is also mechanically scanning and static sonars, which can do either imaging or profiling. Scanning sonars have a servo that rotates the sensor to generate a 360° image.

Other groups of sonar are single and multibeam. As the name suggests, a multibeam has a transducer array that generates multiple beams in specific directions, as shown in Figure 1.1. In contrast, a single beam only has one beam, as illustrated in Figure 1.6c. In a multibeam sonar, a beam needs to have a distinct frequency in order to determine its source. For both multibeam and single beam sonars, there is an imaging and profiling type. There is also a difference between 2D and 3D profiling multibeam sonars [43, 1]. Some other types not mentioned are side-scan sonar and synthetic aperture sonar. See more on sonar in [16].

LBL and SBL are acoustic environmental sensors that compute the distance based on a two-way TOF, or delayed time of arrival, both based on the speed of sound. A possible transponder configuration is having a short baseline mounted on the vehicle as in [63]. Transponders mounted on the vehicle are an advantage, because only one external transponder is required instead of multiple. Another potential sensor technology is the GNSS intelligent buoy, which is a buoy that integrates transponder technology with GNSS to ECEF reference each transponder [89]. For more information on other configurations, see [16].

1.4 Research Objectives

The main research objective was to enhance the spatial and temporal perception of UUVs in aquaculture operation near or in fish cages. This objective may be of help in enabling autonomous vehicles in the future. Figure 1.8 shows an overview of the fish cage environment and acoustic sensor systems relevant to this thesis, and illustrates the research objects.

The first objective is to develop SLAM algorithms for use inside an aquaculture fish cage using acoustic exteroceptive sensors, without any environmental sensors. This objective resulted in articles J1, J2, and C3. Figure 1.8 shows the case where the UUV can localize and map using only sonar, DVL, and other proprioceptive sensors.

Research Objective O1

Research and develop SLAM algorithms for UUVs operating near or in a fish cage based on acoustic exteroceptive sensors.

The second objective aims to develop a mapping method using acoustical tags, which resulted in articles J3 and C4. Figure 1.8 shows a case where acoustic tags and hydrophones localize the anchor line of a fish cage. The acoustic tags transmit depth and ID information to the hydrophones mounted on the fish cage.

Research Objective O2

Research and develop a method for online spatial representation using acoustic tags.

The third objective is to develop algorithms that reduce localization error due to wave motion in environmental sensors, i.e., LBL. The objective is relevant for environmental sensors mounted in the wave zone. This resulted in articles C1 and C2. Figure 1.8 shows the sensor setup for such a system where transducers are mounted on the fish cage and the UUV.

Research Objective O3

Research and develop a method that reduces localization error due to wave disturbances at surface mounted transponder networks.

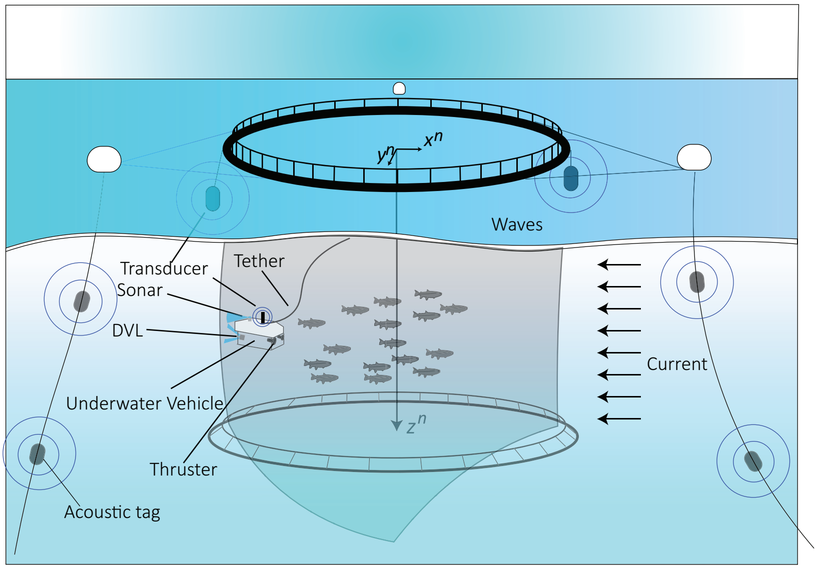

Figure 1.8: UUV localization and mapping in a fish cage.

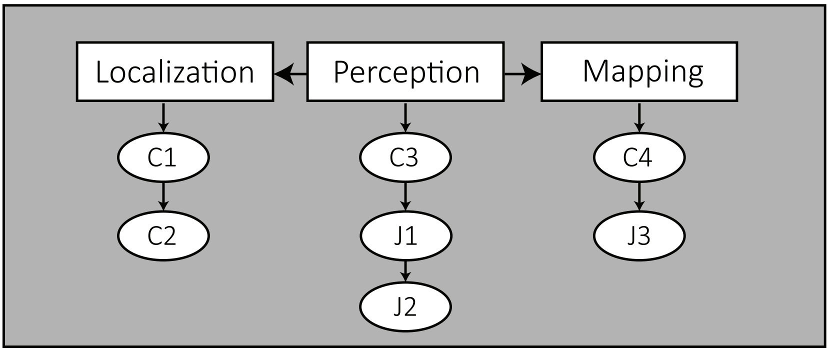

Figure 1.9: Linking each article to the scope of the thesis

1.5 Overview of Articles and Contributions

Table 1.3 presents an overview of the main articles of the thesis. J denotes the Journal articles, and C references the conference articles. Figure 1.9 shows the objectives and the connection between the articles. The first objective is related to localization, the second to mapping, and the third to both mapping and localization. The arrows of each paper indicate the time of origin of each article. Note that the order necessarily connects to when the article was published. The contribution of each article are as follows:

Contributions - J1

- This article is an extension of Article C3. It suggests a new sensor model that makes the SLAM method more robust when sonar measurements are used. A loss function increases the robustness of the algorithm, which is a method that deals with outliers. Outliers are misinformation in the measurements due to errors such as multipathing in acoustic localization. The suggested method is compared with two different range and bearing sensors, namely a multibeam profiling sonar and a mechanical scanning imaging sonar in a tank. Also, the work compares the method with other SLAM algorithms using the same field experiment. This article makes a contribution because it enhances the robustness of UUV perception, thereby introducing more robust information for planning, guidance, and control.

Contributions - J2

- The contribution of this work is a novel map representation that models enclosed vertical structures. The mapping method is memory and run-time efficient, making it an ideal choice in online operations. This approach is also applicable to both static and dynamic environments for adapting temporal change to the environment. The proposed method is also scalable in terms of map resolution, which can benefit fish cage mapping systems that require minimal system memory or computational effort. This article demonstrates the map through a simulated UUV operation for a known location mapping scenario. It also demonstrates the map with the SLAM algorithm proposed in Article J1 and validates it in a tank experiment, where the UUV has no prior knowledge of the environment. The map representation is an essential contribution because it enables online autonomous systems in an aquaculture environment with lower memory consumption and run-time complexity. The method may also be the basis of development for new and more efficient planning, guidance, and control algorithms.

Contributions - J3

- The main contribution of this article is the demonstration of a suggested mapping method that uses off-the-shelf acoustic tags mounted on an anchor line, and hydrophones mounted at the surface. The article presents a second positioning method and compares it to the one presented in Article **??**, in addition to an accuracy analysis. Article J3 makes an essential contribution because it shows the mapping possibilities when using tags and hydrophone network in field experiments.

Contributions - C1

- The main contribution of this paper is a method that minimizes errors due to wave motion in surface mounted transponders. The suggested method separates the UUV dynamics and wave dynamics when using TOF measurements. This work makes a significant contribution because it enables the mounting of transponders near the ocean surface on aquaculture structures and enables higher positioning accuracy in high sea states.

Contributions - C2

- The main contributions of this paper are an experimental verification of the filter presented in Article C1, and a method for computing the parameters of the filter. The work contributes to enabling the mounting of transponders near the ocean surface on aquaculture structures in harsh conditions without fully compromising positioning accuracy.

Contributions - C3

- The main contribution of this article is the implementation of an underwater SLAM method using occupancy grid maps with mechanical scanning imaging sonar measurements. The SLAM method uses dead reckoning through DVL, FOG, and pressure measurements. Simulations and experiments in a tank validate the approach, where the UUV has no prior knowledge of the environment. The work contributes to enhancing the UUV's perception in enclosed environments by providing a location and map to be used in planning, guidance, and control algorithms.

Contributions - C4

- The main contribution of this paper is a method for estimating the map of a flexible structure below the surface of the sea. The work is a conceptual study that uses simulated measurements. The map of the structure is found through the use of acoustical transmitters, herein referred to as tags. The tags emit their respective identification number and depth. Multiple surface mounted hydrophones receive the emitted signal, and from that, they triangulate the position through depth information and time-delay-of-arrival measurements. Using the tag identification number, a probabilistic interpolation between the positing of each tag gives the map of the structure. This map can serve as a tool for robotic vehicles that seek to plan and execute operations autonomously within and around the structure, or as a visualization tool for human operators.

Table 1.3: Overview of articles

	Journal Articles
J1	Sandøy, S. S., Matsuda T., Sangekar M., Schjølberg, I., Maki T., Particle Filter-based Simultaneous Localization and Mapping for Underwater Vehicles with Sonar, Robotic and Autonomous Systems(For review)
J2	Sandøy, S. S., Hegde, J., Schjølberg, I., Utne, I. B., Polar Map: A Digital Representation of Closed Structures for Underwater Robotic Inspection, Aquacultural Engineering, 2020, doi:10.1016/j.aquaeng.2019.102039
J3	Sandøy, S. S., Haugaløkken, B. O. A., Schjølberg, I., Utne, I. B., Localization of a Flexible Underwater Anchor Line using Acoustic Transmitter Tags and Receivers. Applied Acoustics.(For review)
	Conference Articles
C1	Sandøy, S. S., Schjølberg, I., Underwater Positioning Using Near Surface Long Baseline Transponder's Induced by Wave Motion, doi:10.1115/OMAE2017-61742.
C2	Sandøy, S. S., Schjølberg I., Experimental Verification of Underwater Positioning System in Aquaculture, OCEANS 2017 - Aberdeen, Aberdeen, 2017, pp. 1-7. doi: 10.1109/OCEANSE.2017.8084947
C3	Sandøy, S.S., Matsuda, T., Maki, T., Schjølberg, I. (2018) Rao-Blackwellized Particle Filter with Grid-Mapping for AUV SLAM Using Forward-Looking Sonar.Proceedings of MTS/IEEE Oceans'18, Techno-Ocean 2018 - OTO'18.
C4	Arnesen, B. O., Sandøy, S. S., Schjølberg, I. ,Alfredsen, J. A., Utne, I. B., Probabilistic Localization and Mapping of Flexible Underwater Structures Using Octomap, 2018 European Control Conference (ECC), Limassol, 2018, pp. 268-275. doi: 10.23919/ECC.2018.8550498

1.6 Thesis Outline

The thesis is a written summary of the work performed. It is divided into three parts: the main report, a collection of articles, and a list of theses previously published in the Department of Marine Technology at the Norwegian University of Science and Technology. Firstly, Part I contains the main report and is organized as follows.

Chapter 1 This chapter presents an introduction to UUVs and localization and mapping in aquaculture, the research objectives, and an overview of articles and contributions related to the work of this thesis.

Chapter 2 This chapter elaborates on the preliminary methods in order to understand the paper and research methods for validating and verifying the algorithms. It divides the preliminary methods into two parts, namely the underwater positioning problem and the SLAM problem.

Chapter 3 This chapter presents the research methods herein. The methods used for validation are similar to Chapter 2 and are divided by the use of exteroceptive and environmental acoustic sensors.

Chapter 4 This chapter presents a summary of the articles from this work. It divides the work into four sections based on the research objectives of each article. Note that the first objective is divided into two sections because Articles J1 and C3 contain an overall underwater SLAM approach using an occupancy grid map. Article J2 presents a new mapping method along with the suggested underwater SLAM approach.

Chapter 5 This chapter presents conclusions from this work and a summary of recommendations for further work.

Secondly, Part II contains the article collection, and thirdly, Part III contains theses previously published in the Department of Marine Technology at the Norwegian University of Science and Technology.

Chapter 2

Relevant Methods in Localization and Mapping

This chapter presents the algorithms utilized in this work. There are two main sections; localization with acoustic environmental sensors and SLAM, which uses exteroceptive acoustic sensors.

2.1 Underwater Localization with Environmental Acoustics

This section presents two known algorithms for acoustic environmental sensors, namely circular and hyperbolic localization, in addition to the concept of the delusion of precision(DOP). The last subsection reviews the EKF and the PF, which are two well known probabilistic nonlinear estimation methods.

2.1.1 Circular and Hyperbolic Localization

LBL and SBL acoustic positioning systems use different methods to obtain a source position. Even though these strategies are common knowledge, they are reviewed due to their importance in Articles C1, C2, C4, and J3. First, according to the concept of circular acoustic positioning, an acoustic transducer located at the UUV transmits a signal that is received by a transponder. The transponder then sends a new signal back to the transducer, which computes the TOF and the distance between the devices. A second approach uses hyperbolic positioning, where a transmitter sends an acoustic signal, and multiple hydrophones at known locations receive the signal. Based on the signal's arrival time, a computer computes the time difference of arrival (TDOA) between pairs of receivers to determine the position of the transmitter. TOF requires at least three transponders and TDOA at least four hydrophones with positions that are linearly independent in vector space. Linearly independent means that any plane in the space can contain more than two transducers.

Mathematically, the following equation describes the position and TOF relation:

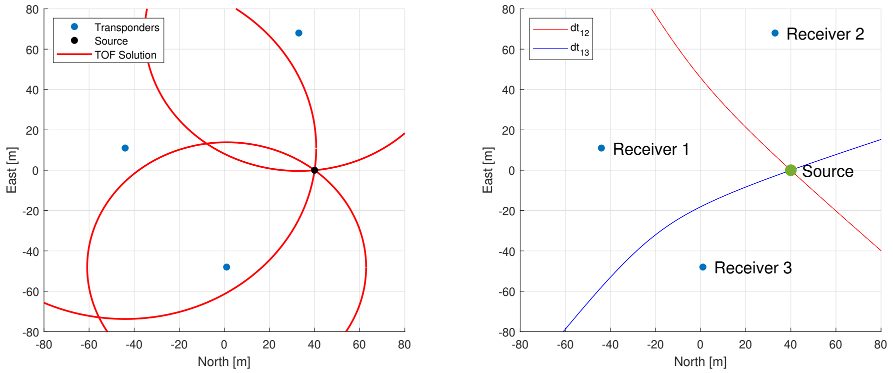

(a) 2D circular localization using TOF measurements.

(b) 2D hyperbolic localization using TDOA measurements.

Figure 2.1: Geometrical solution of circular and hyperbolic localization.

$$\frac{t_{\mathrm{TOF},i}}{2}c_0 = ||\mathbf{x}-\mathbf{p}_i||, i = 1\dots m, \tag{2.1}$$

where $t_{\mathrm{TOF},i}$ is the time of flight, x is the vehicle position, p_i is the position of transponder i and m is the number of transponders. Figure 2.1a shows a 2D geometrical representation with three transponders. Furthermore, the TDOA can be written as:

$$dt_{\mathrm{TDOA},i}c_0 = (||x-\mathbf{p}_i|| - ||\mathbf{x}-\mathbf{p}_{i+1}||), i = 1\dots m-1, \tag{2.2}$$

where $dt_{\mathrm{TDOA},i}$ is the TDOA for the two hydrophones i and $i+1$. Figure 2.1b shows the hyperbolas with three hydrophones [34]. The target position is the intersection of the lines. Note that TDOA gives one less measurement than TOF with the same number of transponders; however, TDOA only requires one-way communication if the position is only topside. “Topside” means above the waterline, where personnel typically do the monitoring.

The reason for the name circular and hyperbolic positioning is that the solution x is determined by the crossing of circles and hyperbolas. This is illustrated by Figure 2.1, where Figure 2.1a shows the circular localization, and Figure 2.1b shows the hyperbolic localization. Without noise, one can find algebraic solutions for the localization problem; however, the result varies when noise is present. Figures 2.2a and 2.2b show a $\pm 10^{-3}$ s error in timing, and the solutions vary by several meters. Large position errors due to small timing errors or other effects are the reason why filtering is an important step in the localization problem.

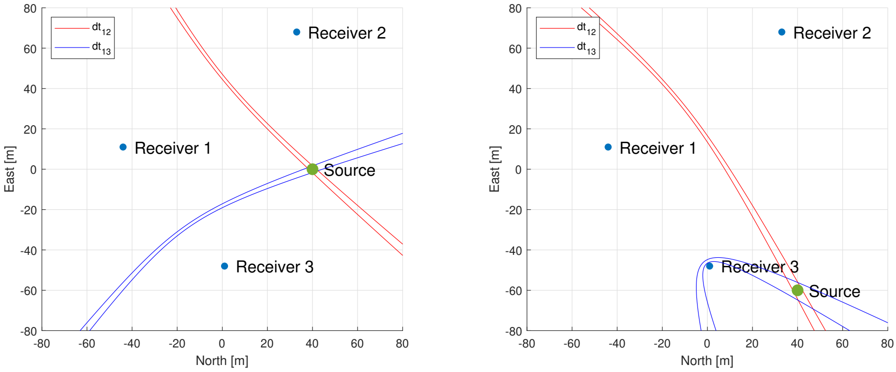

(a) DOP position 1 (b) DOP position 2

Figure 2.2: Geometrical examples of delusion of precision.

2.1.2 Delusion of Precision

The DOP is a measure of the magnitude of an estimate's position accuracy due to the geometrical properties of the triangulation problem [47]. The magnitude of the position certainty relies on the accuracy of the clock, the locators' relative position, and disturbances from environmental factors such as multipathing, ray bending, and errors in the estimate of the speed of sound. The DOP concept is useful because it is possible to investigate the magnitude of all error terms before implementing an estimator. Figure 2.2 shows a geometric representation of the DOP. There is a timing error of $\pm 1e-3$ s, and there are two locators. Case 1, shown in Figure 2.2a, has a lower DOP than Case 2, shown in Figure 2.2b.

2.1.3 Probabilistic Nonlinear Estimators

The most widely used probabilistic filters for nonlinear problems are the EKF [46], and the PF [22]. Using these filters gives the problems a probabilistic representation with parameters that can be determined by the expected amount of noise in the measurement. The EKF assumes uncorrelated additive noise for each measurement, while the PF does not use this assumption. However, the PF is, in most cases, more computationally expensive than the EKF. This work considers only the EKF and the PF but notes that there are also other variants. For example, the unscented Kalman filter [45], extended information filter [91], point mass filter [34], and nonlinear optimization [34].

The nonlinear filtering problem can be defined by the continuous state equations as follows:

$$\dot{\mathbf{x}} = f(\mathbf{x}, \omega) \in \mathbb{R}^n, \tag{2.3}$$

$$\mathbf{y} = h(\mathbf{x}, \omega) \in \mathbb{R}^m, \tag{2.4}$$

where $\mathbf{x}$ is the state vector, f and h are nonlinear vector functions, and ω is a vector of independent normally distributed Gaussian random variables. The process model, $\mathbf{x}$, is typically a kinematics model. The sensor model, $\mathbf{y}$, use proprioceptive, exteroceptive, or environmental sensors.

Extended Kalman Filter

The EKF is a variant of the Kalman filter [46]. The Kalman filter assumes that the system is linear, and the noise is additive and Gaussian, which means that the nonlinear system in Equations (2.3) and (2.4) needs to be written in the following form:

$$
\begin{align}
\dot{\mathbf{x}} &= A\mathbf{x} + \mathit{chol}(Q)\omega \in \mathbb{R}^n, \tag{2.5}\\
\mathbf{y} &= C\mathbf{x} + \mathit{chol}(R)\omega \in \mathbb{R}^m, \tag{2.6}
\end{align}
$$

where

$$
\begin{align}
A &= \frac{\partial f}{\partial \mathbf{x}}, \qquad\qquad C = \frac{\partial h}{\partial \mathbf{x}}, \tag{2.7}\\
Q &= \frac{\partial f}{\partial \omega}^T \frac{\partial f}{\partial \omega}, \quad R = \frac{\partial h}{\partial \omega}^T \frac{\partial h}{\partial \omega}. \tag{2.8}
\end{align}
$$

Running the EKF on a computer requires discretization of (2.5) and (2.6). The appendix in Brown and Hwang [11], shows a method for the discretization of the equations. The following equations review the discrete EKF equations:

$$
\begin{aligned}
K_k &= \bar{P}_k C_k^T (C_k \bar{P} C_k^T + R_k)^{-1}\\
\hat{\mathbf{x}}_k &= \bar{\mathbf{x}}_k + K_k(y_k - h(\bar{x}_k)))\\
\hat{P}_k &= (I_{n\times n} - K_k C_k)\bar{P}_k\\
\bar{\mathbf{x}}_{k+1} &= \hat{\mathbf{x}}_k + f(\hat{\mathbf{x}}_k)\Delta t\\
\bar{P}_{k+1} &= A_k \hat{P}_k A_k^T + Q_k,
\end{aligned}
$$

where K_k is the Kalman gain, $Q_k \in \mathbb{R}^{n\times n}$ and $R \in \mathbb{R}^{m\times m}$ are the process and sensor noise covariance matrices, and $\bar{\mathbf{x}}$ and $\hat{\mathbf{x}}$ denote the predicted and estimated states, respectively. Furthermore, P_k is the covariance matrix, and Δt is the time step. Note that $\bar{(\cdot)}$ marks the posterior estimates. Also, note that the first iteration, $k = 0$, uses the initial values $\bar{\mathbf{x}}_0$ and $\bar{P}_0$.

Particle Filter

This section discusses the sampling importance resampling PF [33]. The PF is more computationally expensive than the EKF; however, the PF does not necessarily need to assume Gaussian density functions and does not require linearization. The PF can also represent multimodal probability density functions, which means that the probability density function does not need to have only one peak. The PF contains three steps:

1. Sampling
2. Importance weighting
3. Resampling

Sampling consist of choosing the hypotheses of the process given in the next time step from (2.3) corresponding to the statistical properties of the process or $p(\mathbf{x}_k|\mathbf{x}_{k-1})$. The particle set and its weights are defined as follows:

$$X_k = \{\mathbf{x}_k^{(1)}, \dots, \mathbf{x}_k^{(N)}\}, \tag{2.9}$$

where $\mathbf{x}_k^{(i)}$ denotes the states representing the hypothesis. Subscript k and superscript i are the time step and particle number, respectively, and N is the number of particles. The importance weighting step assigns a weight w_k^i to each particle. The set of weights are expressed as follows:

$$W_k = \{w_k^{(1)}, \dots, w_k^{(N)}\}, \tag{2.10}$$

The weight of each particle is computed as follows:

$$w_k^{(i)} = \frac{p(\mathbf{x}_k^{(i)}|\bar{\mathbf{y}}_k, \mathbf{x}_{k-1}^{(i)})}{\pi(\mathbf{x}_k^{(i)})}, \tag{2.11}$$

where $p(\mathbf{x}_k^{(i)}|\bar{\mathbf{y}}_k, \mathbf{x}_{k-1}^{(i)})$ is called the target distribution, and $\pi(\mathbf{x}_k^{(i)})$ the proposal distribution. The latter must fit the problem at hand. Figure 2.3 shows an example of a proposal distribution and a target distribution. The particles shown as green circles are chosen based on the proposal distribution

The resampling step consists of choosing the particles for the next iteration with the probability proportional to the weight of the particle. There are multiple ways to resample; one is multinomial resampling [33], where a multinomial distribution is created based on the weights of the particles. The resampling consists of drawing the particle set of the next step from the proposal distribution. The particle set will contain duplicates of the particles that have the highest weights. Note that the initial particle set X_0 depends on the application. It can, for example, be a Gaussian distribution, a uniform grid over a square, or all particles in the same position.

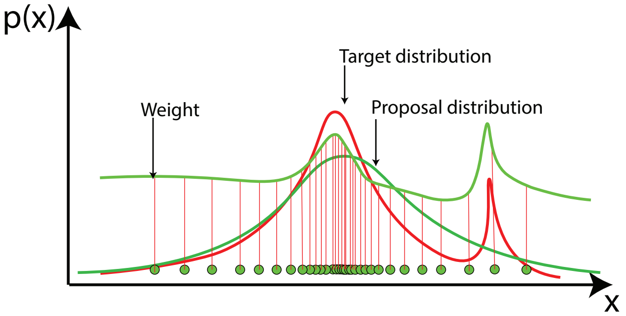

Figure 2.3: Target and proposal distribution in a PF

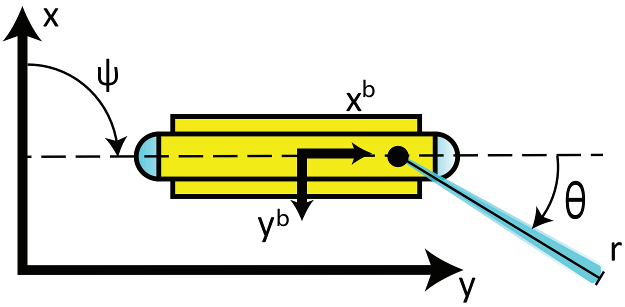

Figure 2.4: Reference systems and notation of the vehicle from the top view.

2.2 Localization and Mapping with Exteroceptive Acoustics

This section presents methods in localization and mapping. The topics are the UUV motion model, sensor model, map representation, scan matching, outlier robustness, and SLAM using the Rao-Blackwellized PF (RBPF). Note that many other methods are also relevant although they are not mentioned here.

2.2.1 Motion Model Using Doppler Velocity Log and Gyro

The motion model uses proprioceptive sensors to perform dead reckoning to estimate position. These sensors measure the internal motion of the vehicle. The equation below presents the differential equations of motion:

$$\dot{\mathbf{x}} = R(\psi)_{xy\psi}\mathbf{u}^b, \tag{2.12}$$

where $\mathbf{x} = \begin{bmatrix} x & y & \psi \end{bmatrix}^T \in \mathbb{R}^3$ is the position of the body frame, (x^b, y^b), relative to the (x, y) map-frame, $\mathbf{u}^b = \begin{bmatrix} u^b_{\text{DVL}} & v^b_{\text{DVL}} & r^b_{\text{G}} \end{bmatrix}^T \in \mathbb{R}^3$ is the velocity of the vehicle given in the body frame, as indicated by b. The rotation matrix, $R_{xy\psi}(\psi) \in \mathbb{R}^{3\times3}$, corresponds to the rotation between a vector in the body frame and one in the reference frame. Figure 2.4 shows the notation of the 2D kinematics for the vehicle. The discrete kinematic equation follows, assuming low velocities and sufficiently small time steps:

$$\boldsymbol{x}_{k+1} = \mathbf{x}_k + R_{xy\psi}(\psi_k)\mathbf{u}_k^b \Delta t + \mathbf{w}_u \Delta t, \tag{2.13}$$

where $\mathbf{w}_u \sim \mathcal{N}(\begin{bmatrix}0 & 0 & 0\end{bmatrix}^T, Q)$ is a Gaussian distribution with mean zero and covariance $Q = \operatorname{diag}(\sigma_{\mathrm{DVL}}^2, \sigma_{\mathrm{DVL}}^2, \sigma_{\mathrm{G}}^2)/\Delta t \in \mathbb{R}^{3\times3}$, and Δt is a small time step. The subscripts DVL and G indicate DVL and gyro measurements, respectively. Note that the equation neglects depth, pitch, and roll motion, because the former was assumed constant, and the latter two were approximately zero. Equation (2.13) contains a probability distribution for the probability of a given position, $\mathbf{x}_{k+1}$, given the last position, $\mathbf{x}_k$. It is written as follows:

$$p(\mathbf{x}_{k+1}|\mathbf{u}_k^b, \mathbf{x}_k) = \frac{1}{\sqrt{2\pi \det(Q)}} \exp(-\frac{1}{2}(\mathbf{x}_{k+1} - \boldsymbol{\mu}_{k+1})^T Q^{-1}(\mathbf{x}_{k+1} - \boldsymbol{\mu}_{k+1})), \tag{2.14}$$

where $\boldsymbol{\mu}_{k+1} \in \mathbb{R}^3$ is equal to (2.13) with $\mathbf{w}_u = \begin{bmatrix}0 & 0 & 0\end{bmatrix}^T$.

2.2.2 Sensor Model Using an Imaging Sonar

The sensor model for a sonar measurement is the representation of a range and bearing measurement to a nearby object. Figure 2.4 illustrates a sonar measurement. The combination of the vehicle position, and the range and bearing information results in an endpoint. The output of the sonar is a series of echoes, as seen in Figure 2.5. The series needs to be interpreted for each echo intensity, as seen at the top of Figure 2.5, to determine the range to the closest object. The simplest method is the threshold model, which sets the range of a measurement to be the first intensity point higher than a given threshold.

The range and bearing measurement, $\mathbf{z}$ at time step k is defined as:

$$\mathbf{z}_k = \begin{bmatrix}r & \theta\end{bmatrix}^T + \begin{bmatrix}\omega_r & \omega_\theta\end{bmatrix}^T, \tag{2.15}$$

where r is the range from the sonar, and θ is the angle of the sonar relative to the vehicle's yaw angle, as seen in Figure 2.4. Furthermore, $\omega_r = \mathcal{N}(0, \sigma_r^2)$ and $\omega_\theta = \mathcal{N}(0, \sigma_\theta^2)$ are both Gaussian random variables with mean zero and standard deviation σ_r and σ_θ, respectively. To obtain the endpoint position relative to the reference frame, the following expression is used:

$$\mathbf{e}(\mathbf{z}_k, \mathbf{x}_k) = R_{xy}(\psi)\left(\begin{bmatrix}r\cos\theta \\ r\sin\theta\end{bmatrix} + \begin{bmatrix}x_{\text{sonar}}^b \\ y_{\text{sonar}}^b\end{bmatrix}\right) + \begin{bmatrix}x \\ y\end{bmatrix}, \tag{2.16}$$

where x_{sonar}^b and y_{sonar}^b are the x- and y-positions of the sonar sensor relative to the origin of the body frame, and the rotation matrix is $R_{xy}(\psi) \in \mathbb{R}^{2\times2}$. The equation

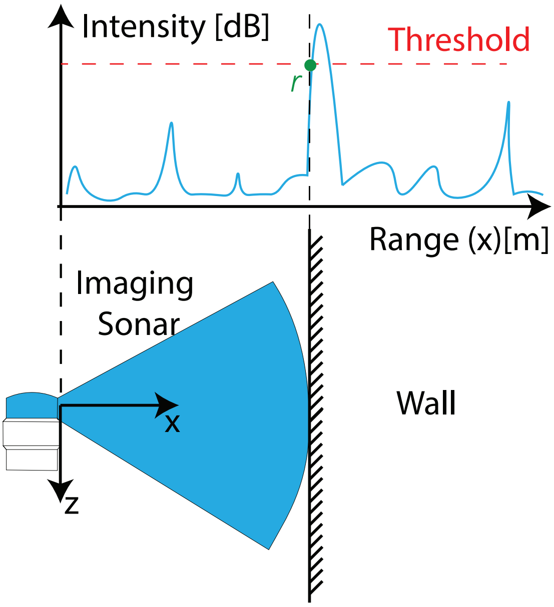

Figure 2.5: Range extraction from echo intensity measurements

assumes that there are no pitch and roll angles when using the MPS. Figure 1.6c shows that the acoustic beam of the MSIS is wider when viewed from the side compared with the MPS. A larger beam width makes it less essential to model the pitch motion.

2.2.3 Occupancy Grid Mapping

Occupancy grid mapping is an old concept [24, 67], that is still heavily utilized in robotics mapping because of its versatility in 2D and 3D applications. In grid maps, the environment is divided into finite cells, as seen in Figure 2.6, where each cell has a probability of being occupied and is independent of all other cells. One downside of the grid map is that the static assumption, meaning the map's actual state, does not change over time. The update scheme of the map consists of inserting a point cloud into it based on the location of each measured endpoint. The scheme updates the cells in the trace of measurement from the vehicle pose to the endpoint. The cells along the trace are updated using a log-odds scheme [91], which is a logarithmic notation for numerical stability. The relation between Log-Odds and probabilities is defined as follows:

$$l(\mathbf{m}_k^{(j)}) = log\left(\frac{p(\mathbf{m}_k^{(j)})}{1 - p(\mathbf{m}_k^{(j)})}\right) \tag{2.17}$$

where $l(\mathbf{m}_k^{(j)})$ is the so-called log-odd ratio for a given cell (j). The scheme updates each cell with a probability p_{hit} if the endpoint of a ray hits a cell, and p_{miss} if the

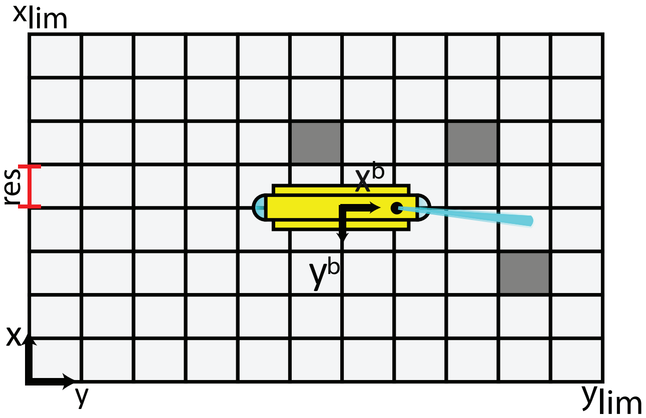

Figure 2.6: Grid mapping

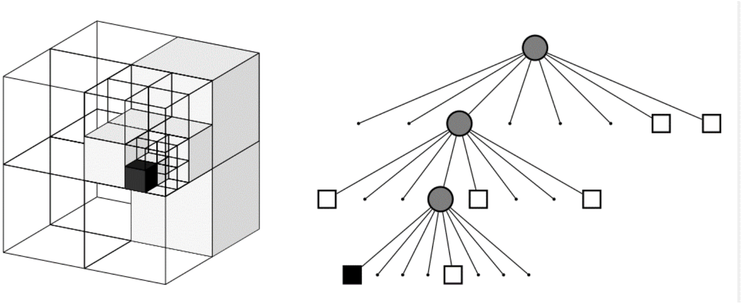

Figure 2.7: Octree representation. Courtesy of [40].

ray only traverses a cell.

There are various representations for occupancy grid mapping, each with its disadvantages and advantages. For example, the classical grid mapping approach from [24] and [67] is computationally efficient for map evaluation, having a runtime complexity of O(1). However, it is not memory efficient for large maps, because the number of cells increases quadratically in 2D and cubically in 3D. Tree-based grid-map representations, such as quadtrees in 2D and octrees in 3D [26, 40], require less memory. These representations have higher computational complexity in the map evaluation step.

Another grid-based map is the 2.5D grid map or bathymetry map, where underwater terrain-based navigation is an application [5]. Figure 2.8 shows the concept. Each mesh point in the north-east plane is associated with a Gaussian distribution uncertainty variable, where the depth corresponds to the mean and the uncertainty corresponds to the variance of the depth. The update procedure is performed independently for each cell using a Kalman filter. The map evaluation complexity, in

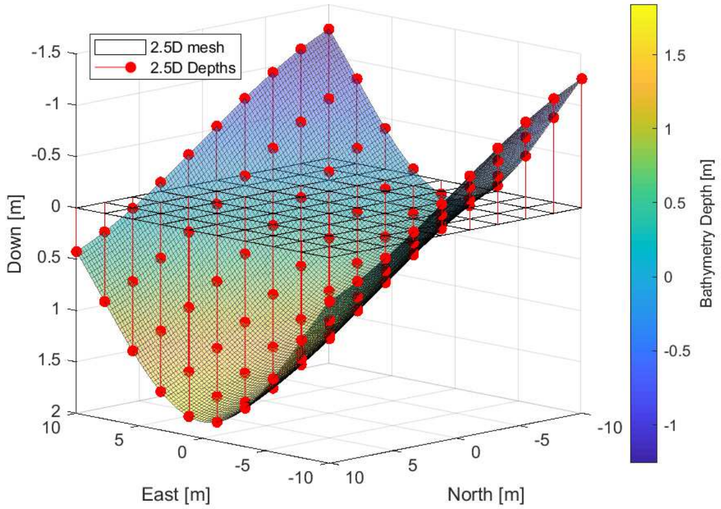

Figure 2.8: The 2.5D bathymetry map

this case, is O(1), and the memory consumption is quadratic. Unlike the previously described models, the 2.5D grid map cannot model vertical environments, such as cliffs on the ocean floor.

There are also other types of representations, like feature-based [57], continuous [73] and Hilbert space-based [79]; however, this work does not evaluate these representations.

2.2.4 Scan Matching

Scan matching is the alignment of a point cloud with a representation of previous measurements used for improving odometry estimates and detecting loop closures. It improves the odometry estimate through optimization of the current range and bearing measurements given by a set $\mathbf{z}_{1:M} = \{\mathbf{z}_1, \ldots, \mathbf{z}_M\}$, with corresponding poses given by a trajectory $\mathbf{x}_{1:M} = \{\mathbf{x}_1, \ldots, \mathbf{x}_M\}$.

Figure 2.9 illustrates the optimization problem. On the left, the believed position deviates from the true position. The scan matching problem aims to find the transformation, $\boldsymbol{\xi}$, to minimize the error between the reference and the map, as shown on the right of Figure 2.9.

There are many different approaches to scan matching [8, 9, 38, 61], but the two types that are important in this work are:

- Point cloud to point cloud matching

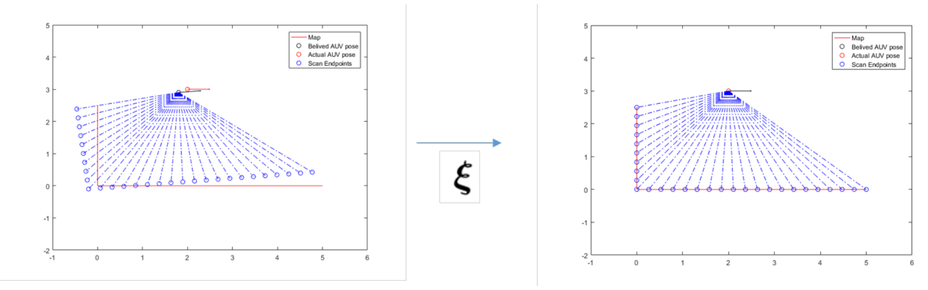

Figure 2.9: Scan matching

- Grid map to point cloud matching

Firstly, point cloud-based scan matching can be solved using the iterative closest point (ICP) method [7]. ICP uses an unaligned point cloud and a reference point cloud as input. First, the ICP determines the correspondence of each point in the point cloud. It then minimizes the distance between the correspondences, and the minimization problem can be defined as follows:

$$F_{icp}(\mathbf{z}_{1:M}, \mathbf{x}_{1:M}, \mathbf{m}_0, \boldsymbol{\xi}) = \underset{\boldsymbol{\xi}}{\operatorname{argmin}} \sum_{i=1}^{M} ||\mathbf{e}(\mathbf{z}_i, T(\mathbf{x}_i, \boldsymbol{\xi})) - \Pi(\mathbf{m}_0, T(\mathbf{x}_i, \boldsymbol{\xi}), \mathbf{z}_i)||^2, \tag{2.18}$$

where

$$T(\mathbf{x}_i, \boldsymbol{\xi}) = \begin{bmatrix} \cos(\xi_\psi)x_i - \sin(\xi_\psi)y_i \\ \sin(\xi_\psi)x_i + \cos(\xi_\psi)y_i \\ \psi_i \end{bmatrix} + \underbrace{\begin{bmatrix} \xi_x \\ \xi_y \\ \xi_\psi \end{bmatrix}}_{\boldsymbol{\xi}} \in \mathbb{R}^3, \tag{2.19}$$

and the transformation parameter $\boldsymbol{\xi}$ rotates and translates the trajectory $\mathbf{x}_{1:M}$ through the following transformation function: Π is the function that finds the point correspondences. Note that $\mathbf{m_0}$ denotes the point cloud. Montesano et al. [65] implemented a variant of the ICP algorithm, termed probabilistic iterative correspondence (pIC). It incorporated the uncertainty of the points by using a probabilistic length, called the Mahalanobis distance, instead of a metric measure, as shown in 2.18. The pIC was developed to account for noisy range measurements and errors in position due to odometry drift. Hernández et al. [38] extended the approach to handle MSIS by removing the distortions at each scan point caused by vehicle motion.

Secondly, point cloud to grid map matching uses a grid map as a reference and a point cloud as input. Kohlbrecher [49] used the approach successfully with Lidar measurements in a cluttered environment. There are multiple methods used within grid map matching as well [49, 75]. The advantage of the point cloud to grid map

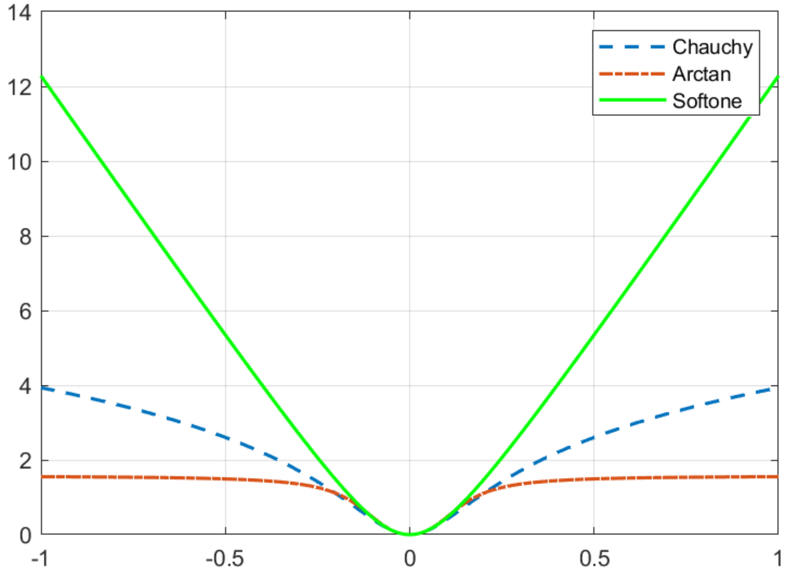

Figure 2.10: Examples of loss functions

approaches is that no point correspondence needs to be determined, which is the most computationally expensive operation in ICP. The methods in this thesis focus on probabilistic matching inspired by Pedrosa [75], which uses likelihood fields that are computed from the grid map. The following equation presents the optimization problem:

$$F_{\text{grid}}(\mathbf{z}_{1:M}, \mathbf{x}_{1:M}, \mathbf{m}_0, \boldsymbol{\xi}) = \underset{\boldsymbol{\xi}}{\operatorname{argmin}} - \prod_{k=1}^{M} p(\mathbf{z}_k | T(\mathbf{x}_k, \boldsymbol{\xi}), \mathbf{m}_0), \tag{2.20}$$

Equation (2.20) may then be optimized using, for example, either the Gauss–Newton [70] or Levenberg–Marquardt [58, 62] methods. Note that $\mathbf{m}_0$ denotes a grid map. There is also a grid map to grid map matching, which has the advantage of also be able to match unoccupied space cells.

2.2.5 Outlier Robustness

The next important principle is the introduction of loss functions into the optimization problem [92]. A loss function is a passive approach to dealing with outliers and excessive noise in probabilistic optimization problems. The use of such functions removes the need for outlier detection, making the optimization problem more robust. Examples of loss functions are the Cauchy (2.21), arctan (2.22), and the soft one loss (2.23) functions, all shown in Figure 2.10.

$$\rho_{\text{chauchy}}(s) = \frac{c}{2} ln(1 + \frac{s}{c}) \tag{2.21}$$

$$\rho_{\text{arctan}}(s) = arctan(s) \tag{2.22}$$

$$\rho_{\text{softone}}(s) = 2((\sqrt{1+s}) - 1) \tag{2.23}$$

2.2.6 SLAM Using RBPF with Occupancy Grid Maps

This section introduces SLAM using RBPF with grid maps [30]. The main idea behind RBPF is to separate mapping and localization such that the localization assumes a known map and the mapping assumes a known vehicle location. In estimating the distribution of the vehicle pose, the distribution consists of particles, where each particle represents a pose with a map constructed from the range and bearing measurements along the trajectory. A particle set is defined as follows:

$$S = \{[\mathbf{x}_k^{(1)}, \mathbf{m}_k^{(1)}, w_t^{(1)}], \dots, [\mathbf{x}_k^{(N)}, \mathbf{m}_k^{(N)}, w_k^{(N)}]\}, \tag{2.24}$$

where k is a time step, (i) is a particle number, $\mathbf{x}_k^{(i)}$ is a pose, $\mathbf{m}_k^{(i)}$ is an occupancy grid map, and $w_k^{(i)}$ denotes a particle weight. Doucet [23] established the theoretical foundation for splitting the process into two, as described in the full SLAM problem equation below:

$$\begin{aligned} p(\mathbf{x}_{1:n}, \mathbf{m}_{1:n} | \mathbf{z}_{1:n}, \mathbf{u}_{0:n-1}, \mathbf{x}_{0:n-1}, \mathbf{m}_{0:n-1}) = \\ \underbrace{p(\mathbf{m}_{1:n} | \mathbf{x}_{t_{1:n}}, \mathbf{z}_{1:n}, \mathbf{m}_{0:n-1})}_{\text{Map estimation}} * \\ \underbrace{p(\mathbf{x}_{1:n} | \mathbf{z}_{1:n}, \mathbf{x}_{0:n-1}, \mathbf{u}_{0:n-1}, \mathbf{m}_{0:n-1})}_{\text{Pose estimation}} . \end{aligned} \tag{2.25}$$

The implemented filter is termed sampling importance resampling PF [33]. In this method, each particle pose is sampled from a distribution given by (2.14). Each particle is then given a weight based on the ratio of the likelihood of its sample being correct, and the range and bearing measurements. This weight was computed using the following equation:

$$w_n^{(i)} = \frac{\overbrace{p(\mathbf{x}_{1:n}^{(i)} | \mathbf{z}_{1:n}, \mathbf{x}_{0:n-1}^{(i)}, \mathbf{u}_{0:n-1}, \mathbf{m}_{0:n-1}^{(i)})}^{\text{Likelihood of being the correct trajectory given all information}}}{\underbrace{\pi(\mathbf{x}_{1:n}^{(i)})}_{\text{The proposal distribution is the likelihood of choosing a sample}}}, \tag{2.26}$$

where $\pi(\mathbf{x}_d^{(i)})$ is known as the proposal distribution.

Once all weights were computed, a normalization of the weights is performed as follows:

$$\tilde{w}_n^{(i)} = \frac{w_n^{(i)}}{\sum_{i=1}^{N} w_n^{(i)}}. \tag{2.27}$$

The effective number of particles quantifies how well the weights were distributed in the particle set [91]. It indicates whether to perform resampling or to leave the particle set unchanged. Avoiding unnecessary resampling is essential to the performance of the algorithm, because resampling increases computational complexity. The following equation computes the effective number of particles:

$$N_{\text{eff}} = \frac{1}{\sum_{i=1}^{N} (\tilde{w}^{(i)})^2}, \tag{2.28}$$

where N is the number of particles, and $\tilde{w}^{(i)}$ is the normalized weight for each particle i. Note that $N_{\text{eff}} = N$ is equivalent to all the particles having equal weight, and $N_{\text{eff}} = 1$ corresponds to having the total weight in one particle.

Algorithm 1 summarizes the steps of a RBPF SLAM approach, and Figures 2.11, 2.12, and 2.13 illustrate the steps. In lines 1 to 4 of the algorithm, the odometry, and range and bearing measurement are gathered until it was considered a full scan using Equations (2.14) and (2.16). Each particle trajectory is then updated in a "for-loop" from lines 5 to 8. An improved trajectory is estimated through scan matching by optimizing Equation (2.20). Finally, an importance weight is given to each particle, as seen in Figure 2.11. The weight of each particle is determined by the likelihood of a scan being correct in relation to the map. Red circles mark the endpoints that have a higher weight. In Figure 2.11, particle number 2 would have the highest weight and particle number 1 would have the lowest. The new particle set is resampled by duplicating the particles with the highest weight. The probability of a particle being picked for the new set is proportional to the importance weight. For example, in Figure 2.12, particle number 2 is chosen twice, and particle number 3 is only chosen once. Lastly, the map is updated for each particle based on the previous map and scan, as shown in Figure 2.13. In this case, the particle's map changed from a bright to a dark color, illustrating an increase from low to high probability of being occupied.

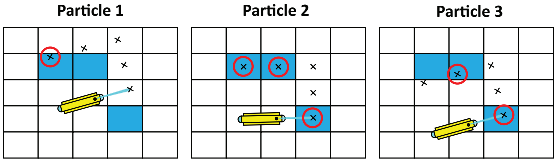

Figure 2.11: RBPF importance weighting with occupancy grid maps

Algorithm 1 Scan matching aided RBPF with occupancy grid maps

```
repeat
    Motion model sampling
    Gather range and bearing measurement
until scan is considered full
for each particle trajectory do
    Scan matching
    Importance weighting
end for
Resampling
Map estimation
```

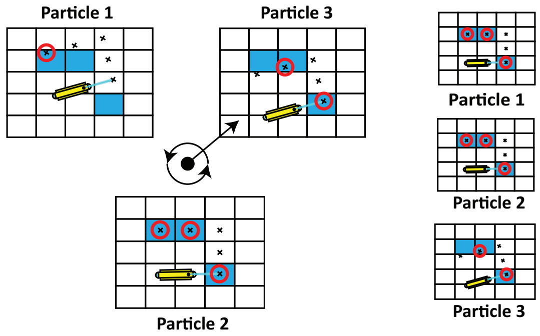

Figure 2.12: RBPF resampling

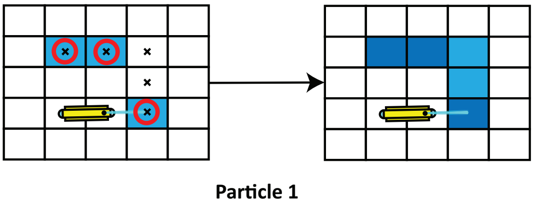

Figure 2.13: Map estimation

The RBPF is the most popular PF solution for online SLAM schemes, and was first suggested in [57] using known landmark associations. In order to use unknown data associations, a grid map representation was customized [30]. The computational complexity of the RBPF is $O(NW)$, where N is the number of particles, and W is the size of the map. The complexity comes from the fact that each particle has a map, and the RBPF requires copies of the map at each resampling step. However, by using adaptive resampling, many of the steps have a complexity of $O(N)$ instead, as adaptive resampling allows for skipping the resampling step.

Another RBPF solution for bathymetry, PF SLAM [4, 5], which uses Gaussian processes, was originally suggested in [96] in order to generate a prediction of the seafloor terrain. The Gaussian processes approach was considerably slower than PF SLAM with 2.5D grid maps [4]. 2.5D grid maps contain a 2D mesh of the seafloor, where each cell contains the estimate and variance of the seafloor depth at a point. Distributed particle SLAM is one possible representation for more memory-efficient storage of the states [25].

Chapter 3

Research Methods

This chapter reviews the research methods herein, where the methods' purpose is to measure the statistical accuracy of the algorithms. Similar to Chapter 2, it is divided into two sections: localization and mapping with exteroceptive acoustic sensors, and underwater localization with environmental acoustic sensors. There are three steps in the validation of the design of the algorithms. The first is statistical simulation of a sensor, vehicle, or an artificial environment. Multiple statistical simulations with averaged results known as Monte Carlo simulations, which is a reliable method determining the robustness of algorithm design. The second is through tank experiments, which allow for testing in a controlled environment. The third step is validation through field experiments.

3.1 Underwater Localization and Mapping with Exteroceptive Acoustics

This section reviews the experimental methods for confirming the accuracy and robustness of the localization and mapping algorithms when using exteroceptive acoustic sensors. The studies that used exteroceptive sensors are C3, J1, and J2. Article C3 used simulations of a vehicle using a dynamic model [28]. The dynamic model, in addition to Gaussian white noise, was used for the DVL, gyro, depth, and sonar measurements. The sonar measurements were the range from the vehicle to the wall of a square tank in the bearing direction. The second validation type was through experimental methods in a tank environment to check that the integration of the system worked in a controlled environment. Articles C3, J1, and J2 used an experimental dataset obtained at the University of Tokyo. Figure 3.1 shows the AUV Tri-Dog 1 and the tank environment. The vehicle took, similar to the simulations, DVL, gyro, depth, and sonar measurements. Also, because the ground truth position was not available, a shell was placed on the tank floor and observed through a camera on the AUV. In post-processing, an algorithm computed the location of the shell for each pass.

The last stage of validation was the field experiments. The author was not able to gather a field experiment in a fish cage. A dataset called the Abandoned Marina

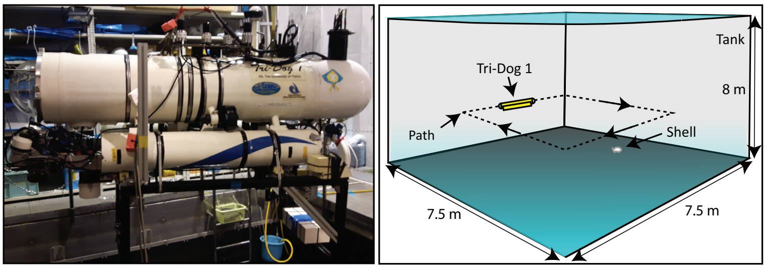

Figure 3.1: The hovering AUV Tri-Dog 1 developed at the University of Tokyo, and the setup of the tank experiment.

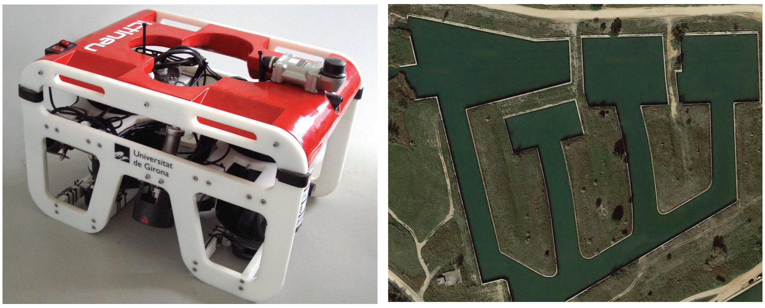

Figure 3.2: On the left: The ROV used for recording the Abandoned Marina Dataset. On the right: an overview of the abandoned marina, courtesy of [80] and Google Maps.

Dataset is frequently used in underwater SLAM articles [81, 61]. The dataset is similar to an aquaculture structure in the sense that it is closed. Figure 3.2 shows the ROV to the left, and a flight photo of the abandoned marina. In addition to gathering DVL, gyro, depth, and sonar measurements, GPS measurements contain actual positioning for algorithm validation.

3.2 Underwater Localization with Environmental Acoustics

The statistical simulation of underwater environmental acoustics is herein performed by calculating the exact ranges between the transponders/hydrophones and the true position of the object of interest, and then adding Gaussian noise. The algorithm design is then tested on the range measurements with noise to test the accuracy and robustness of the algorithm. This was performed in Articles C1, C4, and J3.

For tank experiments, an approach was demonstrated in C2, where an underwater motion capture system called Qualisys was used to track the motion of reflective markers that acted as the position of a transponder. Waves were created in the tank to make the transponders oscillate, as shown in Figure 3.3. The algorithm de-

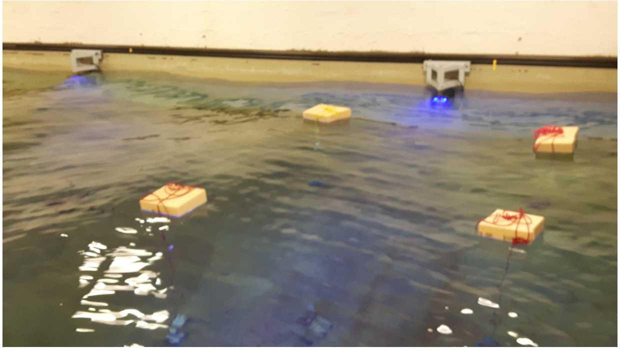

Figure 3.3: Experimental setup in the marine cybernetics lab

sign of interest could, after that, use the data in post-processing as input, instead of using the simulated data.

Further, a field experiment was performed in Article J3 using an array hydrophone at a dock. Figure 3.4a shows the setup of the experiment. The red dots are the hydrophones, where each has an identification number starting with the letter H. The receivers recorded the time of arrival of signals emitted from small tags located at a rope with an anchor, as seen in Figure 3.4b, located at the points noted in Cases 1 and 2. Each tag's signal contained an identification number and a depth measurement that was also recorded by the hydrophones. The validation of the position of the tags was done by distributing the tags along a line and measuring the location of the line at the surface with a DGPS.

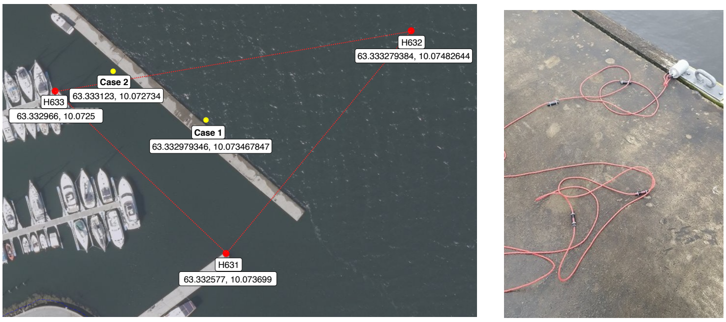
H632
63.333279384, 10.07482644
Case 2
63.333123, 10.072734
H633
63.332966, 10.0725
Case 1
63.332979346, 10.073467847
H631
63.332577, 10.073699

(a) Underwater mapping experiment

(b) Tags mounted on an anchor line

Figure 3.4: Acoustic tag experiment

Chapter 4

Summary of Research Results

This chapter presents a summary of the enclosed articles. The chapter is divided into four sections, where each section presents the novelty, methodology, and results of each topic. The articles are organized in the enumerated sections as follows:

1. Articles C3 and J1,
2. Article J2,
3. Articles C4 and J3, and,
4. Articles C1 and C2.

The reason for the divisions is to follow the ordering of research objectives presented in Section 1.4. Sections 4.1 and 4.2 address O1, Section 4.3 addresses objective O2, and Section 4.4 objective O3.

4.1 Underwater Simultaneous Localization and Mapping

This section summarizes Articles C3 and J1, which address research objective O1.

Problem Description and Novelty

These articles aim to develop underwater SLAM using acoustic exteroceptive sensors. The proposed method performs dead reckoning through a DVL, FOG, and pressure sensor. Figure 4.1 shows an illustration of the acoustic sensor setup of the vehicle, where (a) is the DVL, (b) is the MSIS, and (c) is the multibeam sonar. The contribution of Article C3 is to implement a known RBPF algorithm [30] with sonar measurement. Article J1 extends this by introducing a new likelihood sensor model that makes the SLAM method more robust when using sonar measurements. A loss function enhances the robustness of the likelihood model by dealing with measurement outliers. An outlier means that there is no information in the measurement due to an error, e.g., multipath in acoustic localization.

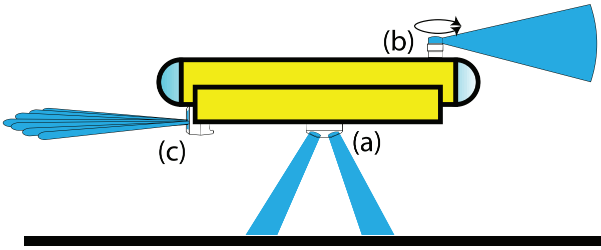

Figure 4.1: Sensor suite

Methodology

Articles C3 and J1 use a modification of the RBPF SLAM introduced by Grisetti [30], with occupancy grid maps for spatial representation, and a scan matching algorithm in order to improve the position estimates based on range and bearing measurements (Section 2.2.6). Article C3 presents an RBPF that uses MSIS range and bearing measurements. The challenge with using an MSIS is that there are outliers in the range measurements. An outlier located far away from the expected position leads to errors in the PF and the scan matcher. In the PF, it may result in more frequent resampling, faster deterioration of the particle set, and false matches in the scan matcher.

Article J1 extends Article C3 by introducing a Cauchy loss function (Section 2.2.5) to make the algorithm more robust to outliers. The following equation is the suggested sonar likelihood model, which includes the Cauchy loss function from (2.21):

$$p(\mathbf{z}_k|\mathbf{x}_k, \mathbf{m}_k) \propto \exp\left(-\frac{1}{2}\rho_{\text{cauchy}}\left(\frac{\Delta\theta_k^2}{\sigma_\theta^2} + \frac{\Delta r_k^2}{\sigma_r^2}\right)\right), \tag{4.1}$$

where Δr_k and $\Delta\theta_k$ are the difference in range and bearing between the closest occupied cell in the map, $\mathbf{m}_k$, and the measurement endpoint given by (2.16). σ_r and σ_θ model the white noise standard deviations of the range and bearing measurements. Both the PF measurement update in (2.11) and the scan matcher in (2.20) uses the a sonar model with the loss function. In the PF, the sonar model is used to compute the particle weight for each step k as following:

$$w_k^{(i)} \propto w_{k-m}^{(i)} \prod_{n=k-m}^{k} p(\mathbf{z}_n|T(\mathbf{x}_n^{(i)}, \boldsymbol{\xi}), \mathbf{m}_{k-m-1}), \tag{4.2}$$

where $T(\mathbf{x}_k^{(i)}, \boldsymbol{\xi})$ is the position found from scan matching, m is the number of range and bearing samples, and (i) is the particle number. Derivation is found in Article J1. The loss function lowers the rate of the effective number of particles and gives the scan matcher a more conservative estimate, preventing large jumps in the

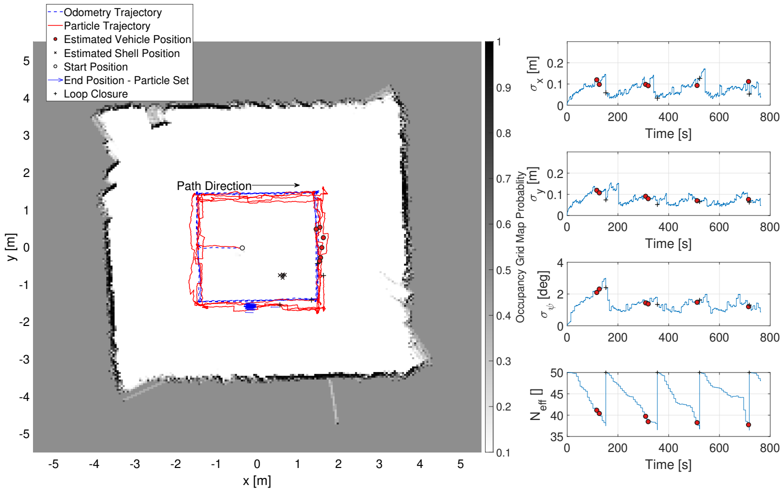

Figure 4.2: SLAM in tank using MSIS

estimates. Article J1 uses an occupancy grid map matcher instead of the ICP scan matcher, which was used in Article C3. The occupancy grid map matcher utilizes local maps within the maximum range of the sensor for increased computational speed. Tank experiments were used to validate the methods in both articles. Figure 3.1 shows Tri-Dog the to the left the vehicle [50], and to the right is an illustration of the tank experiment and the dimensions of the tank shown. Tri-Dog follows the path drawn and uses a shell as a reference through camera images. In Article J1 there were also field experiments from the Abandoned Marina Dataset [80]. Figure 3.2 shows the UUV used to the left, and an overview of the abandoned marina to the right.

Results

The experiments from the final results in Article J1 are shown in Figures 4.2 and 4.3. The former shows the tank occupancy grid map as a color map, and the estimated particle trajectory of the particle with the highest weight in the background. The arrows illustrate the particle set, where each arrow starts in the position of the particle, and the direction of the arrow shows the heading. The right plots, in Figure 4.2, present the covariance of each state in the particle set over time.

The left of the latter figure shows the abandoned marina occupancy grid map along with an overlay of the occupancy grid map with a bird's-eye view photo. The right plots in the figure present the particle set covariance and the effective number of particles. This article makes an important contribution as it enhances the robustness of UUV perception, and thereby introduces more robust information for planning, guidance, and control algorithms.

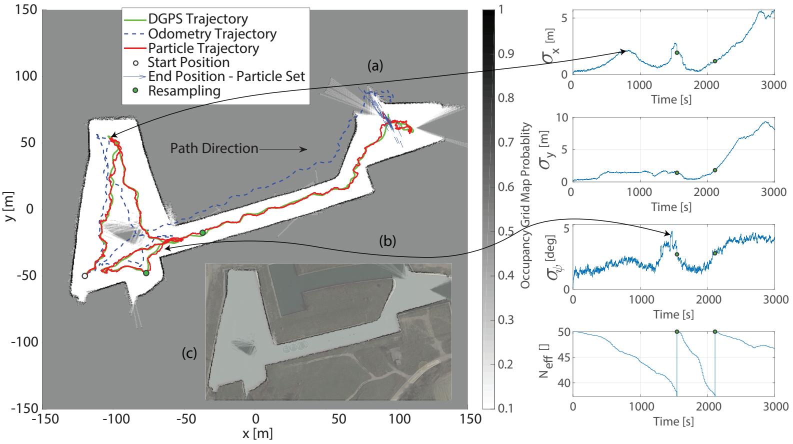

Figure 4.3: Results using the open Abandoned Marina dataset as a test case for the suggested method

4.2 Polar Map: A New Map Representation for Localization and Mapping in Fish Cage Structures

This section summarizes Article J2, which addresses research objective O1. This article presents a grid mapping scheme termed the polar map. It is applicable as a spatial representation in RBPFs. Article J1 is also related to this article.

Problem Description and Novelty

Figure 4.4 shows an illustration of a typical fish cage construction. It has a cylindrical-shaped bag at the top with a diameter and height of 30 m; the cone-shaped bottom has a dimension of approximately 15 m. In order for a UUV to autonomously inspect the construction, it would be beneficial to have a map representation of the fish cage in order to do online planning, guidance, and control. Such a representation would have memory, computational power, and resolution constraints, and must be able to represent the full 3D environment. The present study is restricted to looking at grid map representations, which are one of the most popular representations in robotics. Currently, there is multiple map representation in robotics. Section 2.2.3 presented the most common, namely the 3D occupancy grid map, the octree representation, and the 2.5D terrain map; however, this article presents a new representation that has some beneficial properties in online mapping in enclosed environments.

Methodology

The present study was inspired by the 2.5D mapping solution in [4] for terrain-based SLAM in RBPF, meaning localization and mapping based on the seafloor terrain.

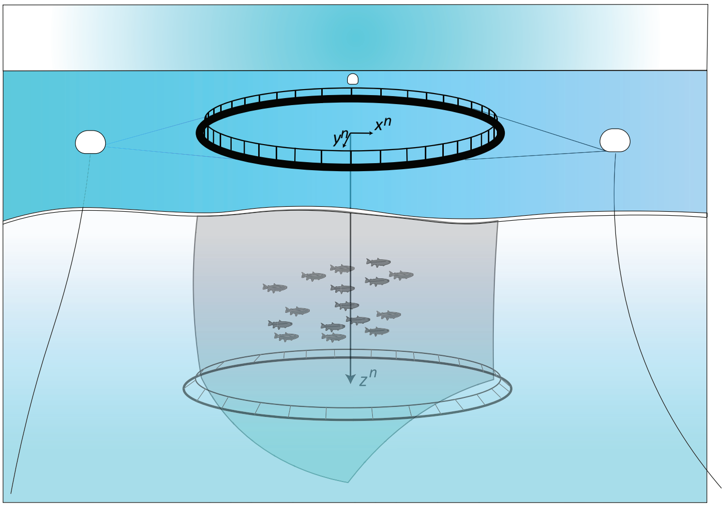

Figure 4.4: Illustration of a typical fish cage

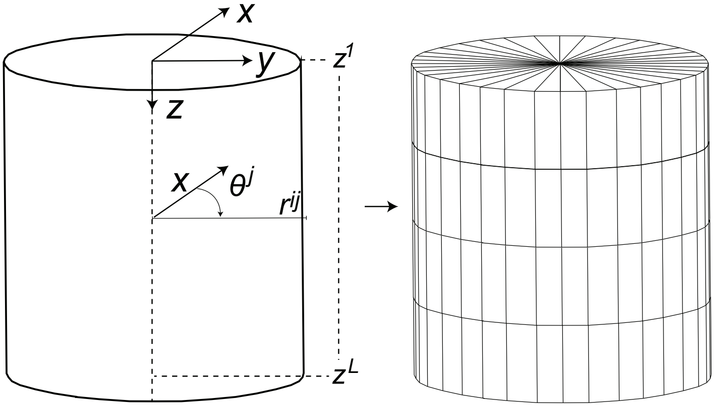

Figure 4.5: Section-wise discretization of a solid cylinder by angle, θ, and depth, z. The range r is the variable that describes the edge of the cylinder for each section.

The 2.5D terrain map, presented in Section 2.2.3, is memory and computationally efficient, as it represents a 3D environment on a projected surface in the x-y plane; however, the representation is not applicable to vertical and enclosed environments. Figure 4.5 shows the concept of the suggested map representation. Sections from a centerline represent the enclosed 3D environment where each section is divided by planes on the z-axis and angles, θ, similar to cylindrical coordinates. The range r for each section gives the outer surface of the enclosed environment.

Figure 4.6 shows how probability is incorporated into the polar map. A Gaussian distribution represents the range of each section with an estimated mean $\hat{r}$, a variance $\hat{P}$, and the indices i and j gives the angle and depth of each section. Fur-

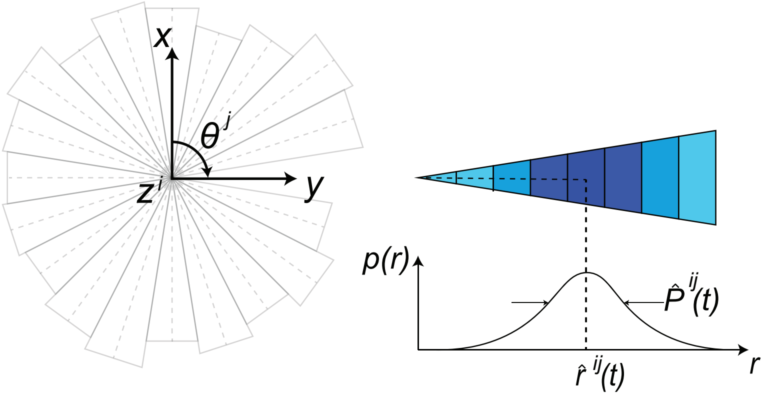

Figure 4.6: Top view of the discretized structure (left) and the uncertainty model of a single section (right) in the 2.5D polar map representation

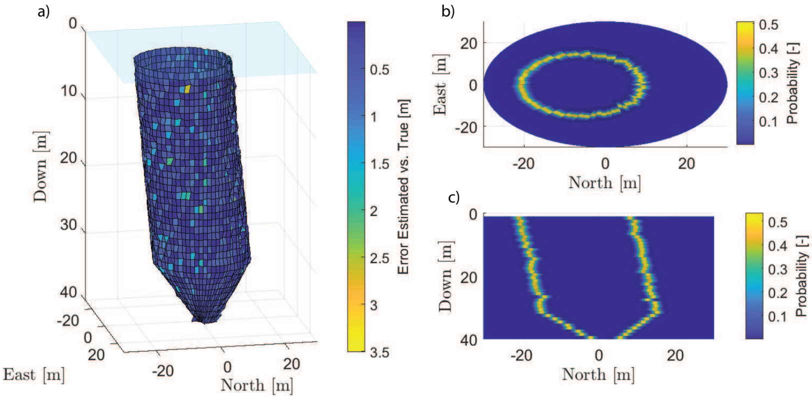

Figure 4.7: 2.5D Polar map representation of a fish cage

thermore, each section is assumed to be independent, and a Kalman filter updates the ranges.

Results

Simulations were carried out to validate the method for mapping with known locations, and tank experiments with the UUV Tri-Dog were used to validate the map for use in SLAM. Figure 4.7 shows a polar map of a fish cage. The mapping scheme uses simulated range measurements to update the polar map. To the left, the figure shows the mean ranges for each section, and the color map represents the distance from the true range. To the right, the figure shows the cross-section of the probability distributions of each section in a top and side view.

Figure 4.8 shows the results of using a polar map in the underwater SLAM approach. The tank environment is the same as that used in Article J1. Comparing

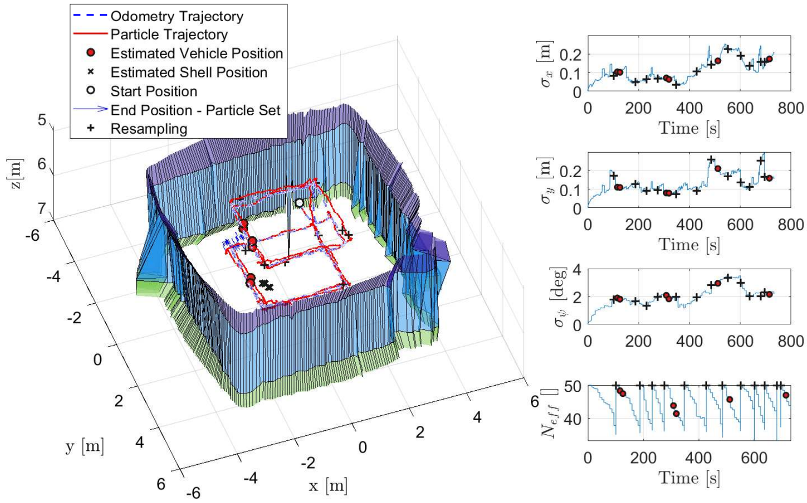

Figure 4.8: PF-based SLAM in tank using polar map

the results of using a polar map versus an octomap in RBPF SLAM, it is clear that the polar map has a lower run time. The main reason is that each particle in the RBPF contains a map, which needs to be copied for each resampling procedure. Because the polar map needs less memory than the other representations, it is easier to copy. The computational complexity of the copy operation increase with memory size.

4.3 Underwater Mapping Using Multiple Acoustic Tags

This section summarizes the results from Articles C4 and J3, which address research objective O2. These articles aim to develop an underwater mapping method for a flexible structure using environmental acoustic sensors. Field experiments with an anchor line were used to validate the suggested procedure.

Problem Description and Novelty

The problem of inspecting underwater equipment in sea-based aquaculture is that the equipment is not always rigid and mounted in one place. The objective of these articles was to use multiple acoustic transmitters or tags [87] and hydrophones [88]. The tags transmitted their respective identification number and depth measurement to the hydrophone receivers through acoustic communication. The procedure needed to compute the positions from the tag information and the TDOA between the hydrophones. Using the tag identification number, a probabilistic interpolation between the positing of each tag gave the map of the structure. This map could serve as a tool for robotic vehicles that seek to plan and execute operations autonomously within and around the structure, or as a visualization tool for human operators.

Methodology

Article C4 presents a conceptual design study, where filters fused the hyperbolic localization and depth information for each tag. The filters used were an EKF [11] and a PF, as presented in Sections 2.1.3 and 2.1.3. They used the equations for hyperbolic localization and depth measurement given in Section 2.1.1. Article C4 suggested a probabilistic parameterized interpolation $\mathbf{v}(t)$, between each point $\mathbf{x} = \begin{bmatrix} \hat{\mathbf{q}}^{\mathrm{ID}_1 T} & \hat{\mathbf{q}}^{\mathrm{ID}_2 T} \end{bmatrix}^T$, where $\mathbf{q} \in \mathbb{R}^3$ is the location of each tag. The parameterization is defined as:

$$\mathbf{v}(t) = A(t)\mathbf{x}, \tag{4.3}$$

where $A(t)$ and $\boldsymbol{x}$ are given as:

$$A(t) = \begin{bmatrix} (1-t) & 0 & 0 & t & 0 & 0 \\ 0 & (1-t) & 0 & 0 & t & 0 \\ 0 & 0 & (1-t) & 0 & 0 & t \end{bmatrix}. \tag{4.4}$$

The function $\mathbf{v}(t)$ has the covariance matrix:

$$\Gamma_{xyz}(t) = \mathrm{covar}(\mathbf{v}_{xyz}(t)) = A(t)\Sigma_{xyz}A(t)^T \in \mathbb{R}^{3\times 3}. \tag{4.5}$$

The uncertainties estimated by the filter can also be interpolated for the two tags and can be found as:

$$\Sigma_{xyz} = \begin{bmatrix} \hat{P}^{\mathrm{ID}_1} & 0 \\ 0 & \hat{P}^{\mathrm{ID}_2} \end{bmatrix} \in \mathbb{R}^{6\times 6}. \tag{4.6}$$

Article C4 validated the method through simulations and inserted the interpolation into the Octomap software. Article J2 extended the previous article by also using a PF, as described in Section 2.1.3, and compared the results from the EKF in the previous article. A DOP analysis was also performed, which used the geometry of the hydrophones and the depth measurement to find the Cramer lower bound, as presented in Section 2.1.2. Figure 3.4 shows two pictures from the acoustic experiments. Figure 3.4a shows the location of the hydrophone and an anchor line, and Figure 3.4b shows the anchor line with the tags mounted.

Results

Figure 4.9 show two time series with RMSE for position estimation using the PF and EKF in the field experiments. It can be seen that the PF has a lower RMSE than the EKF for the lower case. The reason for this is that the DOP of the second case is worse due to the initial position of tag ID 32, and the EKF, therefore, needs more time to converge. A visualization of the interpolated anchor line is shown in Figure 4.10.

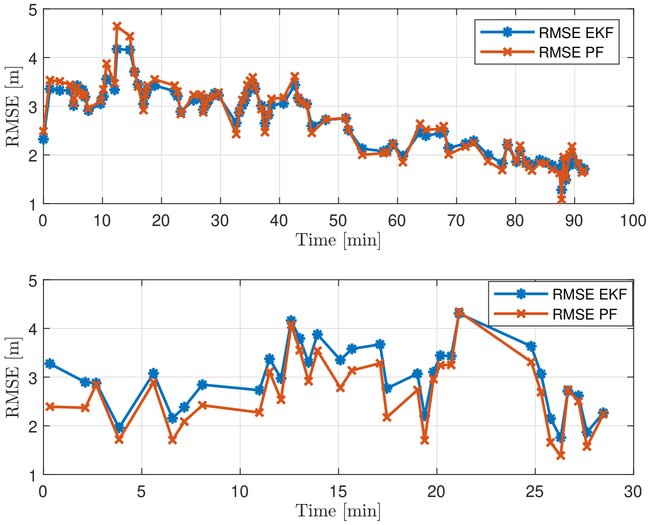

Figure 4.9: Time-series for RMSE of tag ID 32 with the EKF and PF for Case Studies 1 (top subplot) and 2 (bottom subplot). The blue line is the RMSE for the PF, the red line for the EKF.

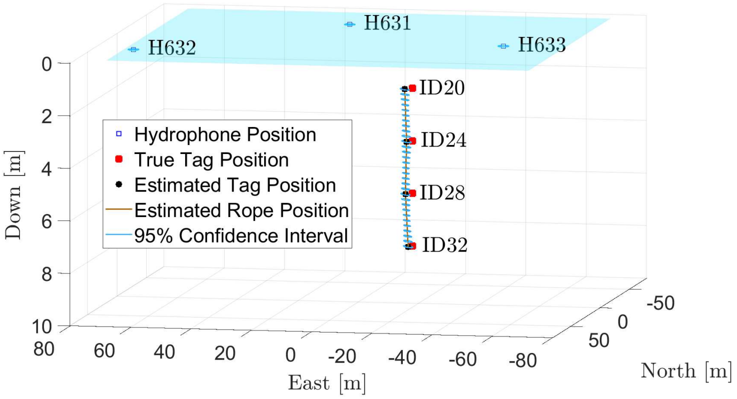

Figure 4.10: Visualization of the interpolated anchor line from Article J1

4.4 Positioning Error Correction for Ocean Wave Induces Long Baseline Navigation System

This section summarizes the research presented in conference Articles C1 and C2. The aim is to estimate a UUV positioning based on an LBL network exposed to wave motion, which addresses research objective O3.

Problem Description and Novelty

These articles aim to estimate a UUV positioning based on an LBL network exposed to wave motion. The wave motion occurs when acoustic transponders are mounted near the sea surface, which is typically done for convenience in aquaculture. The positioning concept used is circular positioning or TOF, as explained in Section 2.1.1. The problem identified in Article C1 is that the transponder position varies periodically with time, which means that the assumed known location of each transponder, $\mathbf{p}_i$, from (2.1) has an unknown periodical error, which gives a time-varying error in the final UUV position estimate. The article aims to find a method that removes this time-varying error in the UUV position estimate. Article C2 extends C1 by including a suggestion for wave spectrum analysis using the transponder position time series.

Methodology

Article C1 proposes a solution that simplifies the UUV position into two parts: the position dynamics and the error dynamics. The position dynamics slowly vary and depend on a random walk process or the UUV dynamics, and a second-order wave model represents the wave error dynamics [2, 28]. The idea behind the wave model is to be able to estimate the error motion from the waves. The wave model assumes that the wave spectrum of ocean waves is known or estimated beforehand. The two parts are then merged in an EKF, as presented in Section 2.1.3 for the general case,

RMSE	$x[m]$	$y[m]$	$z[m]$
Uncompensated	0.0292	0.0281	0.03366
Compensated	0.0062	0.0167	0.0076
Decrease in RMSE	78.8%	40.5%	77.4%

Table 4.1: RMSE for uncompensated versus compensated

along with the TOF measurement equation. Inspired by Bancroft [3], Article C2 extends the work by introducing a method that algebraically computes the UUV position error dynamics. With the algebraic computations, the UUV position error can be extracted from a time series of transponder position measurements. A fast Fourier transform analysis determines the spectrum of the error dynamics from the position error.

Results

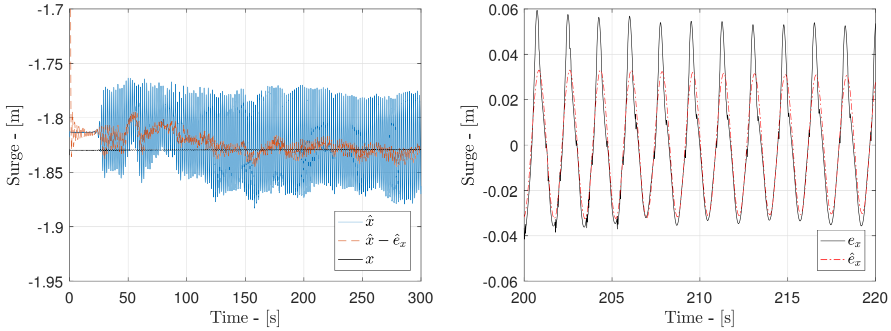

(a) Estimated position in x direction.

(b) Surge error estimated.

Figure 4.11: Estimated states with EKF in x direction

The experiments presented in Article C2 showed that a considerable amount of the error is separate from the wave motion, as seen in Figure 4.11, where the position and error dynamics are separated. Moreover, in the x-direction facing wave direction, there was a 78.4 % decrease in RMSE, as seen in Table 4.1. Figure 4.11a shows the estimated position dynamics with, $\hat{\mathbf{x}} - \hat{\mathbf{e}}$, and without, $\hat{\mathbf{x}}$, compensation in correspondence to the true position, $\mathbf{x}$. Furthermore, Figure 4.11b presents the estimated error dynamics, $\hat{\mathbf{e}}$, versus the true $\mathbf{e}$. Even though there is a large correction, there are still a position error. This is a result of the fact that the error dynamics model does not capture all the nonlinearities of the problem.

Chapter 5

Conclusions and Further Work

Section 1.4 presented three research objectives. This chapter concludes how the work meets the objectives. The last section discusses further work.

5.1 Conclusions

The main topic of this thesis is localization and mapping using acoustic sensors in an underwater aquaculture environment for a UUV. Specifically, the challenges related to perception, meaning how sensory information is processed and represented for decision-making, planning, guidance, and control as required by an underwater inspection operation. The reason for using acoustics is that the electromagnetic sensors are less reliant in a turbid underwater environment, which is the case in aquaculture environments.

Research objective O1 was to develop a SLAM algorithm for UUVs using acoustic exteroceptive sensors in an aquaculture environment. This was mainly addressed in articles J1 and J2. The former presented a PF-based SLAM solution using exteroceptive measurements from a sonar for underwater vehicles in an enclosed environment. The filter design compensated for a high number of outliers and low resolution in sonar measurements by using a novel sonar likelihood model. Furthermore, the efficiency was improved using a sonar update scheme that only utilized map information close to the vehicle. However, the map representation in Article J1 represented a 2D environment, and therefore a suggested 3D map representation termed polar map that was suitable for a 3D aquaculture environment was presented in Article J2. The representation was implemented with the SLAM algorithm in Article J1, and compared with the map representation named octomap. The polar map consumed significantly less memory and required minimal computational effort compared with octomap, meaning that it enabled a large number of sensor readings and could still be used on low-cost computer/circuit boards. The efficiency was beneficial to the methods implemented in a UUV due to its limited space and communication without an umbilical, which called for more memory and computationally efficient methods. The aquaculture environment is also a challenge due to flexible cages, although more rigid constructions are coming to the market.

The fish cages deform in ocean currents, and waves and make the environment unpredictable, and thus an a priori map cannot be used in a UUV planning algorithm. To conclude, the suggested SLAM algorithm and the map representation meet the first research objective of this thesis by suggesting a possible solution for localization and mapping in an aquaculture environment using sonar.

Research objective O2 was to use environmental sensors to generate a probabilistic map of an aquaculture structure. The main work was addressed in Article J3, and presented a novel method for localizing and mapping a submerged anchor line by using acoustic tags and hydrophones. The suggested method was proven through field experiments using both an EKF and a PF, and was shown to have an RMSE of 2–3 m. The work showed that the PF outperformed the EKF in areas with high DOP. The suggested map can be used for operations with underwater vehicles for an enhanced operator or robot perception, or solely for structure monitoring purposes, thereby fulfilling the second objective.

Research objective O3 was to develop an algorithm that reduced localization error when using surface mounted transponder networks. The challenge in using surface mounted networks is that waves induce motion in the transponders, which results in an oscillating position estimation error. Articles C1 and C2 met the research objective by suggesting an EKF that filtered the oscillation by using a wave filter model. Article C2 also suggested a solution for determining the parameters of the wave model. Tank experiments validated the EKF design, and the oscillating error showed an almost 80% decrease in RMSE compared with not using the wave filter.

Thus, to conclude, this thesis has addressed some challenges and solutions for more human-independent UUVs and is, therefore, a step toward autonomous operations in aquaculture. The methods presented may help to build a foundation for planning, guidance, and control algorithms, as well as to enhance the accuracy of localization and mapping during an underwater inspection of an aquaculture environment using a UUV.

5.2 Further Work

As with most work, there is always needed some further investigation or improvement to be performed. For the first research objective, there are still questions related to how well sonar sensors will perform in a fish cage, how much the fish will influence the blocking of the sensor signal, and if the methods presented are able to handle them, or if adjustments are needed in the SLAM method. Difficulties with waves and currents are especially important to consider. For the suggested map representation, a possible improvement is the integration of a Gauss-Markov process model instead of a random walk. A Gauss-Markov model can improve the temporal modeling of a fish cage substantially. Firstly, it does not have a range uncertainty that increase towards infinity, but instead reaches an upper limit. Secondly, the Gauss Markov model can configure the range for each section to be aligned with the expected range, and the range will always tend towards that mean.

Computational speed and memory capacity in computers increase possibilities in the future, and there is also continuous improvement in acoustic sensor technology. For instance, new 3D sonar were presented in [1] and new lens-based sonars with high resolutions are also a important topic that should be further investigated.

This thesis have a limited view on localization and mapping, and there is a multitude of other approaches to investigate in fish cage inspection, for instance, graph-based SLAM [31] and semantic mapping of the environment.

For the second research objective, the most apparent point is the use of the mapping apporach in a fish cage, instead of anchor line. The approach could be integrated to create an initial map of the system and therefore it can be tested along with UUV inspection.

References

[1] R. Adams. Echoscope 4g , surface the future of visualization, mapping sonars. *Sea Technology*, 59(6):10–13, 2018.

[2] J. G. Balchen, N. A. Jenssen, and S. Saelid. Dynamic positioning using kalman filtering and optimal control theory. In *IFAC/IFIP symposium on automation in offshore oil field operation*, volume 183, page 186, 1976.

[3] S. Bancroft. An algebraic solution of the gps equations. *IEEE Transactions on Aerospace and Electronic Systems*, AES-21(1):56–59, 1985. ISSN 0018-9251. doi: 10.1109/TAES.1985.310538.

[4] S. Barkby, S. B. Williams, O. Pizarro, and M. V. Jakuba. A featureless approach to efficient bathymetric slam using distributed particle mapping. *Journal of Field Robotics*, 28(1):19–39, 2011. doi: 10.1002/rob.20382.

[5] S. Barkby, S. B. Williams, O. Pizarro, and M. V. Jakuba. Bathymetric particle filter slam using trajectory maps. *The International Journal of Robotics Research*, 31(12):1409–1430, 2012. ISSN 0278-3649. doi: 10.1177/0278364912459666.

[6] E. Belcher, W. Hanot, and J. Burch. Dual-frequency identification sonar (didson). In *Proceedings of the 2002 Interntional Symposium on Underwater Technology (Cat. No.02EX556)*, pages 187–192, 2002. doi: 10.1109/UT.2002.1002424.

[7] P. J. Besl and N. D. McKay. Method for registration of 3-d shapes. In *Robotics '91*, volume 1611, page 21. SPIE, 1992.

[8] P. J. Besl and N. D. McKay. Method for registration of 3-d shapes. In *Robotics '91*, volume 1611, page 21. SPIE, 1992.

[9] P. Biber and W. Straßer. The normal distributions transform: A new approach to laser scan matching. In *Intelligent Robots and Systems, 2003.(IROS 2003). Proceedings. 2003 IEEE/RSJ International Conference on*, volume 3, pages 2743–2748. IEEE, 2003. ISBN 0780378601.

[10] H. V. Bjelland and et.al. Exposed aquaculture in norway. In *OCEANS 2015 - MTS/IEEE Washington*, pages 1–10, 2015. doi: 10.23919/OCEANS.2015.7404486.

[11] R. G. Brown and P. Y. C. Hwang. *Introduction to Random Signals and Applied Kalman Filtering with Matlab Exercises, 4th Edition.* Introduction to random signals and applied Kalman filtering. John Wiley and Sons, 2012. ISBN 0-470-60969-9.

[12] C. Cadena, L. Carlone, H. Carrillo, Y. Latif, D. Scaramuzza, J. Neira, I. Reid, and J. J. Leonard. Past, present, and future of simultaneous localization and mapping: Toward the robust-perception age. *IEEE Transactions on Robotics*, 32(6):1309–1332, 2016. ISSN 1552-3098. doi: 10.1109/TRO.2016.2624754.

[13] V. Chalkiadakis, N. Papandroulakis, G. Livanos, K. Moirogiorgou, G. Giakos, and M. Zervakis. Designing a small-sized autonomous underwater vehicle architecture for regular periodic fish-cage net inspection. In *2017 IEEE International Conference on Imaging Systems and Techniques (IST)*, pages 1–6, 2017. doi: 10.1109/IST.2017.8261525.

[14] C.-T. Chen. *Linear system theory and design.* The Oxford series in electrical and computer engineering. Oxford University Press, New York, fourth edition. edition, 2013. ISBN 9780199959570 (hardback acid-free paper).

[15] H. M. Choset, S. Hutchinson, K. M. Lynch, G. Kantor, W. Burgard, L. E. Kavraki, and S. Thrun. *Principles of robot motion: theory, algorithms, and implementation.* MIT press, 2005. ISBN 0262033275.

[16] R. D. Christ and R. L. Wernli Sr. *The ROV manual: a user guide for remotely operated vehicles.* Butterworth-Heinemann, 2013.

[17] C. C. Constantinou, S. G. Loizou, and G. P. Georgiades. An underwater laser vision system for relative 3-d posture estimation to mesh-like targets. In *2016 IEEE/RSJ International Conference on Intelligent Robots and Systems (IROS)*, pages 2036–2041, 2016. doi: 10.1109/IROS.2016.7759320.

[18] T. H. Cormen. *Introduction to algorithms.* MIT press, 2009. ISBN 0262533057.

[19] E. W. Dijkstra. A note on two problems in connexion with graphs. *Numerische Mathematik*, 1(1):269–271, 1959. ISSN 0945-3245. doi: 10.1007/bf01386390. URL `https://doi.org/10.1007/BF01386390`.

[20] N. F. Directorate. Antall lokaliteter i 2018 av laks, regnbueoerret og oerret (number of locations in 2018 of salmon and trout; in norwegian), 2018. URL `https://www.fiskeridir.no/content/download/7613/95478/version/30/file/sta-laks-mat-02-lokaliteter.xlsx`. Accessed: 2019-05-02.

[21] Directorate of Fisheries. Escape statistics, 2019. URL `https://www.fiskeridir.no/Akvakultur/Statistikk-akvakultur/Roemmingsstatistikk`.

[22] A. Doucet and A. M. Johansen. A tutorial on particle filtering and smoothing: Fifteen years later. *Handbook of nonlinear filtering*, 12(656-704):3, 2009.

[23] A. Doucet, N. d. Freitas, K. P. Murphy, and S. J. Russell. Rao-blackwellised particle filtering for dynamic bayesian networks. In *Proceedings of the 16th Conference on Uncertainty in Artificial Intelligence*, pages 176–183, 720075, 2000. Morgan Kaufmann Publishers Inc.

[24] A. Elfes. Sonar-based real-world mapping and navigation. *IEEE Journal on Robotics and Automation*, 3(3):249–265, 1987. ISSN 0882-4967. doi: 10.1109/JRA.1987.1087096.

[25] A. Eliazar and R. Parr. Dp-slam: Fast, robust simultaneous localization and mapping without predetermined landmarks. In *IJCAI International Joint Conference on Artificial Intelligence*, pages 1135–1142, 2003.

[26] N. Fairfield, G. Kantor, and D. Wettergreen. Real-time slam with octree evidence grids for exploration in underwater tunnels. *Journal of Field Robotics*, 24(1-2):03–21, 2007. ISSN 1556-4967. doi: 10.1002/rob.20165.

[27] J. Farrell. *Aided Navigation: GPS with High Rate Sensors.* McGraw-Hill Education, 2008. ISBN 9780071642668. URL `https://books.google.no/books?id=yNujEvIMszYC`.

[28] T. I. Fossen. *Handbook of Marine Craft Hydrodynamics and Motion Control.* New York: John Wiley & Sons, 2011.

[29] K. Gade. The seven ways to find heading. *Journal of Navigation*, 69(5): 955–970, 2016. doi: 10.1017/S0373463316000096.

[30] G. Grisetti, C. Stachniss, and W. Burgard. Improved techniques for grid mapping with rao-blackwellized particle filters. *IEEE Transactions on Robotics*, 23(1):34–46, 2007. ISSN 1552-3098. doi: 10.1109/TRO.2006.889486.

[31] G. Grisetti, R. Kummerle, C. Stachniss, and W. Burgard. A tutorial on graph-based slam. *IEEE Intelligent Transportation Systems Magazine*, 2(4):31–43, 2010. ISSN 1939-1390. doi: 10.1109/MITS.2010.939925.

[32] P. D. Groves. *Principles of GNSS, inertial, and multi-sensor integrated navigation systems.* Artech House, Boston/ London, 2008. ISBN 9781580532556.

[33] F. Gustafsson. *Statistical sensor fusion.* Studentlitteratur, Lund, 2nd ed. edition, 2012. ISBN 9144077327.

[34] F. Gustafsson and F. Gunnarsson. Positioning using time-difference of arrival measurements. In *2003 IEEE International Conference on Acoustics, Speech, and Signal Processing, 2003. Proceedings. (ICASSP '03).*, volume 6, pages VI–553, 2012. ISBN 1520-6149. doi: 10.1109/ICASSP.2003.1201741.

[35] P. E. Hart, N. J. Nilsson, and B. Raphael. A formal basis for the heuristic determination of minimum cost paths. *IEEE Transactions on Systems Science and Cybernetics*, 4(2):100–107, 1968. ISSN 0536-1567. doi: 10.1109/TSSC.1968.300136.

[36] A. D. Hawkins and A. D. F. Johnstone. The hearing of the atlantic salmon, salmo salar. *Journal of Fish Biology*, 13(6):655–673, 12 1978. ISSN 1095-8649. doi: 10.1111/j.1095-8649.1978.tb03480.x.

[37] O. Hegrenæs and E. Berglund. Doppler water-track aided inertial navigation for autonomous underwater vehicle. In *OCEANS 2009-EUROPE*, pages 1–10. IEEE, 2009. doi: 10.1109/OCEANSE.2009.5278307.

[38] E. Hernández Bes, P. Ridao Rodríguez, D. Ribas Romagos, and J. Batlle i Grabulosa. Msispic: A probabilistic scan matching algorithm using a mechanical scanned imaging sonar. *Journal of physical agents, 2009, vol. 3, núm. 1, p. 3-11*, 2009. ISSN 1888-0258.

[39] S. M. Holen, I. B. Utne, I. M. Holmen, and H. Aasjord. Occupational safety in aquaculture – part 1: Injuries in norway. *Marine Policy*, 96:184–192, 2018. ISSN 0308597X. doi: 10.1016/j.marpol.2017.08.009.

[40] A. Hornung, K. M. Wurm, M. Bennewitz, C. Stachniss, and W. Burgard. Octomap: an efficient probabilistic 3d mapping framework based on octrees. *Autonomous Robots*, 34(3):189–206, 2013. ISSN 1573-7527. doi: 10.1007/s10514-012-9321-0.

[41] J. M. Hovem. *Marine acoustics : the physics of sound in underwater environments.* Peninsula Publishing, Los Altos Hills, Calif, 2012. ISBN 9780932146656.

[42] F. S. Hover, R. M. Eustice, A. Kim, B. Englot, H. Johannsson, M. Kaess, and J. J. Leonard. Advanced perception, navigation and planning for autonomous in-water ship hull inspection. *The International Journal of Robotics Research*, 31(12):1445–1464, 2012. ISSN 0278-3649. doi: 10.1177/0278364912461059.

[43] IMAGENEX. 837b delta t 1000 m profiling, 2018. Available at: `https://imagenex.com/products/\837b-delta-t-1000-m-profiling` (Accessed: 2018-10-19).

[44] Ø. Jensen, T. Dempster, E. Thorstad, I. Uglem, and A. Fredheim. Escapes of fishes from norwegian sea-cage aquaculture: causes, consequences and prevention. *Aquaculture Environment Interactions*, 1(1):71–83, 2010. doi: 10.3354/aei00008.

[45] S. J. Julier and J. K. Uhlmann. *New extension of the Kalman filter to nonlinear systems*, volume 3068 of *AeroSense '97*. SPIE, 1997. URL `https://doi.org/10.1117/12.280797`.

[46] R. E. Kalman. A new approch to linear filtering and prediction problems. *Journal of Basic Engineering JBE-83*, page 7, 1960.

[47] S. Kay. *Fundamentals of Statistical Signal Processing: Estimation theory*. PTR Prentice-Hall, 1993. ISBN 0133457117.

[48] H. K. Khalil. *Nonlinear systems*. Perntice-Hall. inc., New York, third edition international edition, 1996. ISBN 002363541X.

[49] S. Kohlbrecher, O. von Stryk, J. Meyer, and U. Klingauf. A flexible and scalable slam system with full 3d motion estimation. In *2011 IEEE International Symposium on Safety, Security, and Rescue Robotics*, pages 155–160, Nov 2011. doi: 10.1109/SSRR.2011.6106777.

[50] H. Kondo. Development of an autonomous underwater vehicle "tri-dog" toward practical use in shallow water. *Journal of Robotics and Mechatronics*, 13(2):205–211, 2001.

[51] P. F. Lader and B. Enerhaug. Experimental investigation of forces and geometry of a net cage in uniform flow. *IEEE Journal of Oceanic Engineering*, 30 (1):79–84, 2005. ISSN 0364-9059. doi: 10.1109/joe.2004.841390.

[52] P. F. Lader and A. Fredheim. Dynamic properties of a flexible net sheet in waves and current—a numerical approach. *Aquacultural Engineering*, 35(3): 228–238, 2006. ISSN 01448609. doi: 10.1016/j.aquaeng.2006.02.002.

[53] S. M. LaValle. *Planning algorithms*. Cambridge university press, 2006. ISBN 1139455176.

[54] A. M. Lekkas, R. D. Andreas, M. Breivik, and T. I. Fossen. Continuous-curvature path generation using fermat's spiral. *Modeling, Identification and Control*, 34(4):183–198, 2013. URL `https://search.proquest.com/docview/1655566977?accountid=12870`. Copyright - Copyright Norsk Forening for Automatisering (NFA) 2013; Last updated - 2015-02-19.

[55] J. J. Leonard and H. F. Durrant-Whyte. Mobile robot localization by tracking geometric beacons. *IEEE Transactions on Robotics and Automation*, 7(3): 376–382, 1991. ISSN 1042-296X. doi: 10.1109/70.88147.

[56] J. J. Leonard and H. F. Durrant-Whyte. Simultaneous map building and localization for an autonomous mobile robot. In *Intelligent Robots and Systems '91. 'Intelligence for Mechanical Systems, Proceedings IROS '91. IEEE/RSJ International Workshop on*, pages 1442–1447 vol.3, 1991. doi: 10.1109/IROS.1991.174711.

[57] J. J. Leonard and H. F. Durrant-Whyte. Mobile robot localization by tracking geometric beacons. *IEEE Transactions on Robotics and Automation*, 7(3): 376–382, 1991. ISSN 1042-296X. doi: 10.1109/70.88147.

[58] K. Levenberg. A method for the solution of certain non-linear problems in least squares. *Quarterly of applied mathematics*, 2(2):164–168, 1944. ISSN 0033-569X.

[59] J. Li, M. Kaess, R. Eustice, and M. Johnson-Roberson. Pose-graph slam using forward-looking sonar. *IEEE Robotics and Automation Letters*, PP(99):1–1, 2018. doi: 10.1109/LRA.2018.2809510.

[60] G. Livanos, M. Zervakis, V. Chalkiadakis, K. Moirogiorgou, G. Giakos, and N. Papandroulakis. Intelligent navigation and control of a prototype autonomous underwater vehicle for automated inspection of aquaculture net pen cages. In *2018 IEEE International Conference on Imaging Systems and Techniques (IST)*, pages 1–6. ISBN 1558-2809. doi: 10.1109/IST.2018.8577180.

[61] A. Mallios, P. Ridao, D. Ribas, and E. Hernández. Scan matching slam in underwater environments. *Autonomous Robots*, 36(3):181–198, 2014. ISSN 1573-7527. doi: 10.1007/s10514-013-9345-0.

[62] D. W. Marquardt. An algorithm for least-squares estimation of nonlinear parameters. *Journal of the society for Industrial and Applied Mathematics*, 11 (2):431–441, 1963. ISSN 0368-4245.

[63] T. Matsuda, T. Maki, Y. Sato, T. Sakamaki, and T. Ura. Alternating landmark navigation of multiple auvs for wide seafloor survey: Field experiment and performance verification. *Journal of Field Robotics*, pages n/a–n/a, 2017. ISSN 1556-4967. doi: 10.1002/rob.21742. URL `http://dx.doi.org/10.1002/rob.21742`.

[64] J. Melo and A. Matos. Survey on advances on terrain based navigation for autonomous underwater vehicles. *Ocean Engineering*, 139:250–264, 2017. ISSN 0029-8018. doi: 10.1016/j.oceaneng.2017.04.047.

[65] L. Montesano, J. Minguez, and L. Montano. Probabilistic scan matching for motion estimation in unstructured environments. In *2005 IEEE/RSJ International Conference on Intelligent Robots and Systems*, pages 3499–3504, 2005. doi: 10.1109/IROS.2005.1545182.

[66] G. E. Moore. Cramming more components onto integrated circuits, reprinted from electronics, volume 38, number 8, april 19, 1965, pp.114 ff. *IEEE Solid-State Circuits Society Newsletter*, 11(3):33–35, 2006. ISSN 1098-4232. doi: 10.1109/N-SSC.2006.4785860.

[67] H. P. Moravec. Sensor fusion in certainty grids for mobile robots. *AI magazine*, 9(2):61, 1988. ISSN 0738-4602.

[68] T. Muir, R. W. Toland, T. J. Lemerande, S. H. Ridgway, and S. R. Baker. Experimental evidence for ultra-high frequencies in dolphin sonar signals. In *OCEANS 2017 - Anchorage*, pages 1–6.

[69] T. Nakatani, T. Ura, T. Sakamaki, and J. Kojima. Terrain based localization for pinpoint observation of deep seafloors. In *OCEANS 2009-EUROPE*, pages 1–6. doi: 10.1109/OCEANSE.2009.5278194.

[70] J. Nocedal and S. Wright. *Numerical optimization.* Springer Science and Business Media, 2006. ISBN 0387400656.

[71] S. Norway. Ns 9415.e:2009: Marine fish farms: Requirements for site survey, risk analyses, design, dimensioning, production, installation, and operation. Report, 2009.

[72] S. Norway. Aquaculture, 2017. Available at: `https://www.ssb.no/fiskeoppdrett` (In Norwegian, accessed: 29.1.2018).

[73] S. T. O'Callaghan and F. T. Ramos. Gaussian process occupancy maps. *The International Journal of Robotics Research*, 31(1):42–62, 2012. ISSN 0278-3649. doi: 10.1177/0278364911421039.

[74] L. Paull, S. Saeedi, M. Seto, and H. Li. Auv navigation and localization: A review. *IEEE Journal of Oceanic Engineering*, 39(1):131–149, 2014. ISSN 0364-9059. doi: 10.1109/JOE.2013.2278891.

[75] E. Pedrosa, A. Pereira, and N. Lau. A non-linear least squares approach to slam using a dynamic likelihood field. *Journal of Intelligent and Robotic Systems*, 2017. ISSN 1573-0409. doi: 10.1007/s10846-017-0763-7.

[76] S. Pendleton, H. Andersen, X. Du, X. Shen, M. Meghjani, Y. Eng, D. Rus, and M. Ang. Perception, planning, control, and coordination for autonomous vehicles. *Machines*, 5(1), 2017. ISSN 2075-1702. doi: 10.3390/machines5010006.

[77] S. Potyagaylo and S. G. Loizou. Online adaptive geometry predictor of aquaculture fish-nets. In *22nd Mediterranean Conference on Control and Automation*, pages 1002–1007, 2014. doi: 10.1109/MED.2014.6961505.

[78] S. Potyagaylo, C. C. Constantinou, G. Georgiades, and S. G. Loizou. Asynchronous ukf-based localization of an underwater robotic vehicle for aquaculture inspection operations. In *OCEANS 2015 - MTS/IEEE Washington*, pages 1–6, 2015.

[79] F. Ramos and L. Ott. Hilbert maps: Scalable continuous occupancy mapping with stochastic gradient descent. *The International Journal of Robotics Research*, 35(14):1717–1730, 2016. ISSN 0278-3649. doi: 10.1177/0278364916684382.

[80] D. Ribas, P. Ridao, J. D. Tardós, and J. Neira. Underwater slam in man-made structured environments. *Journal of Field Robotics*, 25(11-12):898–921, 2008. ISSN 1556-4967. doi: 10.1002/rob.20249.

[81] D. Ribas, P. Ridao, J. D. Tardós, and J. Neira. Underwater slam in man-made structured environments. *Journal of Field Robotics*, 25(11-12):898–921, 2008. ISSN 1556-4967. doi: 10.1002/rob.20249.

[82] P. Rundtop and K. Frank. Experimental evaluation of hydroacoustic instruments for rov navigation along aquaculture net pens. *Aquacultural Engineering*, 74:143–156, 2016. ISSN 0144-8609. doi: http://dx.doi.org/10.1016/j.aquaeng.2016.08.002. URL `http://www.sciencedirect.com/science/article/pii/S0144860916300012`.

[83] I. Schjolberg, T. B. Gjersvik, A. A. Transeth, and I. B. Utne. Next generation subsea inspection, maintenance and repair operations. *IFAC-PapersOnLine*, 49(23):434–439, 2016. ISSN 2405-8963. doi: http://dx.doi.org/10.1016/j.ifacol.2016.10.443.

[84] I. A. Sucan, M. Moll, and L. E. Kavraki. The open motion planning library. *IEEE Robotics and Automation Magazine*, 19(4):72–82, 2012. ISSN 1070-9932. doi: 10.1109/MRA.2012.2205651.

[85] P. V. Teixeira, M. Kaess, F. S. Hover, and J. J. Leonard. Underwater inspection using sonar-based volumetric submaps. In *2016 IEEE/RSJ International Conference on Intelligent Robots and Systems (IROS)*, pages 4288–4295. doi: 10.1109/IROS.2016.7759631.

[86] Teledyne. Workhorse navigator - whn 1200, 2018. Available at: `http://www.teledynemarine.com/Lists/\Downloads/navigator_datasheet_lr.pdf` (Accessed: 2018-10-25).

[87] ThelmaBiotel. ID tag 16mm, 2017. URL `http://www.thelmabiotel.com/index.php?pageId=567`. [Accessed: 22.08.2017].

[88] ThelmaBiotel. TBR-700 REALTIME, 2017. `http://www.thelmabiotel.com/index.php?pageId=580`, [Accessed: 22.08.2017].

[89] H. G. Thomas. Gib buoys: an interface between space and depths of the oceans. In *Proceedings of the 1998 Workshop on Autonomous Underwater Vehicles (Cat. No.98CH36290)*, pages 181–184, 1998. doi: 10.1109/AUV.1998.744453.

[90] T. Thorvaldsen, I. M. Holmen, and H. K. Moe. The escape of fish from norwegian fish farms: Causes, risks and the influence of organisational aspects. *Marine Policy*, 55:33 – 38, 2015. ISSN 0308-597X. doi: https://doi.org/10.1016/j.marpol.2015.01.008. URL `http://www.sciencedirect.com/science/article/pii/S0308597X15000196`.

[91] S. Thrun, W. Burgard, and D. Fox. *Probabilistic robotics. 2005.* USA: MIT, 2005.

[92] B. Triggs, P. F. McLauchlan, R. I. Hartley, and A. W. Fitzgibbon. Bundle adjustment — a modern synthesis. In *Lecture Notes in Computer Science*, Vision Algorithms: Theory and Practice, pages 298–372. Springer Berlin Heidelberg, 2000.

[93] I. Utne, I. Schjølberg, and I. Holmen. Reducing risk in aquaculture by implementing autonomous systems and integrated operations. In *Safety and Reliability of Complex Engineered Systems*, sep 2015. doi: 10.1201/b19094-481.

[94] I. B. Utne, A. J. Sørensen, and I. Schjølberg. Risk management of autonomous marine systems and operations. (57663):V03BT02A020, 2017. doi: 10.1115/OMAE2017-61645.

[95] M. Vagia, A. A. Transeth, and S. A. Fjerdingen. A literature review on the levels of automation during the years. what are the different taxonomies that have been proposed? *Applied Ergonomics*, 53:190–202, 2016. ISSN 0003-6870. doi: 10.1016/j.apergo.2015.09.013.

[96] S. Vasudevan, F. Ramos, E. Nettleton, H. Durrant-Whyte, and A. Blair. Gaussian process modeling of large scale terrain. In *2009 IEEE International Conference on Robotics and Automation*, pages 1047–1053, 2009. doi: 10.1109/ROBOT.2009.5152677.

Part II

Collection of Articles

Article J1

Particle Filter-based Simultaneous Localization and Mapping for Underwater Vehicles with Sonar

Stian S. Sandøy, Takumi Matsuda, Mehul Sangekar,
Ingrid Schjølberg, and Toshihiro Maki
Robotic and Autonomous Systems, submitted for review

This article is awaiting publication and is not included in NTNU Open

Article J2

Polar Map: A Digital Representation of Closed Structures for Underwater Robotic Inspection

Stian S. Sandøy, Jeevith Hegde,
Ingrid Schjølberg and Ingrid B. Utne
Aquaculture Engineering, 2020
doi:10.1016/j.aquaeng.2019.102039

Aquacultural Engineering 89 (2020) 102039

Contents lists available at ScienceDirect

Aquacultural Engineering

journal homepage: www.elsevier.com/locate/aque

Polar Map: A Digital Representation of Closed Structures for Underwater Robotic Inspection

Stian S. Sandøy*, Jeevith Hegde, Ingrid Schjølberg, Ingrid B. Utne

Department of Marine Technology, Norwegian University of Science and Technology, Otto Nielsensvei 10, 7052 Trondheim, Norway

ARTICLE INFO

Keywords:
AUV
ROV
SLAM
Navigation
Aquaculture
Octomap

ABSTRACT

This article presents a novel 2.5D map representation, termed polar map, that has a memory consumption of O(*ML*), where *M* and *L* depend on the map's angular and depth resolution, respectively. The map has a computational effort of O(1) in the update and evaluation process, where updates are performed through the use of Kalman filters. The representation can only be applied to structures in an environment that can be represented uniquely in a cylindrical coordinate system, such as fish cages, and square and cylindrical tanks. The work presents two case studies that compare the proposed polar map with the octomap. The first case shows a simulated example when mapping a fish cage. The second, an experiment in a square tank, where an unmanned underwater vehicle performs simultaneous localization and mapping (SLAM) using both the polar map and octomap representation. The results show that the polar map performs better, both in terms of memory consumption and computation effort, in both mapping and SLAM in the selected case studies.

1. Introduction

The Norwegian aquaculture industry produces around 1.3 million tons of fish every year (Norway, 2017). As of December 2018, the production (of mainly salmon and trout) was taking place in 1015 aquaculture fish farms (Directorate, 2018). To increase production volumes, larger structures are installed, and more exposed sites are adopted due to the lack of available sheltered locations. Inspection and maintenance activities are vital for cost efficient and safe aquaculture operations, but sea-based fish farming is a dangerous occupation. The harsh environmental conditions, a high manual workload for the operators, the utilization of heavy equipment, as well as a high work efficiency pressure, contribute to the occupational risks (Holen et al., 2018). Also, there are risks to the environment, such as fish escape. Fish escape incidents have a negative impact on the environment because they are a threat to biodiversity and wild fish (Thorvaldsen et al., 2015). In addition, they cause economic losses, and attract considerable negative attention from the public, with corresponding losses to the fish farm reputation. On average, 372,000 salmon and trout have escaped annually since 2001 (Directorate of Fisheries, 2019).

Sea-based aquaculture fish farms require periodic and conditions-based maintenance, with inspections and maintenance performed by human divers and remotely-operated vehicles (ROVs) (Utne et al., 2015). Diving is hazardous and costly, and the improved utilization of unmanned underwater vehicles (UUVs) for inspection could reduce the risk of human injury and fatality. It is therefore believed that UUVs will become more important for the safe and cost-efficient operation and maintenance of larger and more exposed fish farms. A major challenge for both existing fish farms and future larger ones is that the human divers and ROV operators have to keep track of the inspected areas of the net cages themselves, which is often limited to a localized region within their field of view. This can lead to uncertainty in how well an area is being covered during inspection operations and to undetected damage that can potentially lead to fish escapes.

Interactions with equipment, the hard physical working environment, the operator's workload, work pressure, training, skills, experience, co-operation, communication, and safety management can impact the likelihood of fish escape (Thorvaldsen et al., 2015). Aquaculture nets are not only wore out with time, but also prone to damage, such as holes made by predators and boat collisions. (Jensen et al., 2010). In addition, fish cages in sea-based fish farms are exposed to strong sea currents, which can result in large structural deformations (Lader et al., 2008). These deformations may make inspection and maintenance operations more difficult.

It is envisioned that resident autonomous underwater vehicles (AUVs) will be used for inspection operations in the future. Resident AUVs may increase the sustainability of underwater operations, as well as reducing costs and enhancing efficiency, since a reduced need for

---

* Corresponding author.
E-mail address: stian.s.sandoy@ntnu.no (S.S. Sandøy).

https://doi.org/10.1016/j.aquaeng.2019.102039
Received 27 May 2019; Received in revised form 12 November 2019; Accepted 20 December 2019
Available online 01 February 2020
0144-8609/ © 2020 The Authors. Published by Elsevier B.V. This is an open access article under the CC BY license
(http://creativecommons.org/licenses/BY/4.0/).

equipment transportation could lead to a reduction in greenhouse gas emissions. To enable this type of system, it is necessary that all significant parameters that could affect the operation are taken into account, so that the AUV can make the best possible decisions. Therefore, a global digital representation of the underwater structure is of high value for the AUV for it to be able to position itself and move around safely, whilst having sufficient inspection coverage. Such a representation, however, will not only be useful in future AUV operations, but could also improve ROV operations today.

The work presented in this paper contributes a novel mapping approach that is able to model enclosed vertical structures. The method is highly memory efficient and has low run-time complexity, making it an ideal choice for online applications. Furthermore, the approach is applicable in both static and dynamic environments. The proposed method is scalable, in terms of map resolution, which can benefit fish-cage mapping through its minimal system memory and / or computational effort. Even though the method is described and demonstrated here for fish-cage inspection, it is expected to be highly useful in other applications, such as industrial inspections using drones in confined areas.

The paper is structured as follows: Section 2 provides a brief background of the literature relevant to 2D and 3D map representations. The proposed 2.5D polar map is described in Section 3. The system setup for the proposed method is described in Section 4. Two case studies to test the proposed method are outlined in Section 5. Section 6 presents the results from the simulation trials and lab experiments. The results are discussed in Section 7, followed by the conclusions and scope for future works in Section 8.

2. Related Work on Map Representations

A map is a set of estimated values that describe an environment. Mapping algorithms include two steps: the first step is evaluation of the map, which means obtaining the probability of occupancy of a certain location. The second step is the map update, where detected occupied or free locations are inserted into the representation. The primary motivation for such map is to provide perception to a robot, so that it can localize itself in an environment, hence increasing its autonomy. This localization can be done both through Markov localization (Fox et al., 1999; Maki et al., 2012), which is used when the environment is already known, or through simultaneous localization and mapping (SLAM) (Ribas et al., 2008; Barkby et al., 2012; Mallios et al., 2014; Cadena et al., 2016; Ma et al., 2018; Sandøy et al., 2019) when the environment is unknown. Secondly, the execution of planning algorithms for constrained environments requires a map representation (Lau et al., 2013; Pairet et al., 2018). Thirdly, for ROV operations, these representations improve safety and efficiency because the ROV operator is also provided with increased situational awareness (Utne et al., 2015). Thus, it is crucial to have efficient map representations for autonomous systems. The latter reason (improved safety and efficiency) is an issue that, to a minimal extent, has been discussed in the literature. For the aquaculture industry, AkvaGroup has developed a solution for mapping during fish-cage cleaning operations (Group, 2019), which ensures that the operator has traversed all of the surface area of the fish cage. The system uses a short baseline acoustic network for positioning the vehicle. The limitation of this approach is that it can only define a static cylindrical shape and cannot take into account potential significant deformations in fish cages. This means, firstly, that the representation cannot be used as a map for localization, secondly, it is not possible to use it to plan autonomous operations because of the incomplete map, and thirdly, there are no descriptions of the uncertainties in the map, which makes it difficult to perform risk assessments for operations.

In general, the map representations available can be divided into three types: (i) grid-based (Moravec, 1988; Elfes, 1987); (ii) landmark-based (Leonard and Durrant-Whyte, 1991); and (iii) continuous-space-based (Vallicrosa and Ridao, 2018).

In grid-based maps, the world is divided into a finite number of cells. The probability of each cell being occupied is independent of all other cells, and is assumed to be static. The drawback of grid-based maps is that one cell's true state does not change with time, meaning that it cannot handle dynamic obstacles that change during mission times (i.e., dynamic deformations in fish cages). With finite representations, there are numerous approaches, each with its disadvantages and advantages. For instance, the classical grid-mapping approach of (Moravec, 1988; Elfes, 1987) is computationally efficient for map evaluation, having a runtime complexity of O(1) and being able to describe any type of environment; however, it is not memory efficient for large maps, since the number of cells increases quadratically in 2D and cubically in 3D maps. Tree-based grid-map representations, such as Quadtrees in 2D and Octrees in 3D (Fairfield et al., 2007; Hornung et al., 2013), require less memory; however, these representations come with a higher computational complexity in the map evaluation step. Another type of grid-based map is the so-called 2.5D map, which is used in underwater, terrain-based navigation (Stephen and Oscar, 2011). In this approach, each cell is associated with a depth and a reliability value; the latter corresponds to the probability of the cell having the exact depth. The map evaluation complexity is here O (1), and the memory consumption is low, making it the most efficient grid-based approach; however, unlike the other grid-based approaches, it can only be used to model environments that can be projected onto the x-y plane, and not vertical structures, such as fish cages.

Landmark-based mapping describes the relation between features' positions. A feature, or landmark, is something used to describe a specific location, such as a window or a door. This representation is usually included in an extended Kalman filter, or extended information filter, framework (Thrun et al., 2005). The most challenging part of this type of representation is the identification of the features, which requires the use of machine-learning algorithms that can be error prone, making false associations of features, which can lead to an erroneous location estimate. Landmark-based mapping is a so-called sparse representation that does not model dense maps, which is the most useful representation when planning a path for inspection tasks.

In (Vallicrosa and Ridao, 2018), the continuous-space model of an environment was suggested; however, this approach has a higher computational complexity than the discrete grid-map solution in (Stephen and Oscar, 2011), making it an unsuitable representation for online operations in fish cages. Besides, it cannot model vertical environments. In more recent works, Ramos et al. (Ramos and Ott, 2016) presented a map representation - named a Hilbert map - as an alternative to the Gaussian processes occupancy maps. It utilizes a kernel approximation model and, from this, defines an objective function that is minimized by a stochastic gradient optimizer to find the global optimum map representation. Hilbert maps need the same order of memory (quadratic) as 3D occupancy grid maps because kernel points need to be distributed in the space of interest.

3. Proposed Map Representation: Polar Map

This section describes the proposed novel mapping approach in detail, combining process and sensor models. Note that the sensor and process models, and the Kalman filter are interchangeable with other models or filters; however, the general idea of a cylindrical discretization approach would remain the same.

3.1. Discretization and Uncertainty Modeling

The structure of interest is discretized using cylindrical coordinates, given as $\{\theta, z\}$, where θ and z are the angle and depth, respectively, as shown in Fig. 1. The discretization is given by the set $Z = \{z^1, \ldots, z^L\}$ and $\Theta = \{\theta^1, \ldots, \theta^M\}$, which contains L depths and M angles, respectively, with a fixed resolution of z_{res} and θ_{res} between each discretization point.

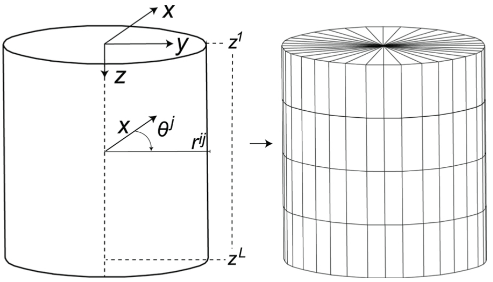

Fig. 1. Section-wise discretization of a solid cylinder by angle, θ, and depth, z. The range r is the variable that describes the edge of the cylinder for each section.

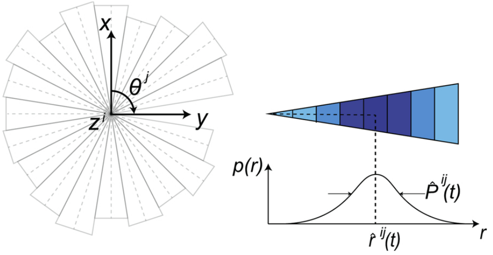

Fig. 2. Top view of the discretized structure (left) and the uncertainty model of a single section (right) in the 2.5D polar map representation.

The range for each section is modeled as a Gaussian distribution, with the probability $p(r)$ given a range of r. The estimated mean is $\hat{r}^{\text{ij}}(t)$, and the estimated variance is $\widehat{P}^{\text{ij}}(t)$, as shown in Fig. 2(right-hand side). The mapping between each section and range is defined as follows:

$$\{z^i, \theta^j\} \rightarrow \{\hat{r}^{\text{ij}}, \widehat{P}^{\text{ij}}\} \quad \forall \quad i \in \{1...L\}, \;\; j \in \{1...M\}. \tag{1}$$

Equation (1) is central for the term 2.5D, which refers to the discretization of a 3D space by using only two variables, namely depth and angle. This separates the representation from other approaches. For instance, in 3D grid mapping, cells are discretized by a Cartesian grid in such a way that free cells are also included; however, this is avoided in the proposed mapping approach, thereby reducing the number of required cells in the representation.

The assumptions that need to be fulfilled when using the proposed mapping approach are:

Assumption 1. The ranges of the sections are statistically independent of each other.

Assumption 2. Each point in the structure can be defined from a vertical line along the z-axis, given an angle and a range.

Assumption 1 says that one section in the structure has no relation to the other sections; however - for instance, in a fish cage - neighboring sections are highly dependent and, if this is ignored, there is a loss of information. On the other hand, it is a very practical assumption because it simplifies the updating process significantly.

Assumption 2 sets a constraint on what type of structure this mapping approach can be used for. The implication of this assumption is that closed shapes that are too complex to be modeled from a single point cannot be mapped. Examples are shown in Fig. 3, where the structure has a shape that can be mapped from the dot in the center (left), while the structure is too complex to be represented by polar coordinates (right).

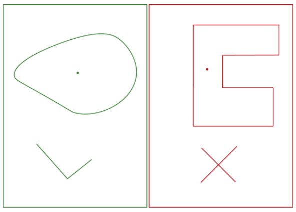

Fig. 3. Shape limitations for a polar map representation.

To convert the cylindrical coordinates to the north-east-down (NED) frame for each section of angle j and depth i, the following known relations are used:

$$x^{\text{ij}} = \hat{r}^{\text{ij}}\cos(\theta^j), \tag{2}$$

$$y^{\text{ij}} = \hat{r}^{\text{ij}}\sin(\theta^j), \tag{3}$$

$$z^{\text{ij}} = z^i. \tag{4}$$

3.2. Process Model

An online mapping approach for a flexible structure needs a model that reflects the change in the structure's position over time. The change in fish cages can be periodically rapid and / or slowly varying, due to ocean waves and currents. In this work, the slowly-varying current effect was modeled as a random walk process, which requires that Assumption 3 is valid.

Assumption 3. The change in the range of each section can be modeled by a random walk process.

The discrete equations for a random walk process can be written as follows:

$$\bar{r}_k^{\text{ij}} = \bar{r}_{k-1}^{\text{ij}} + \omega_r, \quad \omega_r \propto \mathcal{N}(0, Q), \tag{5}$$

where $\bar{r}_k$ is the predicted range for time step k, and ω_r is a Gaussian random variable with variance Q.

3.3. Sensor Model

In order to update the 2.5D polar map, measurements are required. Firstly, this work assumed the range measurements originates from a vehicle with a known pose given as $\mathbf{x} = [\mathbf{p}^T \;\; \psi^n]^T$, where $\mathbf{p} = [x^n \;\; y^n \;\; z^n]^T$ is a position in relation to the NED frame (Fossen, 2011), as indicated by the superscript n, and ψ^n is the heading of vehicle. Note that the pose does not include the roll and pitch angles of the vehicle because they are in this case assumed to be negligible.

The model for the measured range can be written as:

$$y = r + \omega_y, \;\; \omega_y \propto \mathcal{N}(0, R), \tag{6}$$

where r is the true range and ω_y is a normally distributed variable with variance R, which means that Assumption 4 needs to be fulfilled.

Assumption 4. The sensor noise is Gaussian distributed.

To relate a measurement to a section in the structure, given the pose of the sensor, the endpoint $\mathbf{e} = [e_x \;\; e_y]$ of the measurement needs to be related to the fish cage reference frame. The relations are given as:

$$\mathbf{e}(y, \mathbf{x}) = ([y\cos(\psi^n) \;\; y\sin(\psi^n)] + [x^n \;\; y^n])^T, \tag{7}$$

$$\theta = \text{atan2}(e_y, e_x), \tag{8}$$

$$z = z^n, \tag{9}$$

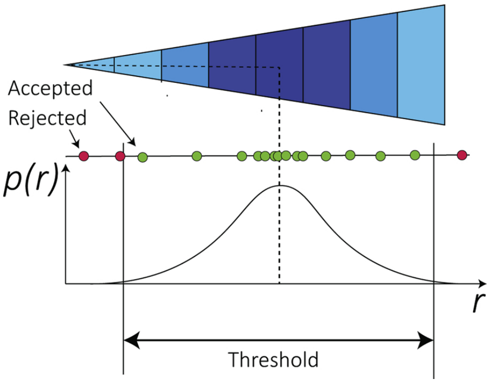

Fig. 4. Outlier rejection scheme.

where atan2 is an inverse of tangents that is valid for all angles (Thrun et al., 2005). The range measurement is then simply computed by taking the Euclidean norm of the endpoint $y_m = ||\mathbf{e}||$, and θ and z are the respective angle and depth of the measurement in relation to the NED frame. The indices i and j are determined by the values in the Z and Θ set closest to z and θ, respectively.

3.4. Outlier Rejection and Initial Smoothing

A weakness of the Gaussian distributed model is that it does not take into account outliers in the sensor measurements, and therefore a separate outlier detection step and initial smoothing need to be performed for each measurement before they enter the Kalman filter. Gustafson (Gustafsson, 2012) suggested a statistical test of two hypotheses for a measurement being an inlier or an outlier. Simplified, the method is a χ^2-test, implemented as:

$$T(y_m) = \frac{(y_m - \bar{r}_k)^2}{\bar{P}_k + R} < \chi^2, \tag{10}$$

where χ^2 represents the threshold shown in Fig. 4, $\bar{r}_k$ is the predicted range, and $\bar{P}_k$ is the predicted covariance. This exploits the Gaussian distribution estimated for each section to accept or reject new measurements. As seen in Fig. 4, measurements outside the threshold are rejected and the others are accepted. All points outside this threshold are rejected.

In addition, initial smoothing steps are necessary to account for potential outlier points. This is done through defining an uncertainty, R_{start}, that decays with each iteration (Gustafsson, 2012).

3.5. Map Update Method Using Kalman Filter

A mapping approach for a flexible structure needs to fuse new information with the estimates over time, as described by the process and sensor model in the previous subsections. A Kalman filter with one state was used for each section, due to the fact that initial conditions can be specified, and both sensor and process updates are performed. In the case where there are no initial conditions, or only the sensor update process is used, an information filter would be more advantageous because it can define the covariance matrix as infinite, thus avoiding the need for initial conditions and reducing the runtime complexity (Stephen and Oscar, 2011; Thrun et al., 2005). The Kalman filter equations are shown, step by step, in Algorithm 5. The algorithm requires the range measurement, along with the index of each section, given as i and j, the previous range in the section, $\bar{r}_{k-1}^{ij}$, and the variance, $\bar{P}_{k-1}^{ij}$.

Algorithm 5. Kalman filter section update including outlier rejection and smoothing

```
Require: $y_m$, $i$, $j$, $\bar{r}_{k-1}^{ij}$, $\bar{P}_{k-1}^{ij}$, $Q$, $R$
for all sections do
    %Process update
    $\bar{r}_k^{ij} = \bar{r}_{k-1}^{ij}$
    $\bar{P}_k^{ij} = \bar{P}_{k-1}^{ij} + Q$
    %Sensor update
    if $T(y_m) < \chi^2$ then
        $K = \bar{P}_k^{ij}(\bar{P}^{ij} + R + \frac{R_{start}}{k^2})^{-1}$
        $\hat{r}_k^{ij} = \bar{r}_k^{ij} + K(y_m - \bar{r}_k^{ij})$
        $\hat{P}_k^{ij} = (1 - K)^2\bar{P}_k^{ij} + K^2(R + \frac{R_{start}}{k^2})$
        $\bar{r}_k^{ij} = \hat{r}_k^{ij}$
        $\bar{P}_k^{ij} = \hat{P}_k^{ij}$
    else
        $\hat{r}_k^{ij} = \bar{r}_k^{ij}$
        $\hat{P}_k^{ij} = \bar{P}_k^{ij}$
    end if
end for
return $\hat{r}_k^{ij}$, $\hat{P}_k$, $\bar{r}_k$, $\bar{P}_k$
```

4. System Setup for Localization and Mapping in Aquaculture

This section presents two different sensor setup scenarios for the localization and mapping of UUVs in aquaculture. The definition of robot localization is finding its position and orientation at a certain time relative to a local environment given a reference frame. A natural point of reference in an aquaculture operation is the center of the fish cage, as shown in Figs. 5 and 6 , where the position and orientation (pose) of the robot is denoted by $\mathbf{x}$. The x^n-axis points north, the z^n-axis downwards, and the y^n-axis completes the right-hand rule. The heading ψ^n relates to the difference in angle between the vehicle's body frame and north. Note that, in this work, pitch and roll were assumed negligible, which is a poor assumption if the UUV is close to the sea surface when there are waves making the attitude of the UUV less stable. The next two subsections present two possible sensor setups for a UUV.

4.1. Underwater Mapping with Known Locations

To obtain the poses of a UUV, a positioning system is required. In underwater environments, acoustic positioning is considered to be the state of art, as opposed to land robots that use the global navigation satellite system. One particular type of acoustic positioning system, termed short base-line (SBL) (Christ and Wernli, 2013), uses the time-

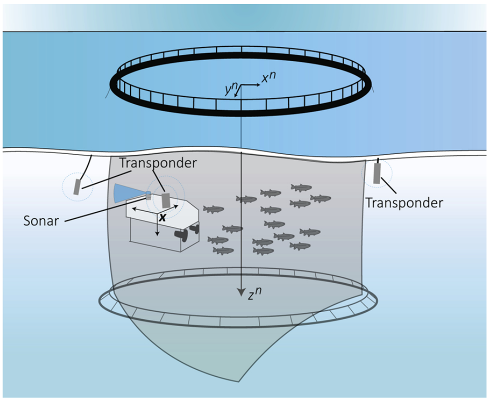

Fig. 5. Illustration of a mapping scenario.

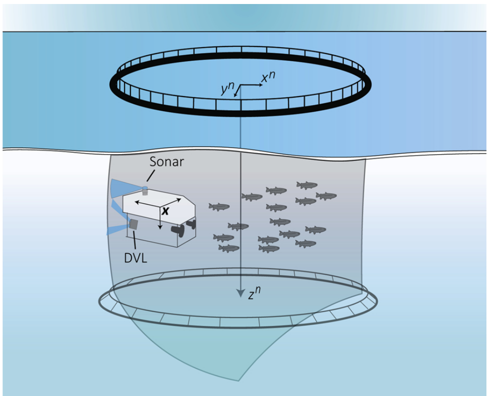

Fig. 6. Illustration of autonomous inspection scenario.

of-flight from a transponder located at a UUV to an array of fixed transponders of known location, as illustrated in Fig. 5. The speed of sound is then used to locate the UUV based on the time-of-flight signals. In order to find the heading of the vehicle, it is necessary to use a magnetic compass or gyro-compass. A magnetic compass is prone to electromagnetic noise, which can be a challenge in some underwater environments, however, a gyro-compass is robust from magnetic disturbances. The range and bearing measurements from the UUV to the edge of the fish cage are then needed. These can be measured by a sonar sensor mounted on the UUV. Sonars use acoustic echo intensities to determine the range to objects. A possible type of sonar is the mechanical scanning imaging sonar as shown in Fig. 5. Finally, a pressure sensor provides the depth measurement, which results in the z^n position, with centimeter accuracy.

4.2. Underwater Simultaneous Localization and Mapping

The SLAM method, as the name indicates, performs the operation of finding the location of the robot and, at the same time, making a representation (map) of the environment. This is particularly difficult because it is considered to be a chicken-and-egg problem, meaning that, in order to localize, the map needs to be known, and vice-versa. The advantage of using SLAM is that only sensors mounted in the UUV are required, as illustrated in Fig. 6. Also, a compass is not essential, which avoids potential heading errors due to magnetic noise. It requires only odometry-type sensors, providing velocity and angular rate; in this case, a Doppler velocity log (DVL) and gyro. Inside an aquaculture fish cage, the DVL can either be faced towards the net pen structure (Rundtop and Frank, 2016), as in Fig. 6, or towards the seafloor. Of course, this assumes that the seafloor is not too deep, and that there are no obstacles to any of the beam paths. The second sensor is the gyro, which measures the rate of the heading angle. As in the previous subsection, sonar is used for ranging to the net pen, and a pressure sensor is used to measure depth.

In this work, two particle-filter-based SLAM methods were implemented and compared. Fig. 7 illustrates the sensor flow for the approaches. Firstly, the sensor measurements are used in both the mapping and localization updates. Secondly, the particle filter has multiple hypotheses for each location and map pair. Thirdly, the mapping approach can be either the occupancy grid map or the proposed polar map. For more information on particle-filter-based SLAM, see (Grisetti et al., 2007; Sandøy et al., 2019).

5. Case Studies

This section presents two case studies for localization and mapping using a UUV for the inspection operations of fish cages. Case Studies 1 and 2 reflect the system setups presented in subsections 4.1 and 4.2, respectively. These cases were of particular interest because they had different degrees of complexity and distinct advantages. Case Study 1 required an SBL network for the vehicle position estimation. Case Study 2 did not require an SBL, and could therefore perform the inspection operation using only local sensors mounted on the vehicle. This could potentially lower the costs and thresholds related to the use of the proposed method.

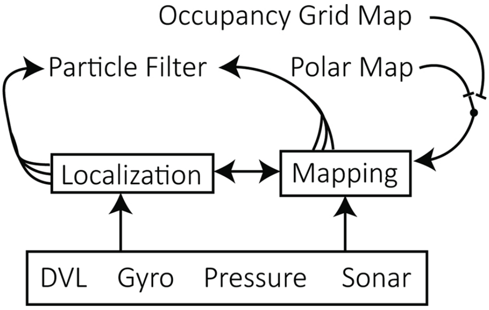

Fig. 7. Flow chart of particle-filter SLAM using polar and occupancy grid maps.

5.1. Case Study 1: Underwater Cage Mapping with Known Pose

The purpose of this case study was to generate a polar map using sonar measurements, assuming known vehicle poses $\mathbf{x}$, as presented in Subsection 4.1. The polar map is compared to an octomap representation (Hornung et al., 2013; Mathworks, 2018).

To simulate a scenario with a UUV having a known position and a sonar, 28,800 range and bearing measurements were generated, evenly distributed over the fish cage surface. To simplify the simulation, it was assumed that the range and bearing sensor was located at the center of the cage and was travelling along the z^n-axis. Gaussian noise, with a standard deviation of 0.1 m, was added to the range measurements. The fish cage had a 15 m radius, was 40 m deep, and had a tilt of 8.53°, which is a realistic scenario for an aquaculture structure, according to (Lader et al., 2008). In addition, a randomly selected 10% of the 28,800 ranges was set to outlier measurements, defined as:

$$y_{\text{outlier}} = 5 + \sigma_{\text{outlier}}\omega_{\text{outlier}}, \tag{11}$$

where $\sigma_{\text{outlier}} = 5$, is the standard deviation, and ω_{outlier} is a random variable with standard distribution. The outlier measurements are to model fish that are blocking the range sensor.

The generated points are scattered as a point cloud in Fig. 11a. As can be seen, the cage is slightly tilted towards the north in order to simulate a case where the fish cage is deformed by the presence of underwater currents. Tables 1 and 2 present the parameters used for the

Table 1
Polar map parameters for Case Study 1

Parameter	Unit	Value
θ_{res}	[deg]	4
z_{res}	[m]	1
z_{min}	[m]	1
z_{max}	[m]	40
$r_{ij}\ \forall\ i, j$	[m]	15
$P_{ij}\ \forall\ i, j$	[m^2]	20^2
R	[m]	0.1^2
R_{start}	[m]	15^2
Q	[m]	0.005^2
χ	[-]	3
Memory usage	[KB]	0.29

Table 2
Occupancy grid map parameters for Case Study 1

Parameter	Unit	Value
Resolution	[*m*]	1.0
p_{hit}	[]	0.7
p_{miss}	[]	0.4
Occupancy threshold	[]	0.71
Memory usage	[KB]	429

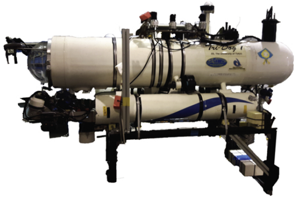

Fig. 8. The UUV Tri-Dog 1 was used in the Case Study 2 tank experiment.

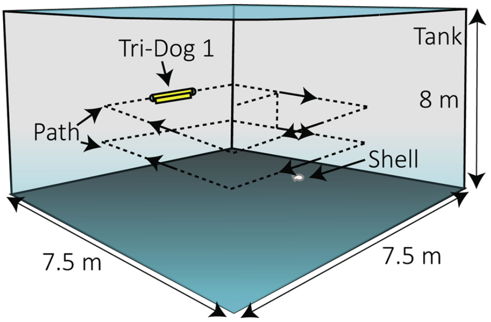

Fig. 9. The path of the vehicle, the size of the tank, and the location of a shell placed on the tank floor for reference.

two methods. Note the large difference in the memory consumption of the two methods in the memory usage column in the tables. Polar map requires only fraction of the memory compared to Octomap, even though both methods have approximately the same resolution at 15 meter range from the center line of the cage.

5.2. *Case Study 2: Underwater Mapping with Unknown Poses*

The purpose of this case study was to analyze an experimental SLAM scenario in a closed environment, such as in a square tank, using a polar map and an octomap. The UUV was equipped with a sonar (Tritech, 2018), an inertial measurement unit (Japan Aviation Electronics Industry, 2018) and a DVL (Teledyne, 2018). The time-series of the sensor data was collected in a tank experiment at the University of Tokyo. The UUV applied in the experiment was Tri-Dog 1 (Kondo, 2001), as shown in Fig. 8, and the size of the tank was 7.5 × 7.5 × 8.0 m, as illustrated in Fig. 9. The time-series was first published in (Sandøy et al., 2019), in which a particle-filter-based SLAM approach, using 2D occupancy grid maps as the spatial representation, was applied to process the data.

6. Results

This section contains the results of the case studies presented in Subsections 5.1 and 5.2.

6.1. *Case Study 1: Underwater Cage Mapping with Known Poses*

Fig. 10 shows the polar map after processing the scattered 28,800 range and bearing measurements from Fig. 11a. The polar map is illustrated by a surface plot that interpolates the estimated ranges for each section. The error of the ranges vs. the true ranges for each section are shown in the color map. The Gaussian distributions of each section are shown in top and side views in a cross-section of the plane $z = 0.5$ and $y = 0$ in Figs. 10b and 10 c, respectively. Fig. 11b shows the results of the occupancy grid map, in which the color bar indicates the depth of the cell.

6.2. *Case Study 2: Underwater Tank Mapping with Unknown Poses*

The parameters of the two mapping methods are shown in Tables 3 and 4 . In the former, note that the polar map was only represented for 4-8 m in depth, at a resolution of 1 m, because the UUV was limited to that region; the angle had a resolution of 1°. Outlier rejection and initial smoothing was not required in this case. The process model was not utilized here either because the tank was a static structure.

The SLAM computer processing time for each iteration using the octomap and the polar map are shown as a time-series budget of each task in Figs. 12 and 13 , respectively. The tasks were divided into resampling, map updating and other. Resampling is the time consumed

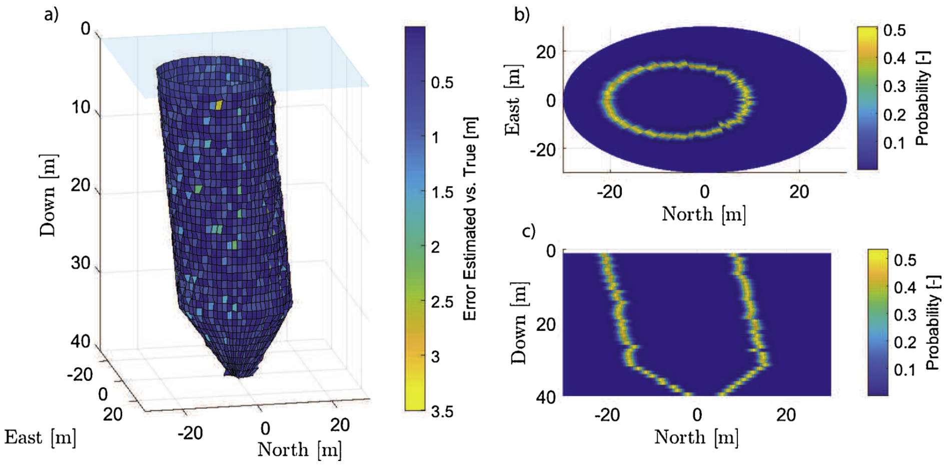

Fig. 10. Case Study 1: 2.5D polar map.

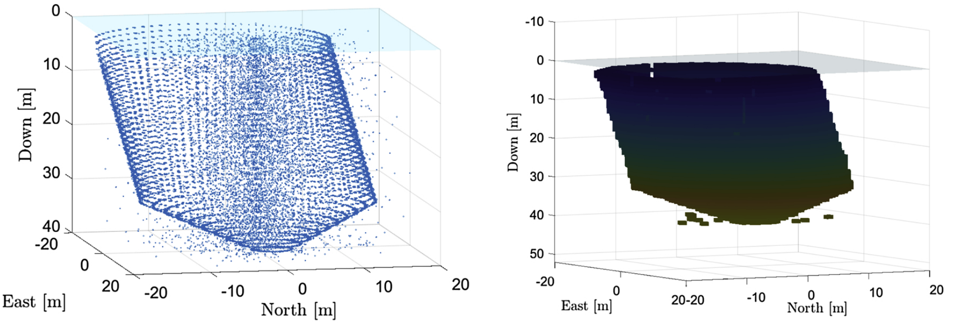

(a) Case study 1: Raw data point cloud

(b) Case Study 1: Octomap

Fig. 11. Raw data point cloud and octomap.

Table 3
Parameters for the polar map in Case Study 2

2.5D polar map	Unit	Value
θ_{res}	[deg]	1
z_{res}	$[m]$	1
$z_{\min}$	$[m]$	4
$z_{\max}$	$[m]$	8
$r_{ij}\ \forall\ i, j$	$[m]$	5
$P_{ij}\ \forall\ i, j$	$[m^2]$	1e10
R	$[m^2]$	$0.\,1^2$

Table 4
Parameters for the octomap in Case Study 2

Octomap	Unit	Value
Resolution	$[m]$	0.05
p_{hit}	[]	0.7
p_{miss}	[]	0.4
Occupancy threshold	[]	0.71

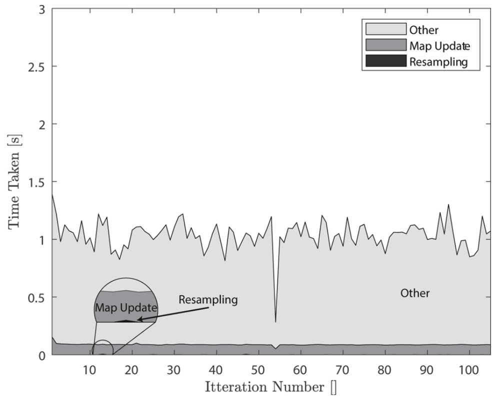

Fig. 12. Update time of SLAM approach when using polar map.

by resampling particles in the particle filter, map updating is the time it takes to update the map, and other represents all other operations.

The resulting outputs of the SLAM approaches are shown in Figs. 14 and 15 . In Fig. 14, the polar map is represented as a surface plot given by the mean range of each section. In Fig. 15, the resulting octomap is shown by boxes marking the occupied cells. The probabilities are not shown

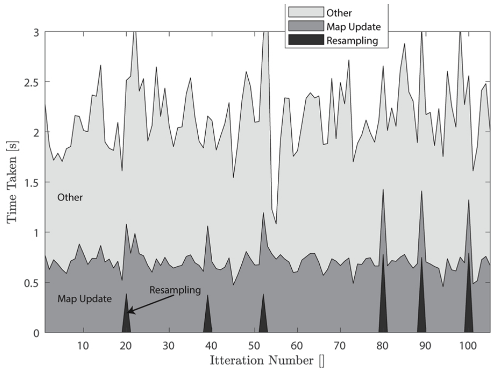

Fig. 13. Update time of SLAM approach when using octomap.

because the concept was proven in Case Study 1. The estimated and odometry trajectories are indicated by solid red and dashed blue lines, respectively. To the right in both figures is the covariance in x, with the y and ψ positions plotted. In addition, the resampling and imaging events are shown by + and a solid red dot, respectively. The image event refers to the event of taking a picture of the shell located on the tank floor as a position reference. The estimated positions of the shell are scattered in the left plot. The number of particles was $N = 50$ for both approaches.

7. Discussion

7.1. Case Study 1: Underwater Fish Cage Mapping with Known Poses

The generated polar map shown in Fig. 10a has a root mean square error (RMSE) of 0.332 m compared to the true fish cage position. The RMSE was found by computing the error between the estimated range and true range in each section of the fish cage. The surface representation gives an intuitive representation due to the ease of interpolating between the mean range points in the polar map. There were some cells that were affected by the outliers, as seen in the error of 3.5 m; however, the smoothing and outlier rejection schemes performed well, considering the low RMSE. Note that it can be a challenge to maintain the validity of Assumption 2. As seen in Fig. 10c, the map is at the limit of Assumption 2 due to the large deformations in the fish cage; however, the centerline can be adjusted to another function to deal with the tilt in depth. The octomap illustrated in Fig. 11b has an RMSE of 0.337 m. The result resembles the RMSE value obtained using the polar mapping approach. The RMSE computations were performed by generating a 3D nearest-neighbor transform, using the binary 3D occupancy grid map and MATLAB function

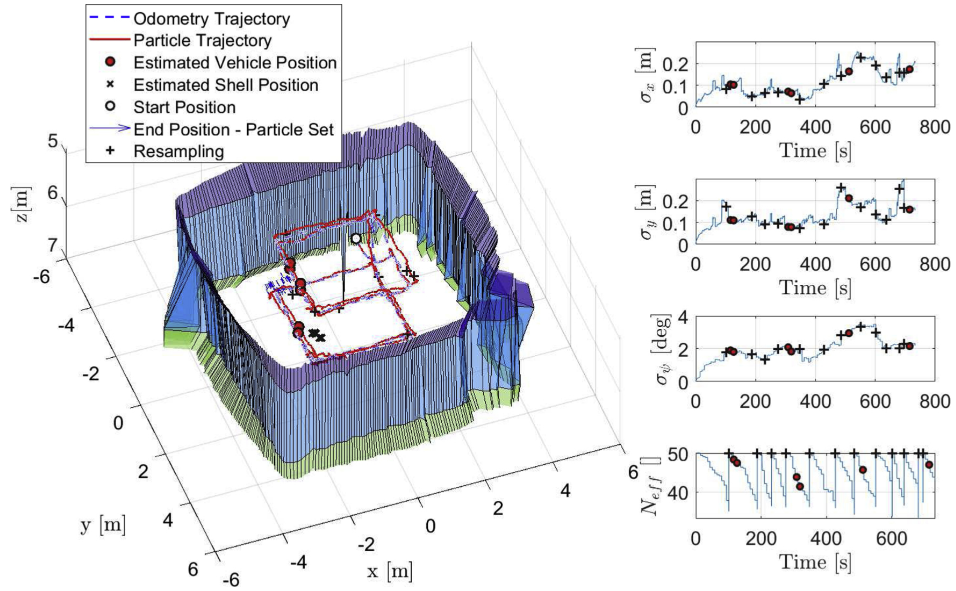

Fig. 14. Particle filter-based SLAM in tank using polar map.

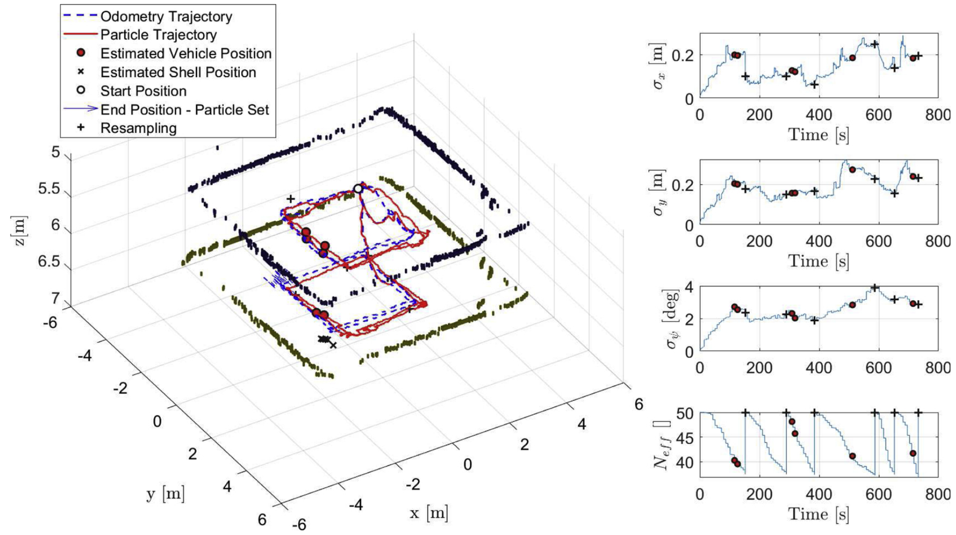

Fig. 15. Particle-filter-based SLAM in tank when using octomap.

bwdist. The nearest neighbor transform is the distance to the nearest occupied cell in a grid. The error was computed by evaluating the true map's position in the generated map's nearest neighbor transform. The occupancy grid map produces a discrete representation. Therefore, it is challenging to generate a continuous surface. This is not the case in the proposed polar mapping approach. When comparing the memory usage shown in Tables 1 and 2, the polar map can be seen to require only a fraction of the memory compared to the occupancy grid map. Although the output of the occupancy grip map is compact (in form of octrees), it still needs to represent a higher number of nodes. The memory for the polar map is computed using the formula $\text{mem}_{\text{polarmap}} = M \times L \times 8\ B$, where M and L are the angular and depth resolution, and B is the unit byte. The memory of the octomap is computed by the formula $\text{mem}_{\text{octomap}} = N_{\text{internalnodes}} \times 40\ \ B + N_{\text{leafnodes}} \times 8\ \ B$ (Hornung et al., 2013), where $N_{\text{internalnodes}}$ is the number of internal nodes and $N_{\text{leafnodes}}$ is the number of leaf nodes. In this work, the octomap's memory was found through octovis[1] .

7.2. Case Study 2: Underwater Tank Mapping with Unknown Poses

The results of the second case study are shown in Figs. 14 and 15 . The polar map and octomap approaches show similar performance in position accuracy, as seen in the consistency of the shell position estimates, although there were some differences in the estimated vehicle trajectory compared to the odometry trajectory in the SLAM approach using octomap. The covariance of the particle set (on the right in the figures) shows a standard deviation of between 0.1 and 0.3 m in the x and y location estimates for both approaches. Note that the covariance increased from 0 to 100 seconds due to the low accuracy of the sonar. Also, there was an increase in covariance at 500 seconds due to the fact that the UUV changed depth and encountered an unexplored map that did not depend on the previous depth, as stated in Assumption 1. In the polar map, this could be handled by relaxing the independence assumption in the depth; for example, by initializing the next depth using the estimate of the previous depth and adding some uncertainty.

---

[1] http://wiki.ros.org/octovis

The most important point for low computational complexity is the cost of updating the map with range and bearing measurements. In an octomap, the update depends on the range of the measurements, since the insertion of a range into a map requires traversal of all cells on the trace of the range measurement. On the other hand, the polar map does not require this traversal, and only the range estimate of the section containing the measurement needs to be updated. This difference is shown clearly in Figs. 12 and 13 by the map update time. They show that the polar map requires one-fifth of the computation time compared to the octomap. The resampling operation gave the most apparent differences in runtime between the two mapping approaches. This is due to the fact that each particle's map needs to be copied, and that the octomap representation is a lot more time-consuming to copy than the polar map. Also, due to the depth change, there was a radical increase in the complexity of the octomap, as shown by the doubling in runtime from the 80th iteration, which would continue to grow for each depth change, while the polar map's copying time will remain the same. Note that the SLAM approaches were run in the post-processing of the sensor data using a desktop computer with an Intel(R) Core(TM) i7-8700 CPU@ 3.20GHz. The SLAM approaches were implemented using MATLAB.

7.3. Other Advantages and Challenges of the Polar Map

Firstly, the polar map considers uncertainties in both the sensor measurements, via the sensor model in Section 3.3, and in the environment, in the form of underwater currents, by the process model described in Section 3.2. However, underwater currents are slowly varying and more rapid motion, such as from wave motion is not taken into account. This means that the suggested method is only applicable for environments where wave motion is negligible.

In nowadays's mapping methods, the static assumption of the maps is strong, as mentioned in Section 2, and there is a need for methods that relax this assumption because of the environmental uncertainties. The proposed polar map is able to handle such uncertainties with the inclusion of a simple random walk process model, although this was not demonstrated in the chosen case studies. The ability to handle outliers in a map strengthens the robot's perception of the environment. This is a big advantage when, for instance, something blocks a range sensor, such as a fish in a fish cage, where noisy sonar data with outliers often occur (Rundtop and Frank, 2016). This was also somewhat dealt with in the octomap representation, but this might not be as robust when it comes to multiple outlier measurements, which can happen when fish block the sensor. In the octomap, a predefined map size is required. In the polar map, this is not required because the range can, in theory, continue infinitely. However, for large ranges, a higher angular resolution is required to maintain accuracy.

A challenge of polar maps is that they cannot model environments outside their scope, meaning environments that cannot be described by a single point, as shown in Fig. 3. In an aquaculture scenario, this can happen when there is an object located inside the fish cage that must be avoided, such as an underwater camera. A possible solution is to use local maps in the ego-space (Fragoso and Anthony, 2019) of the vehicle that can be used for obstacle avoidance. Another difficulty with polar maps for aquaculture application is in situations where a fish cage is highly deformed, which can occur with rapid currents (Lader et al., 2008). This might introduce difficulties when modeling the lower part of the cone, since the centerline that models the structure might fall outside of the structure, which would breach Assumption 2. A possible way to handle this would be to update the centerline from where the polar coordinates are defined; however, this was left for future work. Another factor for the proposed sensor model is waves, which are present close to the wave zone. This might lead to large roll and pitch motions. Herein, the pitch and roll angles were assumed to be small, and would be invalid if waves were considered.

7.4. Discussion of Assumptions

The main drawback associated with Assumption 1 is the loss of information because the dependencies between the sections are removed. Therefore, other interesting techniques that could relax this assumption and utilize the compact 2.5D map, such as Gaussian processes occupancy maps (O'Callaghan and Ramos, 2012) or Hilbert maps (Ramos and Ott, 2016), need to be investigated.

Assumption 2 is necessary for using the polar representation; however, it can be adjusted in the way that the centerline is defined, as mention in the discussion of Case Study 1, by changing the position of the centerline, such that the entire space can be represented. This was, however, not taken into account in this paper.

Assumption 3 is a crude way of modeling a fish cage. Including the modeling of wave and current changes would improve the fish cage model significantly. The benefit of the random walk process model is that no measurement is required; however, if current measurements are available, for instance, it would also be possible to use a more predictive model, based on (Lader et al., 2008), for example.

Assumption 4 could be adjusted if we looked into the use of other estimation algorithms. For instance, multi-modal distributions could be added, such that each section could have multiple means for each section. This would require a higher memory consumption; however, a polar map would still have a lower memory consumption compared to a 3D occupancy grid map or octomap.

7.5. Model for Fish Cage Uncertainty

In addition to a thorough and efficient inspection of the net, provided by the mapping method presented in this paper, it is important to avoid fish escape by preventing holes to develop in the fish net. This means that the UUV should not become tangled in the net or with other types of vulnerable equipment in the cage, which means that precise positioning is very important in reducing risk. Hence, better mapping should also lead to improved localization of the underwater vehicle.

ISO 31000 (International Organization for Standardization, 2018) defines risk as the effect of uncertainty on objectives. The values Q and R represent the uncertainty (variance) associated with an update, or change in the range, in each section of the model, as the vehicle moves around in the cage. Therefore, it is relevant to investigate risk-influencing factors that could impact Q and R during operation of the underwater vehicle. Examples of such factors might include environmental conditions (e.g., currents, waves), sensor quality and measurements, the technical condition and speed of the vehicle, and the distance to the fish net. By developing a model - for example, a Bayesian belief network (BBN) - the various conditions of relevant risk-influencing factors can be represented and updated during operation of the underwater vehicle (Hegde et al., 2018; Utne et al., 2018). Information from the BBN can be used to represent uncertainty, and therefore for choosing the Q and R values. This is subjected to further work.

8. Conclusions and Further Work

This work presented a method to generate a novel map representation, termed a polar map, which can be used in robotic applications. The robotic application examples given included a mapping scenario of a fish cage and an underwater SLAM case performed in a square tank. In both case studies, the polar map was compared with an octomap, in terms of memory consumption and computational effort. The polar map was shown to have significantly lower memory consumption, and required minimal computational effort, compared to the octomap, meaning that it can enable large amount of sensor readings and still be used on low-cost computer / circuit boards. In aquaculture, polar maps can enable automatic inspection / cleaning operations in fish cages, and has the potential to reduce the operational costs and risks related to personnel and the environment. In future works, it will be possible for other estimation algorithms to be considered in the polar map, meaning that the Kalman filter could be replaced with a particle filter or a Gaussian mixture estimation method, so that multiple hypotheses can be obtained for each section. This would increase the computational cost of the method; however, it would improve the accuracy. Other methods might include using the polar representation as a continuous representation through the use of Gaussian process occupancy maps. Another option for further work would be to integrate custom-planned algorithms with the proposed mapping method. There may be an advantage to including computational complexity in the guidance algorithms by exploiting 2.5D representation. Furthermore, the fusion of other sensors into the polar map, such as cameras, or short baseline or different types of sonar sensors, can be explored by exploiting the probabilistic representation of the polar map.

Acknowledgments

This work was funded by the Norwegian University of Science and Technology (NTNU), under the Norwegian Research Council project Reducing Risk in Aquaculture (254913). The authors would like to thank the University of Tokyo, Institute of Industrial Science, Maki Laboratory for support in collecting the tank experiment dataset, and specifically Prof. Toshihiro Maki, Dr. Takumi Matsuda and Dr. Mehul Sangekar. J.H. would also like to acknowledge funding support from the Department of Marine Technology at the NTNU.

References

Barkby, S., Williams, S.B., Pizarro, O., Jakuba, M.V., 2012. Bathymetric particle filter slam using trajectory maps. The International Journal of Robotics Research 31, 1409–1430. https://doi.org/10.1177/0278364912459666.

Cadena, C., Carlone, L., Carrillo, H., Latif, Y., Scaramuzza, D., Neira, J., Reid, I., Leonard, J.J., 2016. Past, present, and future of simultaneous localization and mapping: Toward the robust-perception age. IEEE Transactions on Robotics 32, 1309–1332. https://doi.org/10.1109/TRO.2016.2624754.

Christ, R.D., Wernli Sr., R.L., 2013. The ROV manual: a user guide for remotely operated vehicles. Butterworth-Heinemann.

Directorate, N.F., 2018. Antall lokaliteter i 2018 av laks, regnbueoerret og oerret (number of locations in 2018 of salmon and trout; in norwegian). URL: https://www.fiskeridir.no/content/download/7613/95478/version/30/file/sta-laks-mat-02-lokaliteter.xlsx, accessed: 2019-05-02.

Directorate of Fisheries, 2019. Escape statistics. URL: https://www.fiskeridir.no/Akvakultur/Statistikk-akvakultur/Roemmingsstatistikk.

Elfes, A., 1987. Sonar-based real-world mapping and navigation. IEEE Journal on Robotics and Automation 3, 249–265. https://doi.org/10.1109/JRA.1987.1087096.

Fairfield, N., Kantor, G., Wettergreen, D., 2007. Real-time slam with octree evidence grids for exploration in underwater tunnels. Journal of Field Robotics 24, 03–21. https://doi.org/10.1002/rob.20165.

Fossen, T.I., 2011. Handbook of Marine Craft Hydrodynamics and Motion Control. Wiley.

Fox, D., Burgard, W., Thrun, S., 1999. Markov localization for mobile robots in dynamic environments. Journal of artificial intelligence research 11, 391–427.

Fragoso, C.U., Anthony, T.S., 2019. Los Angeles, Simultaneous representation of moving and static obstacles for automatically controlled vehicles, 20190108764. URL: http://www.freepatentsonline.com/y2019/0108764.html, patent.

Grisetti, G., Stachniss, C., Burgard, W., 2007. Improved techniques for grid mapping with rao-blackwellized particle filters. IEEE Transactions on Robotics 23, 34–46. https://doi.org/10.1109/TRO.2006.889486.

Group, A., 2019. Akva fnc8 v 2.0. URL: http://www.akvagroup.com/cage-farming-aquaculture/net-cleaning/akva-fnc8, accessed: 2019-01-17.

Gustafsson, F., 2012. Statistical sensor fusion, 2nd ed. Studentlitteratur, Lund.

Hegde, J., Utne, I.B., Schjølberg, I., Thorkildsen, B., 2018. A Bayesian approach to risk modeling of autonomous subsea intervention operations. Reliability Engineering & System Safety 175, 142–159. https://doi.org/10.1016/J.RESS.2018.03.019.

Holen, S.M., Utne, I.B., Holmen, I.M., Aasjord, H., 2018. Occupational safety in aquaculture - part 1: Injuries in norway. Marine Policy 96, 184–192. https://doi.org/10.1016/j.marpol.2017.08.009.

Hornung, A., Wurm, K.M., Bennewitz, M., Stachniss, C., Burgard, W., 2013. Octomap: an efficient probabilistic 3d mapping framework based on octrees. Autonomous Robots 34, 189–206. https://doi.org/10.1007/s10514-012-9321-0.

International Organization for Standardization, 2018. ISO 31000 - Risk management - Guidelines. URL: http://www.standard.no/no/Nettbutikk/produktkatalogen/Produktpresentasjon/?ProductID = 970175.

Japan Aviation Electronics Industry, L., 2018. Fiber optical gyro jg-35fd. japan aviation electronics industry, ltd Available at: http://www.jae.com/jp/product/aero/gyro_-spec.html (Accessed: 2018-11-16).

Jensen, Ø., Dempster, T., Thorstad, E., Uglem, I., Fredheim, A., 2010. Escapes of fishes from norwegian sea-cage aquaculture: causes, consequences and prevention. Aquaculture Environment Interactions 1, 71–83. https://doi.org/10.3354/aei00008.

Kondo, H., 2001. Development of an autonomous underwater vehicle “tri-dog” toward practical use in shallow water. J Robot Mechatron 13, 205–211.

Lader, P., Dempster, T., Fredheim, A., Jensen, Ø., 2008. Current induced net deformations in full-scale sea-cages for atlantic salmon (salmo salar). Aquacultural Engineering 38, 52–65.

Lau, B., Sprunk, C., Burgard, W., 2013. Efficient grid-based spatial representations for robot navigation in dynamic environments. Robotics and Autonomous Systems 61, 1116–1130. https://doi.org/10.1016/j.robot.2012.08.010.

Leonard, J.J., Durrant-Whyte, H.F., 1991. Mobile robot localization by tracking geometric beacons. IEEE Transactions on Robotics and Automation 7, 376–382. https://doi.org/10.1109/70.88147.

Ma, T., Li, Y., Wang, R., Cong, Z., Gong, Y., 2018. Auv robust bathymetric simultaneous localization and mapping. Ocean Engineering 166, 336–349. https://doi.org/10.1016/j.oceaneng.2018.08.029.

Maki, T., Mizushima, H., Ura, T., Sakamaki, T., Yanagisawa, M., 2012. Auv navigation around jacket structures i: relative localization based on multi-sensor fusion. Journal of Marine Science and Technology 17, 330–339. https://doi.org/10.1007/s00773-012-0165-2.

Mallios, A., Ridao, P., Ribas, D., Hernández, E., 2014. Scan matching slam in underwater environments. Autonomous Robots 36, 181–198. https://doi.org/10.1007/s10514-013-9345-0.

Mathworks, 2018. robotics.occupancymap3d. URL: https://www.mathworks.com/help/robotics/ref/robotics.occupancymap3d-class.html, accessed: 2019-04-11.

Moravec, H.P., 1988. Sensor fusion in certainty grids for mobile robots. AI magazine 9, 61.

Norway, S., 2017. Aquaculture. Available at: https://www.ssb.no/fiskeoppdrett (In Norwegian, accessed: 29.1.2018).

O’Callaghan, S.T., Ramos, F.T., 2012. Gaussian process occupancy maps. The International Journal of Robotics Research 31, 42–62. https://doi.org/10.1177/0278364911421039.

Pairet, E., Hernández, J.D., Lahijanian, M., Carreras, M., 2018. Uncertainty-based online mapping and motion planning for marine robotics guidance. 2018 IEEE/RSJ International Conference on Intelligent Robots and Systems (IROS) 2367–2374. https://doi.org/10.1109/IROS.2018.8593394.

Ramos, F., Ott, L., 2016. Hilbert maps: Scalable continuous occupancy mapping with stochastic gradient descent. The International Journal of Robotics Research 35, 1717–1730. https://doi.org/10.1177/0278364916684382.

Ribas, D., Ridao, P., Tardós, J.D., Neira, J., 2008. Underwater slam in man-made structured environments. Journal of Field Robotics 25, 898–921. https://doi.org/10.1002/rob.20249.

Rundtop, P., Frank, K., 2016. Experimental evaluation of hydroacoustic instruments for rov navigation along aquaculture net pens. Aquacultural Engineering 74, 143–156. https://doi.org/10.1016/j.aquaeng.2016.08.002.

Sandøy, S., Matsuda, T., Sangekar, M., Schjølberg, I., Maki, T., 2019. Scan matching aided rao-blackwellized particle filter with grid mapping for online underwater slam. Robotics and Autonomous Systems Under review.

Stephen, B., Oscar, W.S.B.P., J.M.V, 2011. A featureless approach to efficient bathymetric slam using distributed particle mapping. Journal of Field Robotics 28, 19–39. https://doi.org/10.1002/rob.20382.

Teledyne, 2018. Workhorse navigator - whn 1200. URL: http://www.teledynemarine.com/Lists/Downloads/navigator_datasheet_lr.pdf, (Accessed: 2018-10-25).

Thorvaldsen, T., Holmen, I.M., Moe, H.K., 2015. The escape of fish from norwegian fish farms: Causes, risks and the influence of organisational aspects. Marine Policy 55, 33–38. https://doi.org/10.1016/j.marpol.2015.01.008. URL: http://www.sciencedirect.com/science/article/pii/S0308597X15000196.

Thrun, S., Burgard, W., Fox, D., 2005. Probabilistic robotics. 2005. Massachusetts Institute of Technology, USA.

Tritech, 2018. Micron sonar - ultra compact imaging sonar. Available at: http://www.tritech.co.uk/product/small-rov-mechanical-sector-scanning-sonar-tritech-micron (Accessed: 2018-10-19).

Utne, I., Schjølberg, I., Holmen, I., 2015. Reducing risk in aquaculture by implementing autonomous systems and integrated operations. Safety and Reliability of Complex Engineered Systems. https://doi.org/10.1201/b19094-481.

Utne, I.B., Schjølberg, I., Sandøy, S., Yang, X., Holmen, I.M., 2018. Reducing risk in aquaculture through autonomous underwater operations. PSAM 2018, LA, USA URL: http://psam14.org/proceedings/paper/paper_98_1.pdf.

Vallicrosa, G., Ridao, P., 2018. H-SLAM: Rao-Blackwellized Particle Filter SLAM Using Hilbert Maps, volume 18. https://doi.org/10.3390/s18051386.

Article J3

Localization of a Flexible Underwater Anchor Line using Acoustic Transmitter Tags and Receivers

Stian S. Sandøy, Bent O. A. Haugaløkken, and Ingrid Schjølberg

Applied Acoustics, Elsevier, submitted for review

This article is awaiting publicaton and is not included in NTNU Open

Article C1

Underwater Positioning Using Near Surface Long Baseline Transponder's Induced by Wave Motion

Stian S. Sandøy and Ingrid Schjølberg

ASME 2017. 36th International Conference on
Offshore Mechanics and Arctic Engineering
doi:10.1115/OMAE2017-61742

Proceedings of the ASME 2017 36th International Conference on Ocean, Offshore and Arctic Engineering
OMAE2017
June 25-30, 2017, Trondheim, Norway

OMAE2017-61742

UNDERWATER POSITIONING USING NEAR SURFACE LONG BASELINE TRANSPONDER'S INDUCED BY WAVE MOTION

Stian S. Sandøy
NTNU Norwegian University
of Science and Technology
Department of Marine Technology
Trondheim 7052, Otto Nielsensvei 10
Email: stian.s.sandoy@ntnu.no

Ingrid Schjølberg
NTNU Norwegian University
of Science and Technology
Department of Marine Technology
Trondheim 7052, Otto Nielsensvei 10
Email: ingrid.schjolberg@ntnu.no

ABSTRACT

This paper presents a filter for underwater positioning in an aquaculture environment with demanding weather conditions. The positioning system is based on acoustic transponders mounted at a net pen on the sea surface. The transponders are exposed to oscillations due to wave disturbance. This will have an impact on the accuracy of the positioning system. An extended Kalman filter (EKF) solution has been proposed including a wave motion model integrated with the pseudo-range measurements from the transponders. Simulations show that the proposed filter compensates well for the disturbances.

1 Introduction

1.1 Background and Motivation

Recently, there has been an increased interest in exposed aquaculture due to environmental and spatial limitations in more sheltered areas [1]. Remoteness and harsh environments motivate the use of Underwater Vehicles (UV) in inspection, maintenance, and repair (IMR) operations. Positioning and localization are key technologies for enabling such operations. Global Navigation Satellite Systems (GNSSs) cannot be used under water. However, other technologies like long baseline (LBL), short baseline (SBL) and ultra short baseline (USBL) systems are available [2]. LBL systems use the same principle as GNSS, namely multiple transponders measuring the distance to a receiver, also known as a pseudo-range measurement. Current LBL systems are expensive and mounted on the sea-bed, which is not optimal in an aquaculture environment. In the aquaculture industry, the overall goal is to reduce on-site manual operations for increased safety and reduced risk for workers [3]. Moreover, to keep the cost of installation, operation and maintenance low. One way of doing this is increased use of remote operations and UVs. For efficient UV operations, there is a need for an underwater positioning system. The configuration of an acoustic transponder system for range measurements is a key challenge and is further assessed. The main idea behind this work is to analyze and reduce negative effects that motion in near surface transponders has on a positioning system. The motion is caused by environmental disturbances like current or waves and can create large errors in the position estimate if not contracted. It is essential that this error is as small as possible to ensure an accurate positioning of the UVs.

1.2 Literature review

There has been a considerable amount of work in navigation, which is meant as finding a position relative to some reference [4]. Especially for GNSS/Inertial Navigation System (INS) [21]. However, the environmental disturbance like ocean current and waves on transponders has not been discussed, and is highly relevant in an aquaculture setting near the ocean surface. Surveys on underwater navigation [5, 6] discuss the sensors available, their accuracy and how state estimation can be applied to fuse sensor information together using both dead reckoning

Copyright © 2017 ASME

sensors like accelerometers and gyros to find orientation. A celebrated nonlinear filter for the latter is the complementary filter from [7] and later enhanced in [8] to an attitude observer. A widely used extended Kalman filter (EKF) approach is presented in [9]. Other, various translation observers using Kalman filter (KF) approaches are discussed in literature like [10]. Examples are Unscented KF, Ensemble KF and particle filter. However, in general, the nonlinear KF's are not proven globally stable in estimating position by pseudo ranges. Recently there has been a suggestion to transform the problem into a quasi-linear. The transformation was first suggested in [11]. Use for KF was first developed in [12], which made the implemented observer Global Exponential Stable (GES), but the transformation is optimal with noisy measurements. This can be resolved by using the Exogenous KF (XKF) presented in [13]. The KF using the quasi-linear model are here used as a linearization point for the next KF inheriting the stability properties and the noise reduction. A complete implementation for navigation using pseudo-range measurements is presented in [14]. Later, it has been implemented in combination with attitude filter in [15] using the attitude filter from [8]. However, this implementation dose not account for the biases in LBL systems. This is implemented using the three stage filter in [16, 17]. Study of wave motions and sea states has been a wide research field. Examples can be found in [18–20].

1.3 Main Contribution and Structure

The main contribution of this paper is the integration of a wave filter model with pseudo-range measurements. This is an important contribution since it enables mounting of transponders near the ocean surface on aquaculture structures, without having the need to calculated the position in real time with GNSS. The solution is simulated with measurements from a LBL system setup near the ocean surface, assuming that the mean transponder position is known and there are only oscillating perturbations. Each measurement correlates and can, therefore, be estimated as a single oscillating term.

This paper will first present the problem statement in Section 2. Further in 3, will necessary mathematical models for the problem at hand be designed. From this will Section 4, develop an extended Kalman filter for each case. Results and discussion are presented in sections 5 and 6, followed by conclusion in Section 7.

1.4 Notation

$(\cdot)^T$ is the transposed of a vector or matrix, and $||\cdot||$ is used as the euclidean norm. As the set of real numbers are noted as $\mathbf{R}^{n\times m}$ with the dimension $n\times m$, where no indication $\mathbf{R}$, implies $m=1$ and $n=1$. $0_{p\times q}$ and $I_{p\times q}$ are the zero and identity matrix respectively, with dimension $p\times q$. Position will always be denoted as a vector $p=\begin{bmatrix}x\ y\ z\end{bmatrix}^T\in\mathbf{R}^{3\times 1}$ where x is surge, y is sway and z is heave. Wave motion vector will be designated $p_w=\begin{bmatrix}x_w\ y_w\ z_w\end{bmatrix}^T\in\mathbf{R}^{3\times 1}$. $N(0,\sigma^2)$ is a Normal Gaussian distribution with variance σ^2 and mean zero. $\hat{(\cdot)}$ is the notation for an estimated variable. For a matrix A and value x_i, $A=diag(x_1,\ldots,x_n)\in\mathbf{R}^{\mathbf{n}\times\mathbf{n}}$ means a matrix with diagonal terms x_1 to x_n and zeros everywhere else. For a function $h(x)$ and vector x, $\frac{\partial h(x)}{\partial x}$ is notation for the partial derivative.

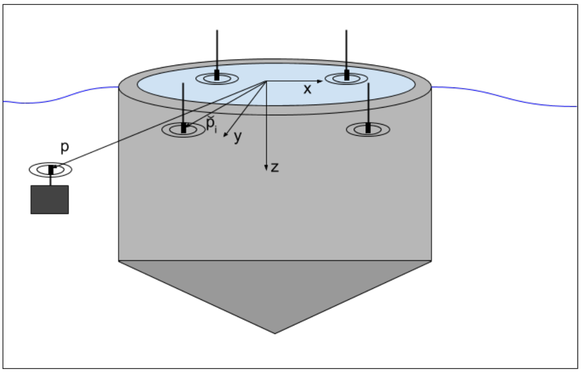

FIGURE 1: **TRANSPONDER CONFIGURATIONS**

2 Problem Statement

The problem of oscillating transponders will be studied in an aquaculture environment around a net pen as seen in Figure 1. Two cases will be discussed. In the former case denoted as A, transponders are rigidly mounted, which is the standard case for a LBL system. In the latter case denoted as B, are transponders mounted near the ocean surface. The case is illustrated in Figure 1. The main difference in these configurations is the near ocean surface disturbance's from wave motion. Here will two different measurement equations describe this deviation. The following section presents these and their assumptions. It should also be mentioned that the reference frame has an origin in the fish cage center at the mean sea surface. Positive z-axis points towards the sea floor and x-axis north. The y-axis complete the right hand, meaning eastward. This is known as the North-East-Down (NED) reference frame [20].

3 Mathematical Modeling

This section presents the mathematical models applied in the EKF. Both measurement and process model equations, are given in this section.

3.1 Measurement Model

Case A: Rigidly Mounted Transponders

Equation (1) assumes that the position for each transponder is known, as stated in Assumption 1. The measurement model is the same formulation as in [16].

$$y_i = \frac{1}{\sqrt{\beta}}(||p - \breve{p}_i|| + \varepsilon_m) = h_i(x) \tag{1}$$

Each pseudo-range measurement from transponder i is noted as $y_i \in \mathbf{R}$. The ROV and transponder position are p and $\breve{p}_i$, respectively. $\beta \in \mathbf{R}$ is a multiplicative bias which account for bias in the speed of sound in water as discussed in [16]. Measurement noise for each transponder is written as $\varepsilon_m \in \mathbf{R}$ in $N(0, \sigma_m^2)$.

Assumption 1. *The transponder position $\breve{p}_i$ is known.*

Case B: Surface Mounted Transponders

The measurement model applied for each pseudo-range from transponder "i" with position $\breve{p}_i$ is modeled in the following equation:

$$y_i = \frac{1}{\sqrt{\beta}}(||p - \breve{p}_i - \breve{p}_{wi}|| + \varepsilon_m) = h_i(x) \tag{2}$$

Equation (2) is similar to (1) with the exception of wave motion term, denoted as $\breve{p}_{wi} \in \mathbf{R}^{3\times 1}$. It assumes that the mean transponder position is known as $\breve{p}_i$ and it is subjected to time varying oscillations, denoted as $\breve{p}_{wi}$. However, each motion $\dot{\breve{p}}_{wi}$ can correlate when placed in a pattern around a fish cage. So estimating all of them will be a waste of computational power. Also, the assumption of uncorrelated process noise in the KF would be violated leading to suboptimal estimates. Therefore, it is simplified to only one wave motion vector p_w, as following:

$$y_i = \frac{1}{\sqrt{\beta}}(||p + p_w - \breve{p}_i|| + \varepsilon_m) = h_i \tag{3}$$

This rough simplification can be justified not only by correlating motion and computational power. If we assume another wave motion spectra different from the transponders, can p_w estimate the oscillations that would be induced in the position estimate without it. Effectively, this can lead to an increased performance without adding too many additional computations or sensors. Finding this spectrum will not be performed here, but a simulation example will be presented in Section 5.

Assumption 2. *The mean transponder position $\breve{p}_i$ is known and the wave frequency spectrum from each transponder can be modeled as a single wave spectrum denoted p_w.*

Mark that for both Case A and B the full measurement vector is denoted as $y = h(x) = \begin{bmatrix} h_1 & \dots & h_m \end{bmatrix}^T \in \mathbf{R}^{m\times 1}$.

3.2 Process Model

Case A and B: Kinematic Model

The EKF process model requires kinematic equations of motion of the vehicle. This model will be the same for Case A and B. The velocity will be modeled as a random walk as following:

$$\dot{p} = A_p p + \varepsilon_p \tag{4}$$

Where $\varepsilon_p \in \mathbf{R}^{3\times 1}$ is $N(0, \sigma_p^2)$ and $A_p = 0_{3\times 3}$. Random walk is used because this case study only takes into account pseudo-range measurements. The velocity is not estimated in this case. It should be remarked that it is simple to also include a velocity state by including accelerometer measurements directly in the process model [14]. This would also improve the position estimates, of course depending on the quality of the accelerometer. However, since this is not the purpose of this paper, it is not taken into account. Only having position estimates also make it possible to further include this in a loosely coupled observer [21].

Case A and B: Bias Model

The sound speed bias in water, β, which are both in Case A and B will be modeled in the same manner as [16], ie. as the following:

$$\dot{\beta} = A_\beta \beta + \varepsilon_\beta \tag{5}$$

Where $A_\beta = 0$ and $\varepsilon_\beta \in \mathbf{R}$ is $N(0, \sigma_\beta^2)$. Note that this is a random walk process.

Case B: Second Order Wave Motion Model

The goal of the wave motion model presented in this section is to separate the low and wave frequency motions. This is illustrated in Figure 2. The blue dashed line is the combined low and wave frequencies, while the red solid and yellow dash-dot line are the separated low and wave frequency motions, respectively. Here is the second-order wave model used for the separation of p and p_w given in Equation (3). This model originated in [19] and can also be found in newer literature [20]. The model is given as following:

$$\begin{bmatrix} \dot{\zeta} \\ \dot{p}_w \end{bmatrix} = A_w \begin{bmatrix} \zeta \\ p_w \end{bmatrix} + E_w \varepsilon_w \in \mathbf{R}^{6\times 1} \tag{6}$$

Copyright © 2017 ASME

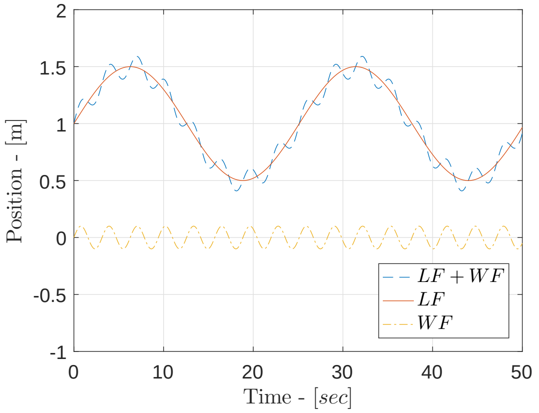

FIGURE 2: **LOW (LF) AND WAVE FREQUENCY (WF) MOTIONS** [20].

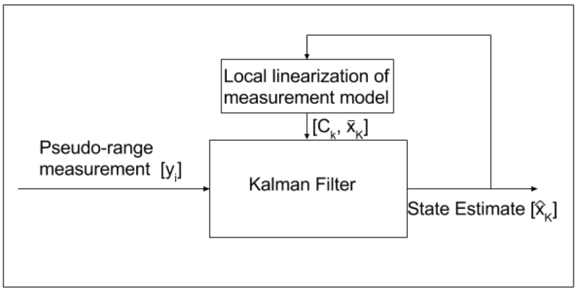

FIGURE 3: **GENERAL STRUCTURE OF EKF** [4].

where $\varepsilon_w \in \mathbf{R}^{3\times1}$ and each noise term is $N(0,1)$. Further, the matrices are defined as the following:

$$A_w = \begin{bmatrix} 0_{3\times3} & I_{3\times3} \\ -\omega_0^2 I_{3\times3} & -2\lambda\,\omega_0 I_{3\times3} \end{bmatrix}, E_w = \begin{bmatrix} 0_{3\times3} \\ K_w \end{bmatrix}$$

where $K_w = diag(\sigma_{w1}, \sigma_{w2}, \sigma_{w3}) \in \mathbf{R}^{3\times3}$.

4 Extended Kalman Filter's Design

The general structure of the EKF for pseudo-range measurements is described in Figure 3 [10]. The filter estimate feedback $\bar{x}_k$, generates a linearized measurement matrix called C_k. Initially in the first iteration $k = 0$, a guess $\bar{x}_0$ is used. The process and measurement equations will in this section be put together to fit the cases. Discrete process model will be defined as following:

$$\dot{x}_k = Ax_{k-1} + D\varepsilon_k \qquad (7)$$

where x_k is the state vector, A is the transition matrix, D is the noise driver matrix and ε_k is the noise vector with uncorrelated white noise terms which is $N(0,\sigma^2)$. The process model of Case A will be on state space form from both Equation (4) and (5). These leads to the following state and noise vectors:

$$x = \begin{bmatrix} p \\ \beta \end{bmatrix}, \varepsilon = \begin{bmatrix} \varepsilon_p \\ \varepsilon_\beta \end{bmatrix}$$

From this it is easy to find the A and D matrix, remark that it needs to be discretized before use in the EKF. Process model of Case B is only an extension of the previous system. The state and noise vectors are defined as following:

$$x = \begin{bmatrix} \zeta \\ p_w \\ p \\ \beta \end{bmatrix}, \varepsilon = \begin{bmatrix} \varepsilon_w \\ \varepsilon_p \\ \varepsilon_\beta \end{bmatrix}$$

Also here are the corresponding A and E matrices easy to derive and is therefore not stated.

For the EKF it is also necessary to have a measurement matrix C_k. This is found by taking the Jacobian of Equation (1) for Case A and (3) for B. This is defined as following:

$$C_k = \frac{\partial h(x)}{\partial x} = \begin{bmatrix} C_{k,1} \\ \vdots \\ C_{k,m} \end{bmatrix} \in \mathbf{R}^{m\times10}$$

where m is the number of pseudo-range measurements. For Case A will the C_k matrix be:

$$\begin{aligned} C_{k,i} &= \frac{\partial h_i(x)}{\partial x}\Big|_{\bar{x}} \\ &= \begin{bmatrix} \frac{p-\check{p}_i}{\sqrt{\beta}||p-\check{p}_i||} & -\frac{||p-\check{p}_i||}{2\beta^{\frac{3}{2}}} \end{bmatrix}\Big|_{\bar{x}} \in \mathbf{R}^{1\times4} \end{aligned}$$

And for each row in Case B it is as following:

$$\begin{aligned} C_{k,i} &= \frac{\partial h_i(x)}{\partial x}\Big|_{\bar{x}} \\ &= \begin{bmatrix} \frac{\partial h_i}{\partial \zeta} & \frac{\partial h_i}{\partial p_w} & \frac{\partial h_i}{\partial p} & \frac{\partial h_i}{\partial \beta} \end{bmatrix}\Big|_{\bar{x}} \end{aligned}$$

Copyright © 2017 ASME

Where

$$
\begin{aligned}
\frac{\partial h_i}{\partial \zeta}\Big|_{\bar{x}} &= 0_{1\times 3} \\
\frac{\partial h_i}{\partial p_w}\Big|_{\bar{x}} = \frac{\partial h_i}{\partial p}\Big|_{\bar{x}} &= \frac{p + p_w - \breve{p}_i}{\sqrt{\beta}||p + p_w - \breve{p}_i||}\Big|_{\bar{x}} \\
\frac{\partial h_i}{\partial \beta}\Big|_{\bar{x}} &= -\frac{||p + p_w - \breve{p}_i||}{2\beta^{\frac{3}{2}}}\Big|_{\bar{x}}
\end{aligned}
$$

Now, that both process and measurement model are derived, can the EKF be stated. The equations are as following [22]:

$$
\begin{aligned}
K_k &= \bar{P}_k C_k^T (C_k \bar{P} C_k^T + R_k)^{-1} \\
\hat{x}_k &= \bar{x}_k + K_k(y_k - h(\bar{x}_k))) \\
P_k &= (I_{n\times n} - K_k C_k)\bar{P}_k \\
\bar{x}_k &= A\hat{x}_{k-1} \\
\bar{P}_k &= AP_{k-1}A^T + D^T QD
\end{aligned}
$$

where $Q \in \mathbf{R}^{n\times n}$ and $R \in \mathbf{R}^{m\times m}$ are the process and sensor noise covariance matrices, respectively. Further, corresponds n and m to the number of states and measurements. P_k is the covariance matrix. Note that $\bar{(\cdot)}$ mark posterior estimates. Also, it should be noted that the first iteration, $k = 0$, are the initial values $\bar{x}_0$ and $\bar{P}_0$ used.

4.1 Observability Analysis

Observability means that we can recreate uniquely all states from the measurement vector y. If this is the case, then the observability matrix of the pair (A, C) have full rank, which means $rank(\mathscr{O}) = n$, where n is the number of states. The matrix is defined as following [10]:

$$
\mathscr{O} = \begin{bmatrix} C_k \\ C_k A \\ \vdots \\ C_k A^{n-1} \end{bmatrix} \tag{8}
$$

Assumption 3. *$m \geq 4$ pseudo-range measurement and all transponder positions is not co-planar.*

Lemma 1. *The pair (A,C) is observable for both Case A and B.*

Proof: It is trivial to calculate the observability matrix in Equation (8). For case A and B, investigating the rank shows that $rank(\mathscr{O}) = 4$ and $\mathscr{O} = 10$, respectively. That is if Assumption 3 is satisfied. From the full rank of Equation (8) in both Case A and B, can observability be concluded. q.e.d.

5 Case Study

This section will present a simulation study of Case A and B. The study includes the two EKF developed in Section 4 and they are implemented in Matlab. The two filters are compared and discussed. The number of transponders are $m = 4$ and are placed such that they are not co-planar with the following positioning:

$$
\begin{aligned}
\breve{p}_1 &= \begin{bmatrix}15 & 0 & 1\end{bmatrix}^T, & \breve{p}_2 &= \begin{bmatrix}0 & 15 & 20\end{bmatrix}^T \\
\breve{p}_3 &= \begin{bmatrix}-15 & 0 & 5\end{bmatrix}^T, & \breve{p}_4 &= \begin{bmatrix}0 & -15 & 16\end{bmatrix}^T
\end{aligned}
$$

The position of the receiver at the ROV is kept constant at $p = \begin{bmatrix}1 & 2 & 3\end{bmatrix}^T$. The measurements for Case A are generated from Equation (1) and correspondingly (3) for B. To simulate the wave motion p_w in Equation (3), a second order wave model was used. Parameters in the wave model are set to $\omega_0 = 0.8$, $\lambda = 0.1017$ and $\sigma_{wi} = 0.8367$ for $i = 1,2,3$. This means that the wave frequency estimated, is defined for a spectrum in each direction. The speed of sound bias in water is set to $\beta = 0.95$ for both cases. The measurement noise is $\sigma_m^2 = 1e-2$. The time step used for discretization and simulation is $\Delta t = 0.2$.

For the initialization of the EKF in Case A is $\bar{x}_0 = \begin{bmatrix}0_{1\times 3} & 1\end{bmatrix}^T$. Further, sensor noise matrix is $R = diag(\sigma_m^2, \sigma_m^2, \sigma_m^2, \sigma_m^2)$ and the process noise is $Q = diag(\sigma_p^2, \sigma_p^2, \sigma_p^2, \sigma_p^2, \sigma_\beta^2) \in \mathbf{R}^{4\times 4}$. Here are $\sigma_p^2 = 1e-4$ and $\sigma_\beta^2 = 1e-6$. The covariance matrix is initial set to $P_0 = diag(0.1, 0.1, 0.1, 1e-4) \in \mathbf{R}^{4\times 4}$.

For Case B the model is the initial states set to $\bar{x}_0 = \begin{bmatrix}0_{1\times 9} & 1\end{bmatrix}^T$. The sensor noise covariance matrix R is the same as in Case A, but the process noise covariance matrix is $Q = diag(1_{1\times 3}, \sigma_p^2, \sigma_p^2, \sigma_p^2, \sigma_p^2, \sigma_\beta^2) \in \mathbf{R}^{7\times 7}$. The inital covariance matrix is set to $P_0 = diag((1e-3)_{1\times 6}, (0.1)_{1\times 3}, 1e-4) \in \mathbf{R}^{10\times 10}$ where the subscripts denote dimensions.

RMS	$x[m]$	$y[m]$	$z[m]$	$beta[]$
EKF Case A	0.009	0.009	0.0336	0.0013
EKF Case B	0.013	0.013	0.049	0.0014

TABLE 1: **RMS ERROR FOR CASE A and B**

6 Simulation Results and Discussion

The simulation results from the case study in the previous section are presented in Table 1 and Figure 5-4. Both case A and B are run for 300 seconds.

Table 1 presents the Root Mean Square (RMS) for the position and bias estimation. It is apparent that the RMS performance

Copyright © 2017 ASME

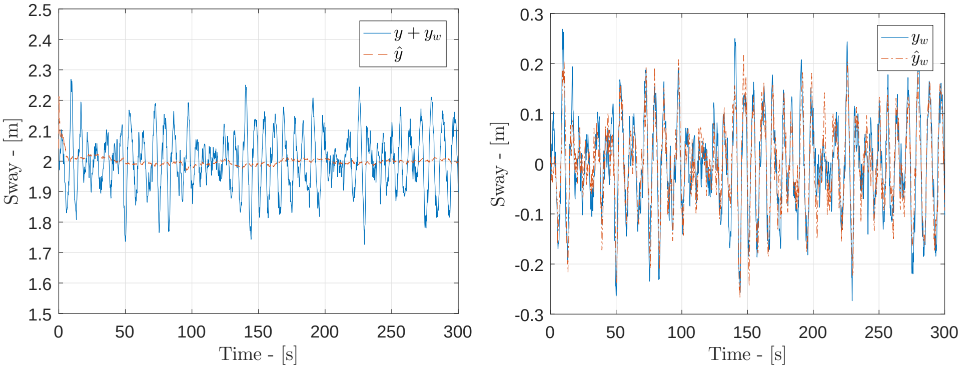

SWAY ESTIMATED POSITION.

(b) SWAY ESTIMATED WAVE POSITION.

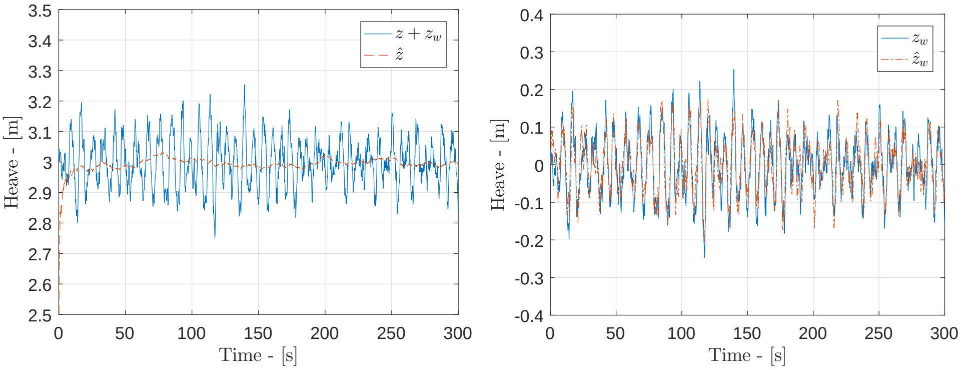

(c) **HEAVE ESTIMATED POSITION.**

(d) **HEAVE ESTIMATED WAVE POSITION.**

FIGURE 4: **ESTIMATED STATES WITH EKF INCLUDING WAVE FILTER.**

is similar for the cases, with naturally slightly worse performance in Case B. Both A and B have a small RMS in surge, sway and heave. However, heave has a larger RMS, which is due to the short transponder placement in z-direction. The estimated biases have very similar RMS performance.

Figure 4 presents how the wave filtering implementation in Case B separates the wave and low-frequency motion in sway and heave as exemplified in Figure 2. Figure 4a has one plot showing the combination of real low and wave frequency motions, $y + y_w$, shown by a solid blue line. The other plot in the figure is estimated low-frequency motion, $\hat{y}$ in a red dashed line. From this, we can see that the estimate converges smoothly to the real position at $y = 2$, as defined in the simulation study. Further, the wave frequency motion is filtered away. It is important to note that the assumed noise variance is relatively low at $\sigma_p^2 = 1e-4$. Meaning that the model is trusted more than the measurements. This is good in this case since $\dot{p} = 0$. Figure 4b shows the simulated wave frequency y_w against estimated $\hat{y}_w$ in the blue solid line. Since the $\hat{y}_w$ is very similar to the simulated y_w means that we have a good estimate. The resulting estimates in heave motion are shown in Figure 4c and 4d. Here does also the heave position estimate, $\hat{z}$ converge towards $z = 3$. The convergence time seems to be a bit longer, but it can be explained by the transponder positions and that it is the state furthest away from the initial condition at $\bar{z} = 0$. The surge results are left out here since the result is very similar to the results in sway. Figure 5 shows how the covariance matrix converges towards steady state values. This effectively means that the filter converges. However, since the EKF is not proven globally stable, this can't be guaranteed. But this simulation shows how well the wave motion can be estimated.

Copyright © 2017 ASME

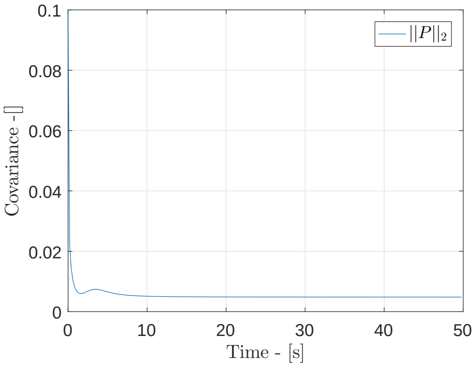

FIGURE 5: **NORM OF COVARIANCE MATRIX IN CASE B** ($||P||_2$)

7 Conclusion and Further Work

In this paper, a filter for underwater positioning in an aquaculture environment is presented. Demanding weather conditions will impose oscillations on the transponders near the surface area. An EKF solution has been proposed including a wave motion model integrated with pseudo-range measurements. This was simulated in Matlab with a predefined case study. The results show that the filter compensates for the wave motion and gives almost the same performance as a system without environmental disturbances. Further work will include experimental analyzes of real wave motion spectra. Fusion of more sensors integrated into the same filter will increase performance.

ACKNOWLEDGMENT

This work is funded by the Norwegian University of Science and Technology (NTNU), Norwegian Research Council projects Reducing Risk in Aquaculture (254913) and SFI Exposed (237790).

REFERENCES

[1] Bjelland, H. V., and et.al. "Exposed aquaculture in norway". In OCEANS 2015 - MTS/IEEE Washington, pp. 1–10.

[2] Christ, R. D., and Wernli Sr, R. L., 2013. *The ROV manual: a user guide for remotely operated vehicles*. Butterworth-Heinemann.

[3] Utne, I. B., Schjolberg, I., and Holmen, I. M., 2015. Reducing risk to aquaculture workers by autonomous systems and operations. i: Safety and reliability of complex engineered systems.

[4] Farrell, J., 2008. *Aided Navigation: GPS with High Rate Sensors*. McGraw-Hill Education.

[5] Kinsey, J. C., Eustice, R. M., and Whitcomb, L. L. "A survey of underwater vehicle navigation: Recent advances and new challenges". In IFAC Conference of Manoeuvering and Control of Marine Craft, Vol. 88.

[6] Leonard, J. J., and Bahr, A., 2016. *Autonomous Underwater Vehicle Navigation*. Springer International Publishing, Cham, pp. 341–358.

[7] Mahony, R., Hamel, T., and Pflimlin, J. M., 2008. "Nonlinear complementary filters on the special orthogonal group". *IEEE Transactions on Automatic Control,* ***53***(5), pp. 1203–1218.

[8] Grip, H. F., Fossen, T. I., Johansen, T. A., and Saberi, A., 2015. "Globally exponentially stable attitude and gyro bias estimation with application to gnss/ins integration". *Automatica,* ***51***, pp. 158–166.

[9] Markley, F. L., 2003. "Attitude error representations for kalman filtering". *Journal of Guidance, Control, and Dynamics,* ***26***(2), pp. 311–317.

[10] Chen, C.-T., 2013. *Linear system theory and design*, fourth edition. ed. The Oxford series in electrical and computer engineering. Oxford University Press, New York.

[11] Bancroft, S., 1985. "An algebraic solution of the gps equations". *IEEE Transactions on Aerospace and Electronic Systems,* ***AES-21***(1), pp. 56–59.

[12] Batista, P. "Ges long baseline navigation with unknown sound velocity and discrete-time range measurements". In 52nd IEEE Conference on Decision and Control, pp. 6176–6181.

[13] Johansen, T. A., and Fossen, T. I., 2016. "The exogenous kalman filter (xkf)". *International Journal of Control*, pp. 1–7.

[14] Johansen, T. A., Fossen, T. I., and Goodwin, G. C., 2016. "Three-stage filter for position estimation using pseudorange measurements". *IEEE Transactions on Aerospace and Electronic Systems,* ***52***(4), pp. 1631–1643.

[15] Johansen, T. A., and Fossen, T. I., 2016. "Nonlinear observer for tightly coupled integration of pseudorange and inertial measurements". *IEEE Transactions on Control Systems Technology,* ***24***(6), pp. 2199–2206.

[16] Stovner, B. B., Johansen, T. A., Fossen, T. I., and Schjolberg, I. "Three-stage filter for position and velocity estimation from long baseline measurements with unknown wave speed". In 2016 American Control Conference (ACC), pp. 4532–4538.

[17] Jorgensen, E. K., Johansen, T. A., and Schjolberg, I., 2016. "Enhanced hydroacoustic range robustness of three-stage position filter based on long baseline measurements with unknown wave speed*". *IFAC-PapersOnLine,* ***49***(23), pp. 61–67.

[18] Faltinsen, O. M., 1990. *Sea loads on ships and offshore structures*. Cambridge ocean technology series. Cambridge University Press, Cambridge.

Copyright © 2017 ASME

[19] Balchen, J. G., Jenssen, N. A., and Saelid, S. "Dynamic positioning using kalman filtering and optimal control theory". In IFAC/IFIP symposium on automation in offshore oil field operation, Vol. 183, p. 186.

[20] Fossen, T. I., 2011. *Handbook of Marine Craft Hydrodynamics and Motion Control*. Wiley.

[21] Groves, P. D., 2008. *Principles of GNSS, inertial, and multi-sensor integrated navigation systems*. Artech House, Boston/ London.

[22] Brown, R. G., and Hwang, P. Y. C., 2012. *Introduction to Random Signals and Applied Kalman Filtering with Matlab Exercises, 4th Edition*. Introduction to random signals and applied Kalman filtering. John Wiley and Sons.

Copyright © 2017 ASME

Article C2

Experimental verification of underwater positioning system in aquaculture

Stian S. Sandøy and Ingrid Schjølberg
IEEE Oceans Aberdeen 2017
10.1109/OCEANSE.2017.8084947

This article is not included due to copyright
available at
https://doi.org/10.1109/OCEANSE.2017.8084947

Article C3

Rao-Blackwellized Particle Filter with Grid-Mapping for AUV SLAM using Forward-Looking Sonar

Stian S. Sandøy, Takumi Matsuda,
Toshihiro Maki and Ingrid Schjølberg
IEEE Oceans Kobe 2018
10.1109/OCEANSKOBE.2018.8559416

This article is not included due to copyright
available at
https://doi.org/10.1109/OCEANSKOBE.2018.8559416

Article C4

Probabilistic Localization and Mapping of Flexible Underwater Structures

Bent O. A. Haugaløkken, Stian S. Sandøy, Ingrid Schjølberg,
Jo A. Alfredsen and Ingrid B. Utne

European Control Conference 2018
10.23919/ECC.2018.8550498

This article is not included due to copyright
available at
https://doi.org/10.23919/ECC.2018.8550498

Part III

Published Theses at Department of Marine Technology - NTNU

Previous PhD theses published at the Department of Marine Technology (earlier: Faculty of Marine Technology)
NORWEGIAN UNIVERSITY OF SCIENCE AND TECHNOLOGY

Report No.	Author	Title
	Kavlie, Dag	Optimization of Plane Elastic Grillages, 1967
	Hansen, Hans R.	Man-Machine Communication and Data-Storage Methods in Ship Structural Design, 1971
	Gisvold, Kaare M.	A Method for non-linear mixed -integer programming and its Application to Design Problems, 1971
	Lund, Sverre	Tanker Frame Optimalization by means of SUMT-Transformation and Behaviour Models, 1971
	Vinje, Tor	On Vibration of Spherical Shells Interacting with Fluid, 1972
	Lorentz, Jan D.	Tank Arrangement for Crude Oil Carriers in Accordance with the new Anti-Pollution Regulations, 1975
	Carlsen, Carl A.	Computer-Aided Design of Tanker Structures, 1975
	Larsen, Carl M.	Static and Dynamic Analysis of Offshore Pipelines during Installation, 1976
UR-79-01	Brigt Hatlestad, MK	The finite element method used in a fatigue evaluation of fixed offshore platforms. (Dr.Ing. Thesis)
UR-79-02	Erik Pettersen, MK	Analysis and design of cellular structures. (Dr.Ing. Thesis)
UR-79-03	Sverre Valsgård, MK	Finite difference and finite element methods applied to nonlinear analysis of plated structures. (Dr.Ing. Thesis)
UR-79-04	Nils T. Nordsve, MK	Finite element collapse analysis of structural members considering imperfections and stresses due to fabrication. (Dr.Ing. Thesis)
UR-79-05	Ivar J. Fylling, MK	Analysis of towline forces in ocean towing systems. (Dr.Ing. Thesis)
UR-80-06	Nils Sandsmark, MM	Analysis of Stationary and Transient Heat Conduction by the Use of the Finite Element Method. (Dr.Ing. Thesis)
UR-80-09	Sverre Haver, MK	Analysis of uncertainties related to the stochastic modeling of ocean waves. (Dr.Ing. Thesis)
UR-81-15	Odland, Jonas	On the Strength of welded Ring stiffened cylindrical Shells primarily subjected to axial Compression
UR-82-17	Engesvik, Knut	Analysis of Uncertainties in the fatigue Capacity of

		Welded Joints
UR-82-18	Rye, Henrik	Ocean wave groups
UR-83-30	Eide, Oddvar Inge	On Cumulative Fatigue Damage in Steel Welded Joints
UR-83-33	Mo, Olav	Stochastic Time Domain Analysis of Slender Offshore Structures
UR-83-34	Amdahl, Jørgen	Energy absorption in Ship-platform impacts
UR-84-37	Mørch, Morten	Motions and mooring forces of semi submersibles as determined by full-scale measurements and theoretical analysis
UR-84-38	Soares, C. Guedes	Probabilistic models for load effects in ship structures
UR-84-39	Aarsnes, Jan V.	Current forces on ships
UR-84-40	Czujko, Jerzy	Collapse Analysis of Plates subjected to Biaxial Compression and Lateral Load
UR-85-46	Alf G. Engseth, MK	Finite element collapse analysis of tubular steel offshore structures. (Dr.Ing. Thesis)
UR-86-47	Dengody Sheshappa, MP	A Computer Design Model for Optimizing Fishing Vessel Designs Based on Techno-Economic Analysis. (Dr.Ing. Thesis)
UR-86-48	Vidar Aanesland, MH	A Theoretical and Numerical Study of Ship Wave Resistance. (Dr.Ing. Thesis)
UR-86-49	Heinz-Joachim Wessel, MK	Fracture Mechanics Analysis of Crack Growth in Plate Girders. (Dr.Ing. Thesis)
UR-86-50	Jon Taby, MK	Ultimate and Post-ultimate Strength of Dented Tubular Members. (Dr.Ing. Thesis)
UR-86-51	Walter Lian, MH	A Numerical Study of Two-Dimensional Separated Flow Past Bluff Bodies at Moderate KC-Numbers. (Dr.Ing. Thesis)
UR-86-52	Bjørn Sortland, MH	Force Measurements in Oscillating Flow on Ship Sections and Circular Cylinders in a U-Tube Water Tank. (Dr.Ing. Thesis)
UR-86-53	Kurt Strand, MM	A System Dynamic Approach to One-dimensional Fluid Flow. (Dr.Ing. Thesis)
UR-86-54	Arne Edvin Løken, MH	Three Dimensional Second Order Hydrodynamic Effects on Ocean Structures in Waves. (Dr.Ing. Thesis)
UR-86-55	Sigurd Falch, MH	A Numerical Study of Slamming of Two-Dimensional Bodies. (Dr.Ing. Thesis)
UR-87-56	Arne Braathen, MH	Application of a Vortex Tracking Method to the Prediction of Roll Damping of a Two-Dimension Floating Body. (Dr.Ing. Thesis)

UR-87-57	Bernt Leira, MK	Gaussian Vector Processes for Reliability Analysis involving Wave-Induced Load Effects. (Dr.Ing. Thesis)
UR-87-58	Magnus Småvik, MM	Thermal Load and Process Characteristics in a Two-Stroke Diesel Engine with Thermal Barriers (in Norwegian). (Dr.Ing. Thesis)
MTA-88-59	Bernt Arild Bremdal, MP	An Investigation of Marine Installation Processes – A Knowledge - Based Planning Approach. (Dr.Ing. Thesis)
MTA-88-60	Xu Jun, MK	Non-linear Dynamic Analysis of Space-framed Offshore Structures. (Dr.Ing. Thesis)
MTA-89-61	Gang Miao, MH	Hydrodynamic Forces and Dynamic Responses of Circular Cylinders in Wave Zones. (Dr.Ing. Thesis)
MTA-89-62	Martin Greenhow, MH	Linear and Non-Linear Studies of Waves and Floating Bodies. Part I and Part II. (Dr.Techn. Thesis)
MTA-89-63	Chang Li, MH	Force Coefficients of Spheres and Cubes in Oscillatory Flow with and without Current. (Dr.Ing. Thesis
MTA-89-64	Hu Ying, MP	A Study of Marketing and Design in Development of Marine Transport Systems. (Dr.Ing. Thesis)
MTA-89-65	Arild Jæger, MH	Seakeeping, Dynamic Stability and Performance of a Wedge Shaped Planing Hull. (Dr.Ing. Thesis)
MTA-89-66	Chan Siu Hung, MM	The dynamic characteristics of tilting-pad bearings
MTA-89-67	Kim Wikstrøm, MP	Analysis av projekteringen for ett offshore projekt. (Licenciat-avhandling)
MTA-89-68	Jiao Guoyang, MK	Reliability Analysis of Crack Growth under Random Loading, considering Model Updating. (Dr.Ing. Thesis)
MTA-89-69	Arnt Olufsen, MK	Uncertainty and Reliability Analysis of Fixed Offshore Structures. (Dr.Ing. Thesis)
MTA-89-70	Wu Yu-Lin, MR	System Reliability Analyses of Offshore Structures using improved Truss and Beam Models. (Dr.Ing. Thesis)
MTA-90-71	Jan Roger Hoff, MH	Three-dimensional Green function of a vessel with forward speed in waves. (Dr.Ing. Thesis)
MTA-90-72	Rong Zhao, MH	Slow-Drift Motions of a Moored Two-Dimensional Body in Irregular Waves. (Dr.Ing. Thesis)
MTA-90-73	Atle Minsaas, MP	Economical Risk Analysis. (Dr.Ing. Thesis)
MTA-90-74	Knut-Aril Farnes, MK	Long-term Statistics of Response in Non-linear Marine Structures. (Dr.Ing. Thesis)
MTA-90-75	Torbjørn Sotberg, MK	Application of Reliability Methods for Safety Assessment of Submarine Pipelines. (Dr.Ing.

		Thesis)
MTA-90-76	Zeuthen, Steffen, MP	SEAMAID. A computational model of the design process in a constraint-based logic programming environment. An example from the offshore domain. (Dr.Ing. Thesis)
MTA-91-77	Haagensen, Sven, MM	Fuel Dependant Cyclic Variability in a Spark Ignition Engine - An Optical Approach. (Dr.Ing. Thesis)
MTA-91-78	Løland, Geir, MH	Current forces on and flow through fish farms. (Dr.Ing. Thesis)
MTA-91-79	Hoen, Christopher, MK	System Identification of Structures Excited by Stochastic Load Processes. (Dr.Ing. Thesis)
MTA-91-80	Haugen, Stein, MK	Probabilistic Evaluation of Frequency of Collision between Ships and Offshore Platforms. (Dr.Ing. Thesis)
MTA-91-81	Sødahl, Nils, MK	Methods for Design and Analysis of Flexible Risers. (Dr.Ing. Thesis)
MTA-91-82	Ormberg, Harald, MK	Non-linear Response Analysis of Floating Fish Farm Systems. (Dr.Ing. Thesis)
MTA-91-83	Marley, Mark J., MK	Time Variant Reliability under Fatigue Degradation. (Dr.Ing. Thesis)
MTA-91-84	Krokstad, Jørgen R., MH	Second-order Loads in Multidirectional Seas. (Dr.Ing. Thesis)
MTA-91-85	Molteberg, Gunnar A., MM	The Application of System Identification Techniques to Performance Monitoring of Four Stroke Turbocharged Diesel Engines. (Dr.Ing. Thesis)
MTA-92-86	Mørch, Hans Jørgen Bjelke, MH	Aspects of Hydrofoil Design: with Emphasis on Hydrofoil Interaction in Calm Water. (Dr.Ing. Thesis)
MTA-92-87	Chan Siu Hung, MM	Nonlinear Analysis of Rotordynamic Instabilities in Highspeed Turbomachinery. (Dr.Ing. Thesis)
MTA-92-88	Bessason, Bjarni, MK	Assessment of Earthquake Loading and Response of Seismically Isolated Bridges. (Dr.Ing. Thesis)
MTA-92-89	Langli, Geir, MP	Improving Operational Safety through exploitation of Design Knowledge - an investigation of offshore platform safety. (Dr.Ing. Thesis)
MTA-92-90	Sævik, Svein, MK	On Stresses and Fatigue in Flexible Pipes. (Dr.Ing. Thesis)
MTA-92-91	Ask, Tor Ø., MM	Ignition and Flame Growth in Lean Gas-Air Mixtures. An Experimental Study with a Schlieren System. (Dr.Ing. Thesis)
MTA-86-92	Hessen, Gunnar, MK	Fracture Mechanics Analysis of Stiffened Tubular Members. (Dr.Ing. Thesis)

MTA-93-93	Steinebach, Christian, MM	Knowledge Based Systems for Diagnosis of Rotating Machinery. (Dr.Ing. Thesis)
MTA-93-94	Dalane, Jan Inge, MK	System Reliability in Design and Maintenance of Fixed Offshore Structures. (Dr.Ing. Thesis)
MTA-93-95	Steen, Sverre, MH	Cobblestone Effect on SES. (Dr.Ing. Thesis)
MTA-93-96	Karunakaran, Daniel, MK	Nonlinear Dynamic Response and Reliability Analysis of Drag-dominated Offshore Platforms. (Dr.Ing. Thesis)
MTA-93-97	Hagen, Arnulf, MP	The Framework of a Design Process Language. (Dr.Ing. Thesis)
MTA-93-98	Nordrik, Rune, MM	Investigation of Spark Ignition and Autoignition in Methane and Air Using Computational Fluid Dynamics and Chemical Reaction Kinetics. A Numerical Study of Ignition Processes in Internal Combustion Engines. (Dr.Ing. Thesis)
MTA-94-99	Passano, Elizabeth, MK	Efficient Analysis of Nonlinear Slender Marine Structures. (Dr.Ing. Thesis)
MTA-94-100	Kvålsvold, Jan, MH	Hydroelastic Modelling of Wetdeck Slamming on Multihull Vessels. (Dr.Ing. Thesis)
MTA-94-102	Bech, Sidsel M., MK	Experimental and Numerical Determination of Stiffness and Strength of GRP/PVC Sandwich Structures. (Dr.Ing. Thesis)
MTA-95-103	Paulsen, Hallvard, MM	A Study of Transient Jet and Spray using a Schlieren Method and Digital Image Processing. (Dr.Ing. Thesis)
MTA-95-104	Hovde, Geir Olav, MK	Fatigue and Overload Reliability of Offshore Structural Systems, Considering the Effect of Inspection and Repair. (Dr.Ing. Thesis)
MTA-95-105	Wang, Xiaozhi, MK	Reliability Analysis of Production Ships with Emphasis on Load Combination and Ultimate Strength. (Dr.Ing. Thesis)
MTA-95-106	Ulstein, Tore, MH	Nonlinear Effects of a Flexible Stern Seal Bag on Cobblestone Oscillations of an SES. (Dr.Ing. Thesis)
MTA-95-107	Solaas, Frøydis, MH	Analytical and Numerical Studies of Sloshing in Tanks. (Dr.Ing. Thesis)
MTA-95-108	Hellan, Øyvind, MK	Nonlinear Pushover and Cyclic Analyses in Ultimate Limit State Design and Reassessment of Tubular Steel Offshore Structures. (Dr.Ing. Thesis)
MTA-95-109	Hermundstad, Ole A., MK	Theoretical and Experimental Hydroelastic Analysis of High Speed Vessels. (Dr.Ing. Thesis)
MTA-96-110	Bratland, Anne K., MH	Wave-Current Interaction Effects on Large-Volume Bodies in Water of Finite Depth. (Dr.Ing. Thesis)
MTA-96-111	Herfjord, Kjell, MH	A Study of Two-dimensional Separated Flow by a Combination of the Finite Element Method and

		Navier-Stokes Equations. (Dr.Ing. Thesis)
MTA-96-112	Æsøy, Vilmar, MM	Hot Surface Assisted Compression Ignition in a Direct Injection Natural Gas Engine. (Dr.Ing. Thesis)
MTA-96-113	Eknes, Monika L., MK	Escalation Scenarios Initiated by Gas Explosions on Offshore Installations. (Dr.Ing. Thesis)
MTA-96-114	Erikstad, Stein O., MP	A Decision Support Model for Preliminary Ship Design. (Dr.Ing. Thesis)
MTA-96-115	Pedersen, Egil, MH	A Nautical Study of Towed Marine Seismic Streamer Cable Configurations. (Dr.Ing. Thesis)
MTA-97-116	Moksnes, Paul O., MM	Modelling Two-Phase Thermo-Fluid Systems Using Bond Graphs. (Dr.Ing. Thesis)
MTA-97-117	Halse, Karl H., MK	On Vortex Shedding and Prediction of Vortex-Induced Vibrations of Circular Cylinders. (Dr.Ing. Thesis)
MTA-97-118	Igland, Ragnar T., MK	Reliability Analysis of Pipelines during Laying, considering Ultimate Strength under Combined Loads. (Dr.Ing. Thesis)
MTA-97-119	Pedersen, Hans-P., MP	Levendefiskteknologi for fiskefartøy. (Dr.Ing. Thesis)
MTA-98-120	Vikestad, Kyrre, MK	Multi-Frequency Response of a Cylinder Subjected to Vortex Shedding and Support Motions. (Dr.Ing. Thesis)
MTA-98-121	Azadi, Mohammad R. E., MK	Analysis of Static and Dynamic Pile-Soil-Jacket Behaviour. (Dr.Ing. Thesis)
MTA-98-122	Ulltang, Terje, MP	A Communication Model for Product Information. (Dr.Ing. Thesis)
MTA-98-123	Torbergsen, Erik, MM	Impeller/Diffuser Interaction Forces in Centrifugal Pumps. (Dr.Ing. Thesis)
MTA-98-124	Hansen, Edmond, MH	A Discrete Element Model to Study Marginal Ice Zone Dynamics and the Behaviour of Vessels Moored in Broken Ice. (Dr.Ing. Thesis)
MTA-98-125	Videiro, Paulo M., MK	Reliability Based Design of Marine Structures. (Dr.Ing. Thesis)
MTA-99-126	Mainçon, Philippe, MK	Fatigue Reliability of Long Welds Application to Titanium Risers. (Dr.Ing. Thesis)
MTA-99-127	Haugen, Elin M., MH	Hydroelastic Analysis of Slamming on Stiffened Plates with Application to Catamaran Wetdecks. (Dr.Ing. Thesis)
MTA-99-128	Langhelle, Nina K., MK	Experimental Validation and Calibration of Nonlinear Finite Element Models for Use in Design of Aluminium Structures Exposed to Fire. (Dr.Ing. Thesis)
MTA-99-	Berstad, Are J., MK	Calculation of Fatigue Damage in Ship Structures.

129		(Dr.Ing. Thesis)
MTA-99-130	Andersen, Trond M., MM	Short Term Maintenance Planning. (Dr.Ing. Thesis)
MTA-99-131	Tveiten, Bård Wathne, MK	Fatigue Assessment of Welded Aluminium Ship Details. (Dr.Ing. Thesis)
MTA-99-132	Søreide, Fredrik, MP	Applications of underwater technology in deep water archaeology. Principles and practice. (Dr.Ing. Thesis)
MTA-99-133	Tønnessen, Rune, MH	A Finite Element Method Applied to Unsteady Viscous Flow Around 2D Blunt Bodies With Sharp Corners. (Dr.Ing. Thesis)
MTA-99-134	Elvekrok, Dag R., MP	Engineering Integration in Field Development Projects in the Norwegian Oil and Gas Industry. The Supplier Management of Norne. (Dr.Ing. Thesis)
MTA-99-135	Fagerholt, Kjetil, MP	Optimeringsbaserte Metoder for Ruteplanlegging innen skipsfart. (Dr.Ing. Thesis)
MTA-99-136	Bysveen, Marie, MM	Visualization in Two Directions on a Dynamic Combustion Rig for Studies of Fuel Quality. (Dr.Ing. Thesis)
MTA-2000-137	Storteig, Eskild, MM	Dynamic characteristics and leakage performance of liquid annular seals in centrifugal pumps. (Dr.Ing. Thesis)
MTA-2000-138	Sagli, Gro, MK	Model uncertainty and simplified estimates of long term extremes of hull girder loads in ships. (Dr.Ing. Thesis)
MTA-2000-139	Tronstad, Harald, MK	Nonlinear analysis and design of cable net structures like fishing gear based on the finite element method. (Dr.Ing. Thesis)
MTA-2000-140	Kroneberg, André, MP	Innovation in shipping by using scenarios. (Dr.Ing. Thesis)
MTA-2000-141	Haslum, Herbjørn Alf, MH	Simplified methods applied to nonlinear motion of spar platforms. (Dr.Ing. Thesis)
MTA-2001-142	Samdal, Ole Johan, MM	Modelling of Degradation Mechanisms and Stressor Interaction on Static Mechanical Equipment Residual Lifetime. (Dr.Ing. Thesis)
MTA-2001-143	Baarholm, Rolf Jarle, MH	Theoretical and experimental studies of wave impact underneath decks of offshore platforms. (Dr.Ing. Thesis)
MTA-2001-144	Wang, Lihua, MK	Probabilistic Analysis of Nonlinear Wave-induced Loads on Ships. (Dr.Ing. Thesis)
MTA-2001-145	Kristensen, Odd H. Holt, MK	Ultimate Capacity of Aluminium Plates under Multiple Loads, Considering HAZ Properties. (Dr.Ing. Thesis)
MTA-2001-146	Greco, Marilena, MH	A Two-Dimensional Study of Green-Water

		Loading. (Dr.Ing. Thesis)
MTA-2001-147	Heggelund, Svein E., MK	Calculation of Global Design Loads and Load Effects in Large High Speed Catamarans. (Dr.Ing. Thesis)
MTA-2001-148	Babalola, Olusegun T., MK	Fatigue Strength of Titanium Risers – Defect Sensitivity. (Dr.Ing. Thesis)
MTA-2001-149	Mohammed, Abuu K., MK	Nonlinear Shell Finite Elements for Ultimate Strength and Collapse Analysis of Ship Structures. (Dr.Ing. Thesis)
MTA-2002-150	Holmedal, Lars E., MH	Wave-current interactions in the vicinity of the sea bed. (Dr.Ing. Thesis)
MTA-2002-151	Rognebakke, Olav F., MH	Sloshing in rectangular tanks and interaction with ship motions. (Dr.Ing. Thesis)
MTA-2002-152	Lader, Pål Furset, MH	Geometry and Kinematics of Breaking Waves. (Dr.Ing. Thesis)
MTA-2002-153	Yang, Qinzheng, MH	Wash and wave resistance of ships in finite water depth. (Dr.Ing. Thesis)
MTA-2002-154	Melhus, Øyvin, MM	Utilization of VOC in Diesel Engines. Ignition and combustion of VOC released by crude oil tankers. (Dr.Ing. Thesis)
MTA-2002-155	Ronæss, Marit, MH	Wave Induced Motions of Two Ships Advancing on Parallel Course. (Dr.Ing. Thesis)
MTA-2002-156	Økland, Ole D., MK	Numerical and experimental investigation of whipping in twin hull vessels exposed to severe wet deck slamming. (Dr.Ing. Thesis)
MTA-2002-157	Ge, Chunhua, MK	Global Hydroelastic Response of Catamarans due to Wet Deck Slamming. (Dr.Ing. Thesis)
MTA-2002-158	Byklum, Eirik, MK	Nonlinear Shell Finite Elements for Ultimate Strength and Collapse Analysis of Ship Structures. (Dr.Ing. Thesis)
IMT-2003-1	Chen, Haibo, MK	Probabilistic Evaluation of FPSO-Tanker Collision in Tandem Offloading Operation. (Dr.Ing. Thesis)
IMT-2003-2	Skaugset, Kjetil Bjørn, MK	On the Suppression of Vortex Induced Vibrations of Circular Cylinders by Radial Water Jets. (Dr.Ing. Thesis)
IMT-2003-3	Chezhian, Muthu	Three-Dimensional Analysis of Slamming. (Dr.Ing. Thesis)
IMT-2003-4	Buhaug, Øyvind	Deposit Formation on Cylinder Liner Surfaces in Medium Speed Engines. (Dr.Ing. Thesis)
IMT-2003-5	Tregde, Vidar	Aspects of Ship Design: Optimization of Aft Hull with Inverse Geometry Design. (Dr.Ing. Thesis)
IMT-	Wist, Hanne Therese	Statistical Properties of Successive Ocean Wave

2003-6		Parameters. (Dr.Ing. Thesis)
IMT-2004-7	Ransau, Samuel	Numerical Methods for Flows with Evolving Interfaces. (Dr.Ing. Thesis)
IMT-2004-8	Soma, Torkel	Blue-Chip or Sub-Standard. A data interrogation approach of identity safety characteristics of shipping organization. (Dr.Ing. Thesis)
IMT-2004-9	Ersdal, Svein	An experimental study of hydrodynamic forces on cylinders and cables in near axial flow. (Dr.Ing. Thesis)
IMT-2005-10	Brodtkorb, Per Andreas	The Probability of Occurrence of Dangerous Wave Situations at Sea. (Dr.Ing. Thesis)
IMT-2005-11	Yttervik, Rune	Ocean current variability in relation to offshore engineering. (Dr.Ing. Thesis)
IMT-2005-12	Fredheim, Arne	Current Forces on Net-Structures. (Dr.Ing. Thesis)
IMT-2005-13	Heggernes, Kjetil	Flow around marine structures. (Dr.Ing. Thesis
IMT-2005-14	Fouques, Sebastien	Lagrangian Modelling of Ocean Surface Waves and Synthetic Aperture Radar Wave Measurements. (Dr.Ing. Thesis)
IMT-2006-15	Holm, Håvard	Numerical calculation of viscous free surface flow around marine structures. (Dr.Ing. Thesis)
IMT-2006-16	Bjørheim, Lars G.	Failure Assessment of Long Through Thickness Fatigue Cracks in Ship Hulls. (Dr.Ing. Thesis)
IMT-2006-17	Hansson, Lisbeth	Safety Management for Prevention of Occupational Accidents. (Dr.Ing. Thesis)
IMT-2006-18	Zhu, Xinying	Application of the CIP Method to Strongly Nonlinear Wave-Body Interaction Problems. (Dr.Ing. Thesis)
IMT-2006-19	Reite, Karl Johan	Modelling and Control of Trawl Systems. (Dr.Ing. Thesis)
IMT-2006-20	Smogeli, Øyvind Notland	Control of Marine Propellers. From Normal to Extreme Conditions. (Dr.Ing. Thesis)
IMT-2007-21	Storhaug, Gaute	Experimental Investigation of Wave Induced Vibrations and Their Effect on the Fatigue Loading of Ships. (Dr.Ing. Thesis)
IMT-2007-22	Sun, Hui	A Boundary Element Method Applied to Strongly Nonlinear Wave-Body Interaction Problems. (PhD Thesis, CeSOS)
IMT-2007-23	Rustad, Anne Marthine	Modelling and Control of Top Tensioned Risers. (PhD Thesis, CeSOS)
IMT-2007-24	Johansen, Vegar	Modelling flexible slender system for real-time simulations and control applications
IMT-2007-25	Wroldsen, Anders Sunde	Modelling and control of tensegrity structures.

		(PhD Thesis, CeSOS)
IMT-2007-26	Aronsen, Kristoffer Høye	An experimental investigation of in-line and combined inline and cross flow vortex induced vibrations. (Dr. avhandling, IMT)
IMT-2007-27	Gao, Zhen	Stochastic Response Analysis of Mooring Systems with Emphasis on Frequency-domain Analysis of Fatigue due to Wide-band Response Processes (PhD Thesis, CeSOS)
IMT-2007-28	Thorstensen, Tom Anders	Lifetime Profit Modelling of Ageing Systems Utilizing Information about Technical Condition. (Dr.ing. thesis, IMT)
IMT-2008-29	Refsnes, Jon Erling Gorset	Nonlinear Model-Based Control of Slender Body AUVs (PhD Thesis, IMT)
IMT-2008-30	Berntsen, Per Ivar B.	Structural Reliability Based Position Mooring. (PhD-Thesis, IMT)
IMT-2008-31	Ye, Naiquan	Fatigue Assessment of Aluminium Welded Box-stiffener Joints in Ships (Dr.ing. thesis, IMT)
IMT-2008-32	Radan, Damir	Integrated Control of Marine Electrical Power Systems. (PhD-Thesis, IMT)
IMT-2008-33	Thomassen, Paul	Methods for Dynamic Response Analysis and Fatigue Life Estimation of Floating Fish Cages. (Dr.ing. thesis, IMT)
IMT-2008-34	Pákozdi, Csaba	A Smoothed Particle Hydrodynamics Study of Two-dimensional Nonlinear Sloshing in Rectangular Tanks. (Dr.ing.thesis, IMT/ CeSOS)
IMT-2007-35	Grytøyr, Guttorm	A Higher-Order Boundary Element Method and Applications to Marine Hydrodynamics. (Dr.ing.thesis, IMT)
IMT-2008-36	Drummen, Ingo	Experimental and Numerical Investigation of Nonlinear Wave-Induced Load Effects in Containerships considering Hydroelasticity. (PhD thesis, CeSOS)
IMT-2008-37	Skejic, Renato	Maneuvering and Seakeeping of a Singel Ship and of Two Ships in Interaction. (PhD-Thesis, CeSOS)
IMT-2008-38	Harlem, Alf	An Age-Based Replacement Model for Repairable Systems with Attention to High-Speed Marine Diesel Engines. (PhD-Thesis, IMT)
IMT-2008-39	Alsos, Hagbart S.	Ship Grounding. Analysis of Ductile Fracture, Bottom Damage and Hull Girder Response. (PhD-thesis, IMT)
IMT-2008-40	Graczyk, Mateusz	Experimental Investigation of Sloshing Loading and Load Effects in Membrane LNG Tanks Subjected to Random Excitation. (PhD-thesis, CeSOS)
IMT-2008-41	Taghipour, Reza	Efficient Prediction of Dynamic Response for Flexible amd Multi-body Marine Structures. (PhD-

		thesis, CeSOS)
IMT-2008-42	Ruth, Eivind	Propulsion control and thrust allocation on marine vessels. (PhD thesis, CeSOS)
IMT-2008-43	Nystad, Bent Helge	Technical Condition Indexes and Remaining Useful Life of Aggregated Systems. PhD thesis, IMT
IMT-2008-44	Soni, Prashant Kumar	Hydrodynamic Coefficients for Vortex Induced Vibrations of Flexible Beams, PhD thesis, CeSOS
IMT-2009-45	Amlashi, Hadi K.K.	Ultimate Strength and Reliability-based Design of Ship Hulls with Emphasis on Combined Global and Local Loads. PhD Thesis, IMT
IMT-2009-46	Pedersen, Tom Arne	Bond Graph Modelling of Marine Power Systems. PhD Thesis, IMT
IMT-2009-47	Kristiansen, Trygve	Two-Dimensional Numerical and Experimental Studies of Piston-Mode Resonance. PhD-Thesis, CeSOS
IMT-2009-48	Ong, Muk Chen	Applications of a Standard High Reynolds Number Model and a Stochastic Scour Prediction Model for Marine Structures. PhD-thesis, IMT
IMT-2009-49	Hong, Lin	Simplified Analysis and Design of Ships subjected to Collision and Grounding. PhD-thesis, IMT
IMT-2009-50	Koushan, Kamran	Vortex Induced Vibrations of Free Span Pipelines, PhD thesis, IMT
IMT-2009-51	Korsvik, Jarl Eirik	Heuristic Methods for Ship Routing and Scheduling. PhD-thesis, IMT
IMT-2009-52	Lee, Jihoon	Experimental Investigation and Numerical in Analyzing the Ocean Current Displacement of Longlines. Ph.d.-Thesis, IMT.
IMT-2009-53	Vestbøstad, Tone Gran	A Numerical Study of Wave-in-Deck Impact usin a Two-Dimensional Constrained Interpolation Profile Method, Ph.d.thesis, CeSOS.
IMT-2009-54	Bruun, Kristine	Bond Graph Modelling of Fuel Cells for Marine Power Plants. Ph.d.-thesis, IMT
IMT 2009-55	Holstad, Anders	Numerical Investigation of Turbulence in a Sekwed Three-Dimensional Channel Flow, Ph.d.-thesis, IMT.
IMT 2009-56	Ayala-Uraga, Efren	Reliability-Based Assessment of Deteriorating Ship-shaped Offshore Structures, Ph.d.-thesis, IMT
IMT 2009-57	Kong, Xiangjun	A Numerical Study of a Damaged Ship in Beam Sea Waves. Ph.d.-thesis, IMT/CeSOS.
IMT 2010-58	Kristiansen, David	Wave Induced Effects on Floaters of Aquaculture Plants, Ph.d.-thesis, CeSOS.

IMT 2010-59	Ludvigsen, Martin	An ROV-Toolbox for Optical and Acoustic Scientific Seabed Investigation. Ph.d.-thesis IMT.
IMT 2010-60	Hals, Jørgen	Modelling and Phase Control of Wave-Energy Converters. Ph.d.thesis, CeSOS.
IMT 2010- 61	Shu, Zhi	Uncertainty Assessment of Wave Loads and Ultimate Strength of Tankers and Bulk Carriers in a Reliability Framework. Ph.d. Thesis, IMT/ CeSOS
IMT 2010-62	Shao, Yanlin	Numerical Potential-Flow Studies on Weakly-Nonlinear Wave-Body Interactions with/without Small Forward Speed, Ph.d.thesis,CeSOS.
IMT 2010-63	Califano, Andrea	Dynamic Loads on Marine Propellers due to Intermittent Ventilation. Ph.d.thesis, IMT.
IMT 2010-64	El Khoury, George	Numerical Simulations of Massively Separated Turbulent Flows, Ph.d.-thesis, IMT
IMT 2010-65	Seim, Knut Sponheim	Mixing Process in Dense Overflows with Emphasis on the Faroe Bank Channel Overflow. Ph.d.thesis, IMT
IMT 2010-66	Jia, Huirong	Structural Analysis of Intect and Damaged Ships in a Collission Risk Analysis Perspective. Ph.d.thesis CeSoS.
IMT 2010-67	Jiao, Linlin	Wave-Induced Effects on a Pontoon-type Very Large Floating Structures (VLFS). Ph.D.-thesis, CeSOS.
IMT 2010-68	Abrahamsen, Bjørn Christian	Sloshing Induced Tank Roof with Entrapped Air Pocket. Ph.d.thesis, CeSOS.
IMT 2011-69	Karimirad, Madjid	Stochastic Dynamic Response Analysis of Spar-Type Wind Turbines with Catenary or Taut Mooring Systems. Ph.d.-thesis, CeSOS.
IMT - 2011-70	Erlend Meland	Condition Monitoring of Safety Critical Valves. Ph.d.-thesis, IMT.
IMT – 2011-71	Yang, Limin	Stochastic Dynamic System Analysis of Wave Energy Converter with Hydraulic Power Take-Off, with Particular Reference to Wear Damage Analysis, Ph.d. Thesis, CeSOS.
IMT – 2011-72	Visscher, Jan	Application of Particla Image Velocimetry on Turbulent Marine Flows, Ph.d.Thesis, IMT.
IMT – 2011-73	Su, Biao	Numerical Predictions of Global and Local Ice Loads on Ships. Ph.d.Thesis, CeSOS.
IMT – 2011-74	Liu, Zhenhui	Analytical and Numerical Analysis of Iceberg Collision with Ship Structures. Ph.d.Thesis, IMT.
IMT – 2011-75	Aarsæther, Karl Gunnar	Modeling and Analysis of Ship Traffic by Observation and Numerical Simulation. Ph.d.Thesis, IMT.

Imt – 2011-76	Wu, Jie	Hydrodynamic Force Identification from Stochastic Vortex Induced Vibration Experiments with Slender Beams. Ph.d.Thesis, IMT.
Imt – 2011-77	Amini, Hamid	Azimuth Propulsors in Off-design Conditions. Ph.d.Thesis, IMT.
IMT – 2011-78	Nguyen, Tan-Hoi	Toward a System of Real-Time Prediction and Monitoring of Bottom Damage Conditions During Ship Grounding. Ph.d.thesis, IMT.
IMT-2011-79	Tavakoli, Mohammad T.	Assessment of Oil Spill in Ship Collision and Grounding, Ph.d.thesis, IMT.
IMT-2011-80	Guo, Bingjie	Numerical and Experimental Investigation of Added Resistance in Waves. Ph.d.Thesis, IMT.
IMT-2011-81	Chen, Qiaofeng	Ultimate Strength of Aluminium Panels, considering HAZ Effects, IMT
IMT-2012-82	Kota, Ravikiran S.	Wave Loads on Decks of Offshore Structures in Random Seas, CeSOS.
IMT-2012-83	Sten, Ronny	Dynamic Simulation of Deep Water Drilling Risers with Heave Compensating System, IMT.
IMT-2012-84	Berle, Øyvind	Risk and resilience in global maritime supply chains, IMT.
IMT-2012-85	Fang, Shaoji	Fault Tolerant Position Mooring Control Based on Structural Reliability, CeSOS.
IMT-2012-86	You, Jikun	Numerical studies on wave forces and moored ship motions in intermediate and shallow water, CeSOS.
IMT-2012-87	Xiang ,Xu	Maneuvering of two interacting ships in waves, CeSOS
IMT-2012-88	Dong, Wenbin	Time-domain fatigue response and reliability analysis of offshore wind turbines with emphasis on welded tubular joints and gear components, CeSOS
IMT-2012-89	Zhu, Suji	Investigation of Wave-Induced Nonlinear Load Effects in Open Ships considering Hull Girder Vibrations in Bending and Torsion, CeSOS
IMT-2012-90	Zhou, Li	Numerical and Experimental Investigation of Station-keeping in Level Ice, CeSOS
IMT-2012-91	Ushakov, Sergey	Particulate matter emission characteristics from diesel enignes operating on conventional and alternative marine fuels, IMT
IMT-2013-1	Yin, Decao	Experimental and Numerical Analysis of Combined In-line and Cross-flow Vortex Induced Vibrations, CeSOS

IMT-2013-2	Kurniawan, Adi	Modelling and geometry optimisation of wave energy converters, CeSOS
IMT-2013-3	Al Ryati, Nabil	Technical condition indexes doe auxiliary marine diesel engines, IMT
IMT-2013-4	Firoozkoohi, Reza	Experimental, numerical and analytical investigation of the effect of screens on sloshing, CeSOS
IMT-2013-5	Ommani, Babak	Potential-Flow Predictions of a Semi-Displacement Vessel Including Applications to Calm Water Broaching, CeSOS
IMT-2013-6	Xing, Yihan	Modelling and analysis of the gearbox in a floating spar-type wind turbine, CeSOS
IMT-7-2013	Balland, Océane	Optimization models for reducing air emissions from ships, IMT
IMT-8-2013	Yang, Dan	Transitional wake flow behind an inclined flat plate-----Computation and analysis, IMT
IMT-9-2013	Abdillah, Suyuthi	Prediction of Extreme Loads and Fatigue Damage for a Ship Hull due to Ice Action, IMT
IMT-10-2013	Ramìrez, Pedro Agustìn Pèrez	Ageing management and life extension of technical systems- Concepts and methods applied to oil and gas facilities, IMT
IMT-11-2013	Chuang, Zhenju	Experimental and Numerical Investigation of Speed Loss due to Seakeeping and Maneuvering. IMT
IMT-12-2013	Etemaddar, Mahmoud	Load and Response Analysis of Wind Turbines under Atmospheric Icing and Controller System Faults with Emphasis on Spar Type Floating Wind Turbines, IMT
IMT-13-2013	Lindstad, Haakon	Strategies and measures for reducing maritime CO2 emissons, IMT
IMT-14-2013	Haris, Sabril	Damage interaction analysis of ship collisions, IMT
IMT-15-2013	Shainee, Mohamed	Conceptual Design, Numerical and Experimental Investigation of a SPM Cage Concept for Offshore Mariculture, IMT
IMT-16-2013	Gansel, Lars	Flow past porous cylinders and effects of biofouling and fish behavior on the flow in and around Atlantic salmon net cages, IMT
IMT-17-2013	Gaspar, Henrique	Handling Aspects of Complexity in Conceptual Ship Design, IMT
IMT-18-2013	Thys, Maxime	Theoretical and Experimental Investigation of a Free Running Fishing Vessel at Small Frequency of Encounter, CeSOS
IMT-19-2013	Aglen, Ida	VIV in Free Spanning Pipelines, CeSOS

IMT-1-2014	Song, An	Theoretical and experimental studies of wave diffraction and radiation loads on a horizontally submerged perforated plate, CeSOS
IMT-2-2014	Rogne, Øyvind Ygre	Numerical and Experimental Investigation of a Hinged 5-body Wave Energy Converter, CeSOS
IMT-3-2014	Dai, Lijuan	Safe and efficient operation and maintenance of offshore wind farms ,IMT
IMT-4-2014	Bachynski, Erin Elizabeth	Design and Dynamic Analysis of Tension Leg Platform Wind Turbines, CeSOS
IMT-5-2014	Wang, Jingbo	Water Entry of Freefall Wedged – Wedge motions and Cavity Dynamics, CeSOS
IMT-6-2014	Kim, Ekaterina	Experimental and numerical studies related to the coupled behavior of ice mass and steel structures during accidental collisions, IMT
IMT-7-2014	Tan, Xiang	Numerical investigation of ship’s continuous- mode icebreaking in leverl ice, CeSOS
IMT-8-2014	Muliawan, Made Jaya	Design and Analysis of Combined Floating Wave and Wind Power Facilities, with Emphasis on Extreme Load Effects of the Mooring System, CeSOS
IMT-9-2014	Jiang, Zhiyu	Long-term response analysis of wind turbines with an emphasis on fault and shutdown conditions, IMT
IMT-10-2014	Dukan, Fredrik	ROV Motion Control Systems, IMT
IMT-11-2014	Grimsmo, Nils I.	Dynamic simulations of hydraulic cylinder for heave compensation of deep water drilling risers, IMT
IMT-12-2014	Kvittem, Marit I.	Modelling and response analysis for fatigue design of a semisubmersible wind turbine, CeSOS
IMT-13-2014	Akhtar, Juned	The Effects of Human Fatigue on Risk at Sea, IMT
IMT-14-2014	Syahroni, Nur	Fatigue Assessment of Welded Joints Taking into Account Effects of Residual Stress, IMT
IMT-1-2015	Bøckmann, Eirik	Wave Propulsion of ships, IMT
IMT-2-2015	Wang, Kai	Modelling and dynamic analysis of a semi-submersible floating vertical axis wind turbine, CeSOS
IMT-3-2015	Fredriksen, Arnt Gunvald	A numerical and experimental study of a two-dimensional body with moonpool in waves and current, CeSOS
IMT-4-2015	Jose Patricio Gallardo Canabes	Numerical studies of viscous flow around bluff bodies, IMT

IMT-5-2015	Vegard Longva	Formulation and application of finite element techniques for slender marine structures subjected to contact interactions, IMT
IMT-6-2015	Jacobus De Vaal	Aerodynamic modelling of floating wind turbines, CeSOS
IMT-7-2015	Fachri Nasution	Fatigue Performance of Copper Power Conductors, IMT
IMT-8-2015	Oleh I Karpa	Development of bivariate extreme value distributions for applications in marine technology,CeSOS
IMT-9-2015	Daniel de Almeida Fernandes	An output feedback motion control system for ROVs, AMOS
IMT-10-2015	Bo Zhao	Particle Filter for Fault Diagnosis: Application to Dynamic Positioning Vessel and Underwater Robotics, CeSOS
IMT-11-2015	Wenting Zhu	Impact of emission allocation in maritime transportation, IMT
IMT-12-2015	Amir Rasekhi Nejad	Dynamic Analysis and Design of Gearboxes in Offshore Wind Turbines in a Structural Reliability Perspective, CeSOS
IMT-13-2015	Arturo Jesùs Ortega Malca	Dynamic Response of Flexibles Risers due to Unsteady Slug Flow, CeSOS
IMT-14-2015	Dagfinn Husjord	Guidance and decision-support system for safe navigation of ships operating in close proximity, IMT
IMT-15-2015	Anirban Bhattacharyya	Ducted Propellers: Behaviour in Waves and Scale Effects, IMT
IMT-16-2015	Qin Zhang	Image Processing for Ice Parameter Identification in Ice Management, IMT
IMT-1-2016	Vincentius Rumawas	Human Factors in Ship Design and Operation: An Experiential Learning, IMT
IMT-2-2016	Martin Storheim	Structural response in ship-platform and ship-ice collisions, IMT
IMT-3-2016	Mia Abrahamsen Prsic	Numerical Simulations of the Flow around single and Tandem Circular Cylinders Close to a Plane Wall, IMT
IMT-4-2016	Tufan Arslan	Large-eddy simulations of cross-flow around ship sections, IMT

IMT-5-2016	Pierre Yves-Henry	Parametrisation of aquatic vegetation in hydraulic and coastal research,IMT
IMT-6-2016	Lin Li	Dynamic Analysis of the Instalation of Monopiles for Offshore Wind Turbines, CeSOS
IMT-7-2016	Øivind Kåre Kjerstad	Dynamic Positioning of Marine Vessels in Ice, IMT
IMT-8-2016	Xiaopeng Wu	Numerical Analysis of Anchor Handling and Fish Trawling Operations in a Safety Perspective, CeSOS
IMT-9-2016	Zhengshun Cheng	Integrated Dynamic Analysis of Floating Vertical Axis Wind Turbines, CeSOS
IMT-10-2016	Ling Wan	Experimental and Numerical Study of a Combined Offshore Wind and Wave Energy Converter Concept
IMT-11-2016	Wei Chai	Stochastic dynamic analysis and reliability evaluation of the roll motion for ships in random seas, CeSOS
IMT-12-2016	Øyvind Selnes Patricksson	Decision support for conceptual ship design with focus on a changing life cycle and future uncertainty, IMT
IMT-13-2016	Mats Jørgen Thorsen	Time domain analysis of vortex-induced vibrations, IMT
IMT-14-2016	Edgar McGuinness	Safety in the Norwegian Fishing Fleet – Analysis and measures for improvement, IMT
IMT-15-2016	Sepideh Jafarzadeh	Energy effiency and emission abatement in the fishing fleet, IMT
IMT-16-2016	Wilson Ivan Guachamin Acero	Assessment of marine operations for offshore wind turbine installation with emphasis on response-based operational limits, IMT
IMT-17-2016	Mauro Candeloro	Tools and Methods for Autonomous Operations on Seabed and Water Coumn using Underwater Vehicles, IMT
IMT-18-2016	Valentin Chabaud	Real-Time Hybrid Model Testing of Floating Wind Tubines, IMT
IMT-1-2017	Mohammad Saud Afzal	Three-dimensional streaming in a sea bed boundary layer
IMT-2-2017	Peng Li	A Theoretical and Experimental Study of Wave-induced Hydroelastic Response of a Circular Floating Collar
IMT-3-2017	Martin Bergström	A simulation-based design method for arctic maritime transport systems

IMT-4-2017	Bhushan Taskar	The effect of waves on marine propellers and propulsion
IMT-5-2017	Mohsen Bardestani	A two-dimensional numerical and experimental study of a floater with net and sinker tube in waves and current
IMT-6-2017	Fatemeh Hoseini Dadmarzi	Direct Numerical Simualtion of turbulent wakes behind different plate configurations
IMT-7-2017	Michel R. Miyazaki	Modeling and control of hybrid marine power plants
IMT-8-2017	Giri Rajasekhar Gunnu	Safety and effiency enhancement of anchor handling operations with particular emphasis on the stability of anchor handling vessels
IMT-9-2017	Kevin Koosup Yum	Transient Performance and Emissions of a Turbocharged Diesel Engine for Marine Power Plants
IMT-10-2017	Zhaolong Yu	Hydrodynamic and structural aspects of ship collisions
IMT-11-2017	Martin Hassel	Risk Analysis and Modelling of Allisions between Passing Vessels and Offshore Installations
IMT-12-2017	Astrid H. Brodtkorb	Hybrid Control of Marine Vessels – Dynamic Positioning in Varying Conditions
IMT-13-2017	Kjersti Bruserud	Simultaneous stochastic model of waves and current for prediction of structural design loads
IMT-14-2017	Finn-Idar Grøtta Giske	Long-Term Extreme Response Analysis of Marine Structures Using Inverse Reliability Methods
IMT-15-2017	Stian Skjong	Modeling and Simulation of Maritime Systems and Operations for Virtual Prototyping using co-Simulations
IMT-1-2018	Yingguang Chu	Virtual Prototyping for Marine Crane Design and Operations
IMT-2-2018	Sergey Gavrilin	Validation of ship manoeuvring simulation models
IMT-3-2018	Jeevith Hegde	Tools and methods to manage risk in autonomous subsea inspection,maintenance and repair operations
IMT-4-2018	Ida M. Strand	Sea Loads on Closed Flexible Fish Cages
IMT-5-2018	Erlend Kvinge Jørgensen	Navigation and Control of Underwater Robotic Vehicles

IMT-6-2018	Bård Stovner	Aided Intertial Navigation of Underwater Vehicles
IMT-7-2018	Erlend Liavåg Grotle	Thermodynamic Response Enhanced by Sloshing in Marine LNG Fuel Tanks
IMT-8-2018	Børge Rokseth	Safety and Verification of Advanced Maritime Vessels
IMT-9-2018	Jan Vidar Ulveseter	Advances in Semi-Empirical Time Domain Modelling of Vortex-Induced Vibrations
IMT-10-2018	Chenyu Luan	Design and analysis for a steel braceless semi-submersible hull for supporting a 5-MW horizontal axis wind turbine
IMT-11-2018	Carl Fredrik Rehn	Ship Design under Uncertainty
IMT-12-2018	Øyvind Ødegård	Towards Autonomous Operations and Systems in Marine Archaeology
IMT-13-2018	Stein Melvær Nornes	Guidance and Control of Marine Robotics for Ocean Mapping and Monitoring
IMT-14-2018	Petter Norgren	Autonomous Underwater Vehicles in Arctic Marine Operations: Arctic marine research and ice monitoring
IMT-15-2018	Minjoo Choi	Modular Adaptable Ship Design for Handling Uncertainty in the Future Operating Context
MT-16-2018	Ole Alexander Eidsvik	Dynamics of Remotely Operated Underwater Vehicle Systems
IMT-17-2018	Mahdi Ghane	Fault Diagnosis of Floating Wind Turbine Drivetrain- Methodologies and Applications
IMT-18-2018	Christoph Alexander Thieme	Risk Analysis and Modelling of Autonomous Marine Systems
IMT-19-2018	Yugao Shen	Operational limits for floating-collar fish farms in waves and current, without and with well-boat presence
IMT-20-2018	Tianjiao Dai	Investigations of Shear Interaction and Stresses in Flexible Pipes and Umbilicals
IMT-21-2018	Sigurd Solheim Pettersen	Resilience by Latent Capabilities in Marine Systems
IMT-22-2018	Thomas Sauder	Fidelity of Cyber-physical Empirical Methods. Application to the Active Truncation of Slender Marine Structures
IMT-23-2018	Jan-Tore Horn	Statistical and Modelling Uncertainties in the Design of Offshore Wind Turbines

IMT-24-2018	Anna Swider	Data Mining Methods for the Analysis of Power Systems of Vessels
IMT-1-2019	Zhao He	Hydrodynamic study of a moored fish farming cage with fish influence
IMT-2-2019	Isar Ghamari	Numerical and Experimental Study on the Ship Parametric Roll Resonance and the Effect of Anti-Roll Tank
IMT-3-2019	Håkon Strandenes	Turbulent Flow Simulations at Higher Reynolds Numbers
IMT-4-2019	Siri Mariane Holen	Safety in Norwegian Fish Farming – Concepts and Methods for Improvement
IMT-5-2019	Ping Fu	Reliability Analysis of Wake-Induced Riser Collision
IMT-6-2019	Vladimir Krivopolianskii	Experimental Investigation of Injection and Combustion Processes in Marine Gas Engines using Constant Volume Rig
IMT-7-2019	Anna Maria Kozlowska	Hydrodynamic Loads on Marine Propellers Subject to Ventilation and out of Water Condition.
IMT-8-2019	Hans-Martin Heyn	Motion Sensing on Vessels Operating in Sea Ice: A Local Ice Monitoring System for Transit and Stationkeeping Operations under the Influence of Sea Ice
IMT-9-2019	Stefan Vilsen	Method for Real-Time Hybrid Model Testing of Ocean Structures – Case on Slender Marine Systems
IMT-10-2019	Finn-Christian W. Hanssen	Non-Linear Wave-Body Interaction in Severe Waves
IMT-11-2019	Trygve Olav Fossum	Adaptive Sampling for Marine Robotics
IMT-12-2019	Jørgen Bremnes Nielsen	Modeling and Simulation for Design Evaluation
IMT-13-2019	Yuna Zhao	Numerical modelling and dyncamic analysis of offshore wind turbine blade installation
IMT-14-2019	Daniela Myland	Experimental and Theoretical Investigations on the Ship Resistance in Level Ice
IMT-15-2019	Zhengru Ren	Advanced control algorithms to support automated offshore wind turbine installation
IMT-16-2019	Drazen Polic	Ice-propeller impact analysis using an inverse propulsion machinery simulation approach
IMT-17-2019	Endre Sandvik	Sea passage scenario simulation for ship system performance evaluation

IMT-18-2019	Loup Suja-Thauvin	Response of Monopile Wind Turbines to Higher Order Wave Loads
IMT-19-20119	Emil Smilden	Structural control of offshore wind turbines – Increasing the role of control design in offshore wind farm development
IMT-20-2019	Aleksandar-Sasa Milakovic	On equivalent ice thickness and machine learning in ship ice transit simulations
IMT-1-2020	Amrit Shankar Verma	Modelling, Analysis and Response-based Operability Assessment of Offshore Wind Turbine Blade Installation with Emphasis on Impact Damages
IMT-2-2020	Bent Oddvar Arnesen Haugaløkken	Autonomous Technology for Inspection, Maintenance and Repair Operations in the Norwegian Aquaculture
IMT-3-2020	Seongpil Cho	Model-based fault detection and diagnosis of a blade pitch system in floating wind turbines
IMT-4-2020	Jose Jorge Garcia Agis	Effectiveness in Decision-Making in Ship Design under Uncertainty
IMT-5-2020	Thomas H. Viuff	Uncertainty assessment of wave-and current-induced global response of floating bridges
IMT-6-2020	Fredrik Mentzoni	Hydrodynamic Loads on Complex Structures in the Wave Zone
IMT-7-2020	Senthuran Ravinthrakumar	Numerical and Experimental Studies of Resonant Flow in Moonpools in Operational Conditions
IMT-8-2020	Stian Skaalvik Sandøy	Acoustic-Based Probabilistic Localization and Mapping for Unmanned Underwater Vehicles in Aquaculture Operations

Errata:

Title: Cover and title page**:** **Acoustics-Based** to **Acoustic-Based**

Author name on cover and title page: **Skaavik** to **Skaalvik.**

Add blue page at: p.1 and p. 69

Acknowledgements: 4th paragraph: training -> workout

Nomenclature:

- List of abbreviations
  - p. xv: Removed LoA as an abbreviation
- List of symbols
  - p. xvi: u and x units description switched
  - p. xvi : Fixed R^{n x m} and R^{n} compilation error

p.3: Tabel 1.3: Space between authors in article J1

p.6: Figure 1.4 : Changed figure by centering the text: Scope of thesis.

p.11: Caption table 1.1: Lower case s in sensor.

p.14: Equation (1.1): Equation is now on one line.

p.26, second last paragraph. x (hat and bar) vector set to bold font.

p.27, 1st paragraph: The PF contains three steps:

p.28, Equation 2.12: Removed the superscript n from x in equation a following paragraph.

p.33: Equation 2.18: Corrections in equation

p.34: Last paragraph in section 2.2.4: Added: "Note that **m**_0 denotes a grid map"

p.37: Section 2.2.6: Added missing paragraph and algorithm.

p.35: Second paragraph after equation 2.24: Fixed parenthesis in variables in paragraph

p.44: Methodology section: Changed section reference to 2.2.6

p.44: Added missing equation 4.2 + definition of variables

p.48: First paragraph in Result section: Figure 4.8 changed to 4.7

p.53: Last paragraph: Variables put to bold, facing the wave motion

p.57: Last paragraph: Typo: approach

p. = page